

Lipid foulant interactions during the chromatographic purification of virus-like particles from *Saccharomyces cerevisiae*

A thesis submitted to University College London
for the degree of
DOCTOR OF PHILOSOPHY

By

Jing Jin

September 2010

The Advanced Centre for Biochemical Engineering
Department of Biochemical Engineering
University College London,
Torrington Place, London WC1E 7JE, UK

I, Jing Jin confirm that the work presented in this thesis is my own. Where information has been derived from other sources, I confirm that this has been indicated in the thesis.

Abstract

The objective of this study was to understand the mechanism of lipid fouling in chromatography through the investigation of a hydrophobic interaction chromatography (HIC) operation. This was motivated by the need to understand this phenomenon during the manufacture of biological products such as vaccines. The systematic approach and novel analytical techniques employed create a unique platform to study fouling of other chromatographic adsorbents and process feed materials.

HIC is employed as a primary capture step in the purification of yeast derived hepatitis B surface antigen (HBsAg), where the required cell disruption and detergent liberation steps release high levels of lipid content into the feed stream. From lipid-rich and lipid-depleted feedstocks, comparative analysis was able to quantify the deterioration in HIC performance (binding capacities, purities and recoveries) under successive cycles. Furthermore, a full mass balance on host lipids identified the highly hydrophobic triacylglyceride as the main foulant. Intra-particle distribution and progression of lipid fouling and its effects on material adsorption and diffusion were then examined under confocal laser scanning microscopy (CLSM). In addition, high-resolution scanning electron microscopy (SEM) images of the fouled bead (after 40 cycles) confirmed that a thick lipid layer was building up on the outer bead surface. Based on these findings, the mechanism of fouling was thought to be the rapid accumulation of lipid foulant at the rim of the bead, which was aggravated by the possible diffusion hindrance resulting from multilayer adsorption. Finally, pretreatments to reduce this mechanism of chromatography fouling were evaluated in terms of improvement on feed quality and HIC performance. Selective adsorbent polystyrene XAD-4 demonstrated promising lipid removal capabilities with satisfactory HBsAg VLP recoveries. The improved feed into the column resulted in a three-fold increase in product capacity, whilst the overall yield remained constant over 40 cycles.

Acknowledgement

Looking back, I am really grateful for all the kind support that I have received during my PhD journey making it an exciting and rewarding experience, which certainly will be an invaluable part of my life. This thesis would not have been possible without the help and encouragement from the following people.

First and foremost, I would like to thank my supervisor Dr Daniel Bracewell for his dedication, encouragement and guidance, all of which have been the inspiration carrying me past all the obstacles in the research. It also gives me great pleasure in acknowledging the support and help from my advisor Professor Nigel Titchener-Hooker.

It has been a great honour to work alongside many outstanding academic staffs and PhD colleagues at UCL. I especially wish to thank Dr Sunil Chhatre for his generous and invaluable contribution to many aspects of my research. I cannot imagine how life would be like working alone on such a challenging material as VLP without the insightful exchanges and support from Dr Gaik Sui Kee and Claire Burden (the VLP team), for which I am immensely grateful. I would also like to acknowledge the training and support that I received from Dr Gareth Mannall in ACBE pilot plant and Dr Mark Turmaine (Division of Biosciences) in electron microscopy.

Last but not the least, I would like to show my deepest gratitude to my family, especially my mother Xiaoyan and my wife Aika, for their unfailing love and support.

This thesis is lovingly dedicated to my mother who lost her fight with cancer in 2008.
I am forever indebted to her for all the love, encouragement and inspiration she has
given me.

Table of Contents

Abstract.....	3
Acknowledgement	4
Table of Contents	6
Table of Figures.....	11
Lists of Tables.....	15
Table of Symbols and Abbreviations	16
Chapter 1: Introduction	20
1.1 Chromatography	21
1.1.1 Principles	21
1.1.2 Performance parameters	23
1.1.3 Resins.....	24
1.1.4 Techniques.....	28
1.1.5 Hydrophobic Interaction Chromatography	29
1.2 Virus-like particle (VLP).....	32
1.2.1 VLP advantages	32
1.2.2 VLP applications	34
1.2.3 VLP manufacturing process.....	36
1.2.4 Hepatitis B virus surface antigen (HBsAg)	37
1.3 Fouling in Chromatography.....	42
1.3.1 Type of foulants.....	44
1.3.1.1 Proteins	45
1.3.1.2 Lipids	47
1.3.1.3 Nucleic acids.....	51
1.3.1.4 Particulates.....	52
1.3.2 Fouling effects	53
1.3.3 CIP and validation	55
1.4 Confocal and Electron Microscopy	58
1.4.1 The study of mass transfer in chromatography.....	58
1.4.2 Confocal Microscopy in chromatography research	61
1.4.3 Principles of CLSM	62
1.4.4 Scanning electron microscopy (SEM)	64

1.5 Research Aims	66
1.5.1 Quantification of the deterioration in column performance from lipid fouling	66
1.5.2 Investigation of the lipid fouling mechanism	67
1.5.3 Investigation lipid removal strategies	67
1.6 Organisation of this thesis	68
Chapter 2: Materials and Methods	70
2.1 Materials	71
2.1.1 Chemicals	71
2.1.2 HBsAg VLP cell line	71
2.2 Analytical.....	71
2.2.1 Optical density measurements	71
2.2.2 Dry cell weight measurements.....	72
2.2.3 Glucose & galactose measurements	72
2.2.4 Enzyme Linked ImmunoSorbent Assay (ELISA) for VLP	72
2.2.5 Lipid quantitation by HPLC	73
2.2.6 Protein quantitation.....	73
2.2.7 Scanning electron microscopy (SEM)	74
2.2.8 Confocal laser scanning microscopy (CLSM).....	75
2.2.8.1 Description of equipment.....	75
2.2.8.2 Fluorescent labelling.....	77
2.2.8.3 Column sectioning tool.....	77
2.3 Experiments in Chapter 3	79
2.3.1 Fermentation	79
2.3.2 Primary recovery	80
2.3.3 Preparation of low lipid feedstock.....	80
2.3.4 Hydrophobic interaction chromatography (HIC).....	82
2.4 Experiments in Chapter 4	83
2.4.1 Adsorption isotherm measurements.....	83
2.4.2 Uptake rate measurements	84
2.4.3 Effect of salt concentrations on diffusion profile (flow cell).....	85
2.4.4 Effect of lipid fouling on protein diffusion (flow cell)	85
2.4.5 Lipid displacement (flow cell).....	86
2.4.6 Lipid foulant distribution within the column	87
2.4.7 Progression of lipid fouling within the column	87
2.5 Experiments in Chapter 5	88

2.5.1 Homogenisation pressure and centrifugation.....	88
2.5.2 Triton X-100 concentrations.....	89
2.5.3 Additional lipid removal steps.....	89
Chapter 3: Quantification of the deterioration in column performance from lipid fouling	91
3.1 Introduction	92
3.2 Results and Discussions.....	95
3.2.1 Fermentation	95
3.2.2 HIC chromatogram	96
3.2.3 Lipid composition in the feed	97
3.2.4 Lipid deposition into the column	101
3.2.5 Column performance with lipid fouling	103
3.3 Conclusion	109
Chapter 4: Investigation of lipid fouling mechanism.....	111
4.1 Introduction	112
4.2 Theory.....	114
4.2.1 Fluorescence	114
4.2.2 Fluorescent dyes	117
4.2.2.1 Amine-reactive dyes	117
4.2.2.2 Lipophilic dyes.....	118
4.2.3 CLSM data processing.....	120
4.2.3.1 Light attenuation correction	120
4.2.3.2 Relative capacity calculation	122
4.2.4 Pore and surface diffusion	124
4.3 Results and Discussion	127
4.3.1 Experimental errors	127
4.3.1.1 Photobleaching.....	127
4.3.1.2 Particle size distribution.....	128
4.3.2 Experimental controls.....	129
4.3.2.1 Fluorescent labelling effects on adsorption	129
4.3.2.2 Material autofluorescence and cross-talks	130
4.3.3 Thermodynamic characterisation of process material uptake	132
4.3.3.1 Adsorption isotherms	132
4.3.3.2 Material batch uptake rates	135
4.3.3.3 Effects of material interactions on uptake rates	137

4.3.4 Investigation of material uptakes under the effect of fouling by CLSM	142
4.3.4.1 Effect on mass transport by salt concentrations	142
4.3.4.2 Effects of diffusion hindrance	146
4.3.4.3 Irreversible adsorption of lipids	150
4.3.5 Visualisation of lipid fouling by SEM	154
4.3.6 Investigation of lipid fouling within a column	158
4.3.6.1 Quantitation of lipid fouling within a column	158
4.3.6.2 Progression of lipid fouling within a column	163
4.3.6.3 Dual-peak phenomenon	165
4.4 Conclusions and proposed lipid fouling mechanism	167
4.4.1 Summary of findings	167
4.4.2 Characteristics of lipids and their roles in fouling	169
4.4.3 Effect of adsorption condition on diffusion	170
4.4.4 Multilayer adsorption	171
4.4.5 Pore blockage	173
4.4.6 Lipid fouling mechanism	174
Chapter 5: Investigating the efficacy of pretreatments in lipid removal	175
5.1 Introduction	176
5.2 Theory	178
5.2.1 Homogenisation	178
5.2.2 Detergent: Triton X-100	180
5.2.3 Ammonium sulphate precipitation	181
5.2.4 LRA (Lipid Removal Agent)	182
5.2.5 Amberlite® XAD-4	183
5.2.6 CUNO Zeta Plus® depth filtration	184
5.3 Results and Discussion	185
5.3.1 Effect of homogenisation pressure and centrifugation	185
5.3.2 Effect of Triton X-100 concentration	190
5.3.3 Additional lipid removal step	194
5.3.4 HIC performance improvement	200
5.4 Conclusions	203
Chapter 6: Conclusions and Recommendations for future work	205
6.1 Overview	206
6.2 Quantification of the deterioration in column performance from lipid fouling	
(Chapter 3)	207

6.2.1 Study objectives (Chapter 3).....	207
6.2.2 Summary of findings (Chapter 3)	208
6.3 Investigation on lipid fouling mechanism (Chapter 4)	209
6.3.1 Study objectives (Chapter 4).....	209
6.3.2 Summary of findings (Chapter 4)	209
6.4 Investigating on the efficacy of pretreatments in lipid removal (Chapter 5).....	211
6.4.1 Study objectives (Chapter 5).....	211
6.4.2 Summary of findings (Chapter 5)	212
6.5 Recommendation for future work.....	213
6.5.1 HBsAg VLP quantification.....	213
6.5.2 Further characterisation of HBsAg stability	214
6.5.3 Improved labelling techniques and conditions	215
6.5.4 Alternative lipid removal strategies	215
6.5.5 Alternative capture step chromatography	216
6.5.6 Column design	217
6.5.7 Resin design.....	218
Chapter 7: References	219
Appendix.....	243

Table of Figures

Figure 1-1: Structure of fresh Sepharose [®] Butyl-S 6 Fast Flow resin	25
Figure 1-2: Sepharose [®] 6 Fast Flow HIC resin:spacer arm and ligand substituted)	27
Figure 1-3: Diagrammatic representation of hepatitis B virus surface antigen.	38
Figure 1-4: Process flow chart of VLP purification.....	40
Figure 1-5: Structures of triacylglycerols, cholesterol and phospholipids	48
Figure 1-6: Schematic illustration of solute mass transport into a chromatography bead.	59
Figure 1-7: Light paths in a confocal scanning laser microscopy.....	63
Figure 2-1: Flow cell used in CLSM live imaging..	76
Figure 2-2: Flow cell setting within a confocal microscope.	76
Figure 2-3: Column sectioning tool and procedures of column sectioning.	78
Figure 2-4: Process flow chart for HBsAg VLP purification.	81
Figure 3-1: Recombinant <i>Saccharomyces cerevisiae</i> HBsAg VLP fermentation.	95
Figure 3-2: The HIC loading and elution profile..	97
Figure 3-3: Chromatogram of the lipids composition in the feed.....	99
Figure 3-4: Confocal laser scanning microscopy image of Sepharose [®] Butyl-S 6 Fast Flow beads after repeated loading cycles.....	101
Figure 3-5: Percentage of VLP bound during loading	104
Figure 3-6: Comparison of amount of total materials during low salt and 30% isopropanol elutions.	105
Figure 3-7: Percentage of VLP eluted during the low salt elution of total VLP bound	106
Figure 4-1: Jablonski diagram.....	114
Figure 4-2: Molecular structure of Alexa Fluor [®]	117
Figure 4-3: Excitation and emission spectra of Alexa Fluor [®] 555.	118

Figure 4-4: Molecular structure of Bodipy [®] 493/503.	118
Figure 4-5: Excitation and emission spectra of Bodipy [®] 493/503.	119
Figure 4-6: Molecular structure of Nile red.	119
Figure 4-7: Excitation and emission spectra of Nile red.	120
Figure 4-8: Coordinate system in the cross-section at the centre of a bead.	121
Figure 4-9: Illustrates of pore and surface diffusions in porous particles.	124
Figure 4-10: Photobleaching profiles of Alexa [®] Fluor 555 and Cy3 dyes	127
Figure 4-11: Adsorption equilibriums of HBsAg VLP, neutral lipids and proteins in process feed by Sepharose [®] Butyl-S 6 Fast Flow	132
Figure 4-12: Batch uptake curves of HBsAg VLP, neutral lipids and proteins in process feed by Sepharose [®] Butyl-S 6 Fast Flow.	136
Figure 4-13: Batch uptake curves of neutral lipids in process feed by Sepharose [®] Butyl-S 6 Fast Flow at 0.6 and 0.3 M (NH ₄) ₂ SO ₄	139
Figure 4-14: Batch uptake curves of HBsAg VLP in process feed by Sepharose [®] Butyl-S 6 Fast Flow at 0.6 and 0.3 M (NH ₄) ₂ SO ₄	140
Figure 4-15: Batch uptake curves of proteins in process feed by Sepharose [®] Butyl-S 6 Fast Flow at 0.6 and 0.3 M (NH ₄) ₂ SO ₄	141
Figure 4-16: Time series of bead cross-sections (10, 15, 30, 60, and 90 min) during the uptake of Bodipy [®] 493/503 labelled lipids from process feed to fresh Sepharose [®] Butyl-S 6 Fast Flow beads at 0.6 M (NH ₄) ₂ SO ₄ concentration.	143
Figure 4-17: Time series of bead cross-sections (1, 5, 10, 15, and 20 min) during the uptake of Bodipy [®] 493/503 labelled lipids from process feed stream to fresh Sepharose [®] Butyl-S 6 Fast Flow beads at 0.3 M (NH ₄) ₂ SO ₄ concentration.	144
Figure 4-18: Time series of bead cross-sections (0.5, 1, 1.5, and 2 min) during the uptake of Bodipy [®] 493/503 labelled lipids from process feed to fresh Sepharose [®] Butyl-S 6 Fast Flow beads in the absence of (NH ₄) ₂ SO ₄	145
Figure 4-19: Time series of bead cross-sections (10, 20, and 30 min) during the uptake of pure BSA-Alexa [®] 555 to fresh Sepharose [®] Butyl-S 6 Fast Flow beads at 0.6 M (NH ₄) ₂ SO ₄	148
Figure 4-20: Time series of bead cross-sections (1, 5, 10, and 20 min) during the competitive uptake of Bodipy [®] 493/503 labelled lipids and BSA-Alexa [®]	

555 from process feed to fresh Sepharose [®] Butyl-S 6 Fast Flow beads at 0.6 M (NH ₄) ₂ SO ₄ .	149
Figure 4-21: Time series of bead cross-sections (11, 13, 15, and 20 min) during the uptake of neutral lipids from process feed to fresh Sepharose [®] Butyl-S 6 Fast Flow beads.	152
Figure 4-22: Fractions of the remaining adsorbed Nile red labelled lipids from the previous 10 minute during the continuous loading of Bodipy [®] 493/503 labelled lipids from the process feed.	153
Figure 4-23: Scanning electron microscopy images of Sepharose [®] Butyl-S 6 Fast Flow bead from fresh resin and those at and the end of 1 and 40 cycles of operation.	155
Figure 4-24: Scanning electron microscopy images of Sepharose [®] Butyl-S 6 Fast Flow bead at the end of 40 cycles of operation.	156
Figure 4-25: Scanning electron microscopy images of a fouled Sepharose [®] Butyl-S 6 Fast Flow bead showing an area of contact between beads, i.e. bead contact point.	157
Figure 4-26: Scanning electron microscopy images from secondary emissions of a fouled Sepharose Butyl-S 6 Fast Flow bead labelled with Osmium showing an area of contact between beads.	158
Figure 4-27: Typical beads chosen from the three column sections (top, middle and bottom) after 1 cycle, 10 cycles and 40 cycles of operation.	159
Figure 4-28: Intra-particle relative volumetric intensity of fluorescence from the Bodipy [®] 493/503 labelled process feed at top, middle and bottom section of the column, after 1 cycle, 10 cycles and 40 cycles of operation.	160
Figure 4-29: Bead cross-section intensity profiles of Bodipy [®] 493/503 labelled lipids from process feed after 1 cycle, 10 cycles and 40 cycles of operation. Bead samples were from top third section of the column.	162
Figure 4-30: Fluorescence intensity of Bodipy [®] 493/503 labelled lipids from process feed at various intra-particle radial position during the uptake by Sepharose [®] Butyl-S 6 Fast Flow beads.	163
Figure 4-31: Intra-particle distribution of lipid foulant.	164
Figure 4-32: Dual-peak phenomenon.	166
Figure 4-33: Interaction between adsorptive and diffusive forces on a molecule in HIC at low, medium and high adsorption conditions.	170
Figure 4-34: Proposed multilayer adsorption in the presence of lipid foulants.	172

Figure 4-35: Pore blockage due to multilayer adsorption. L: lipids or lipid aggregates. P: proteins.	173
Figure 4-36: Proposed lipid fouling mechanism during the chromatographic purification of yeast-derived HBsAg VLP.	174
Figure 5-1: Schematic diagram of a typical vale unit inside the high-pressure Manton- Gaulin homogeniser.	178
Figure 5-2: Molecular structure of Triton X-100 detergent.	180
Figure 5-3: CUNO Zeta Plus [®] DEL depth filtration cartridges.	184
Figure 5-4: The yields of HBsAg VLP at various homogenisation pressures in both conventional and selective methods.	186
Figure 5-5: The levels of lipid released at various homogenisation pressures in both conventional and selective methods.	188
Figure 5-6: Screening of optimal homogenisation pressure condition.	189
Figure 5-7: The yield of HBsAg VLP versus the levels of lipid release at various Triton X-100 concentrations	191
Figure 5-8: Screening of optimal Triton X-100 concentration	192
Figure 5-9: The effects of ammonium sulphate precipitation on HBsAg VLP recovery and remaining lipid levels	196
Figure 5-10: The effects of LRA treatment on HBsAg VLP recovery and remaining lipid levels.	197
Figure 5-11: The effects of XAD-4 treatment on HBsAg VLP recovery and remaining lipid levels.	197
Figure 5-12: The effects of CUNO Zeta Plus [®] Delipid filtration on HBsAg VLP recovery and remaining lipid levels.	198
Figure 5-13: Screening of lipid removal performance.	199
Figure 5-14: Revised process flow chart for HBsAg VLP purification.	204
Figure 6-1: Chromatograph column with two guard columns.	218

Lists of Tables

Table 1-1: Chromatography resin properties and their implications.	24
Table 1-2: Common foulants in the feed stream and possible source.....	44
Table 1-3: Foulants and commonly used cleaning agents.	57
Table 3-1: Lipid compositions in the conventional feed, low lipid feed, <i>Saccharomyces cerevisiae</i> cells and <i>S.C.</i> lipid particles	100
Table 3-2: Lipid mass balance for conventional and low lipid feed in the first HIC cycle	102
Table 4-1: Control experiments performed for CLSM.	130
Table 4-2: Control experiment performed for cross-talks of Bodipy [®] 493/503.	131
Table 4-3: Control experiment performed for cross-talks of Nile red.	131
Table 4-4: Control experiment performed for cross-talks of BSA-Alexa [®] 555.	131
Table 4-5: Estimated values of Q_{\max} and K_d using Langmuir isotherm model.....	133
Table 4-6: The amounts of material in the adsorbed and free state at the end of the two-hour batch uptake.....	138
Table 4-7: Percentage of beads displaying dual-peak phenomenon	167
Table 5-1: LRA lipid removal capacity.	183
Table 5-2: HIC performance from the four selected feed streams.....	201

Table of Symbols and Abbreviations

Symbols

C_M	Solute concentration in mobile phase (mM)
C_S	Solute concentration in stationary phase (mM)
D_p	Pore diffusion coefficient (cm^2/s)
D_s	Surface diffusion coefficient (cm^2/s)
Ex_{\max}	Excitation maximum (nm)
Ex_{\max}	Emission maximum (nm)
$h\nu_{EM}$	Photon emission energy (joule)
$h\nu_{EX}$	Photon excitation energy (joule)
I_{corr}	Corrected fluorescence intensity (arb. unit)
I_{em}	Emission fluorescence intensity (arb. unit)
I_{pv}	Volumetric intensity (arb. unit)
I_{shell}	Intensity of shell (arb. unit)
K	Henry constant of adsorption ($\text{Pa}\cdot\text{m}^3/\text{mol}$)
k	Rate constant (per bar \cdot pass)
k'	Retention factor
K_D	Distribution coefficient (mL/g)
K_d	Equilibrium dissociation constant (mg/mL)
N	Number of passes
\emptyset	Phase ratio (arb. unit)
P	P value
Q_{\max}	Maximum adsorption capacity (mg/mL of resin)
Q_{rel}	Relative capacity (intensity/ μm^3)
R	Bead radius (μm)
R	Amount of protein released (mg)
r_a	Outer radii of a pixel within the cross-section of the particle (μm)
r_i	Inner radii of a pixel within the cross-section of the particle (μm)
R_m	Maximum amount of protein available for release (mg)

R_S	Resolution/Resolution factor (arb. unit)
S_0	Ground state
S_1	Relaxed singlet excited state
S_1'	Excited electronic singlet state
V_M	Volume of mobile phase (mL)
V_R	Retention volume (mL)
V_S	Volume of stationary phase (mL)
W_b	Base width (cm)
W_M	Amount of solute mobile phase (mg)
W_S	Amount of solute in stationary phase (mg)
x	x-axis
z	z-axis
α	Selectivity factor (arb. unit)
α (exponent)	Resistance to disruption from the cells (arb. unit)
ϵ_{resin}	Extinction coefficient of resin (cm^{-1})
ρ_k	Particle density (Kg/cm^3)

Abbreviation

$^{\circ}\text{C}$	Degree Celsius
μL	Microlitres
μm	Micrometers
AC	Affinity chromatography
AIDS	Acquired immune deficiency syndrome
Au	Arbiter units
BCA	Bicinchoninic acid assay
BSA	Bovine serum albumin
CCD	Charge coupled device
cGMP	Current good manufacturing practice
CIP	Clean-in-place
CLSM	Confocal scanning laser microscopy

cm	Centemeters
CMC	Critical micellar concentration
CV	Column volume
D/P	Dye to protein ratio
DCW	Dry cell weight
DNA	Deoxyribose nucleic acid
DNases	Deoxyribonuclease
DOT	Dissolved oxygen tension
EBA	Expanded bed adsorption
ELISA	Enzyme linked immunosorbent assay
ELSD	Evaporative Light Scattering Detector
ER	Endoplasmic reticulum
FF	Fast flow
FRET	Fluorescence resonance energy transfer
g	Grams
Gal	Galactose
GLU	Glucose
GSK	GlaxoSmithKline
h	Hours
HBsAg	Hepatitis B virus surface antigen
HBV	Hepatitis B virus
HCP	Host cell proteins
HDL	High-density lipoprotein
HIC	Hydrophobic interaction chromatography
HPLC	High-performance liquid chromatography
HPV	Human papillomavirus
IEX	Ion exchange chromatography
IgG	Immunoglobulin G
kbp	Kilobasepairs
kDa	Kilodaltons
L	Litres
LAS	Leica Application Suite
LRA	Lipid removal agent
M	Molar
mAB	Monoclonal antibody

MDa	Megadaltons
mg	Milligram
min	Minutes
mL	Millilitres
mm	Millimetres
mM	Millimolars
Mr	Relative molecular weight
N.A	Not available
N.D.	Not determined
NHS	National Health Services
nm	Nanometers
OD	Optical densities
PDI	Protein disulphide isomerase
PSD	Pore size distribution
RAC	Reducing agent-compatible
RNA	Ribose nucleic acid
rpm	Rotation per minute
S.C	Saccharomyces cerevisiae
SEC	Size exclusion chromatography
SEM	Scanning electron microscopy
TFA	Trifluoroacetic acid
UV	Ultraviolet
v/v	Volume by volume
VLP	Virus-like particles
w/w	Weight by weight

Chapter 1

Introduction

This chapter introduces the project and discusses the fundamentals and challenges in process chromatography. The relevance of fouling studying is addressed by examining the various deleterious effects it has on chromatography performance. The novel confocal and electron microscopic investigation platform is introduced. In addition, a literature review on the history, biology and downstream processing of VLPs in general and specifically the HBsAg particle were also presented.

1.1 Chromatography

1.1.1 Principles

Chromatography is used to develop and manufacture biopharmaceuticals and must follow stringent quality and safety requirements. Since the rise of biological medicines, it has become the core operation about which the downstream processing is centred due to the unparalleled resolution it is capable of achieving. Chromatography separations are based on the difference in interaction between targets and impurities with a chromatographic resin, and this important property of the resin is generally referred to as selectivity (Hagel et al., 2007). For example, in elution chromatography for a given resin, conditions that favour interactions with the targets but not with the impurities are adapted. When the feed stream that passes through the column under such conditions, chromatography resin retains the target solutes more strongly than the impurities. The condition is then reversed during elution allowing for desorption of the targets. Resolution of chromatographic separation is determined by two factors, selectivity and dispersion. The higher the selectivity of a resin, the higher the discriminating power it possesses, hence the larger the difference between target and impurity retentions. Dispersion, resulting from operating conditions and physical properties of the resin, however, causes zone-broadening leading to a less defined boundary between the peaks at the base level. Therefore, the resolution (R_S), calculated from the retention volumes (V_R) and average base widths (W_b) of two peaks, is favored by high selectivity and low dispersion (Equation 1-1).

$$R_s = \frac{2(V_{R_2} - V_{R_1})}{W_{b_2} + W_{b_1}} \quad (1-1)$$

Selectivity factor (α), the quantitative measure of selectivity, for two solutes under the same operating conditions can be expressed by their relative retention factors (Equation 1-2). Retention factor (k') is defined as the ratio of amount of the solute in the stationary phase (W_S) to that in the mobile phase (W_M). Thus, retention factor can be expressed as a product of distribution coefficient (K_D) and phase ratio (\emptyset), where K_D is the fraction of solute concentration in the stationary phase (C_S) over that in the mobile phase (C_M) and \emptyset is the volume of the stationary phase (V_S) with respect to the volume of the mobile phase (V_M) (Equation 1-3).

$$\alpha = \frac{k'_2}{k'_1} \quad (1-2)$$

$$k' = \frac{W_S}{W_M} = \frac{C_S \cdot V_S}{C_M \cdot V_M} = K_D \emptyset \quad (1-3)$$

In essence, K_D captures the thermodynamic elements and \emptyset reflects the structural ones in retention of a solute to stationary phase. In most cases, the impact of selectivity, and hence retention, on resolution is far more significant than dispersion. Consequently, efforts have been put into providing a greater understanding of the

underlying principle of retention in chromatography, and this remains an active research area for process optimisation to date.

1.1.2 Performance parameters

In process chromatography design, the utmost important objective is high productivity, contributed from high purity, high recovery and high capacity and given as

$$\text{Productivity} = \frac{\text{amount of purified product}}{\text{column volume} \times \text{time}} = \frac{\text{capacity} \times \text{recovery} \times \text{purity}}{\text{time}}$$

High purity requires a high-selectivity chromatography resin that can give a high resolution between the product and closely eluting impurities. In practice, a resolution factor of 1.5 would yield a complete separation of peaks. The recovery, however, is dependent on the resolution attained and the requirement for purity. In some cases, products are irreversibly lost on the chromatography resin or degraded, leading to a lowered recovery, even though the purity and the capacity are high. High purity requirement will generally lead to low recovery, this adversity improves with resolution factor though. For example, with a resolution factor (R_S) of 0.5, 98% purity requirement for a sample containing 10% impurities will give a recovery of just 86%, whereas the same purity requirement will give an almost complete recovery with a resolution factor of 1.5. Similarly, material may be lost at very high loadings, and

symmetrical peaks are typically only found at column loads up to 30% of the maximum capacity (Yamamoto et al., 1988).

Thus, optimisation is essential to establish the fine balance between these interlinked performance parameters in order to achieve the highest productivity. Important factors to consider may include resin properties, operating techniques, running conditions and feed stream impurities.

1.1.3 Resins

Table 1-1: Chromatography resin properties and their implications (Hagel et al., 2007).

Resin property	Implication
Mechanical properties	Throughput, potential scale of manufacturing, maximum operating velocity
Ligand density and distribution	Binding capacity, selectivity, recovery
Pore size and pore size distribution	Dynamic-binding capacity
Particle size and particle size distribution	Resolution, product purity, removal of impurities, dynamic capacity
Chemical stability	Lifespan, sanitisability and reusability
Hydrophilicity/hydrophobicity	Product recovery, cleanability

Resins are the essence of chromatography. They are made from the polymerisation of various materials, such as polystyrene with divinylbenzene, methacrylate, latexes, dextrans and agarose. These materials, either as they are or

further modified through the addition of functional groups, function as the stationary support in different type of chromatographic separations. Resin properties (Table 1-1) can be highly customised to accommodate the requirements of a particular purification process, and its design is mainly driven by process factors including speed of separation, quantity, product purity and cost.

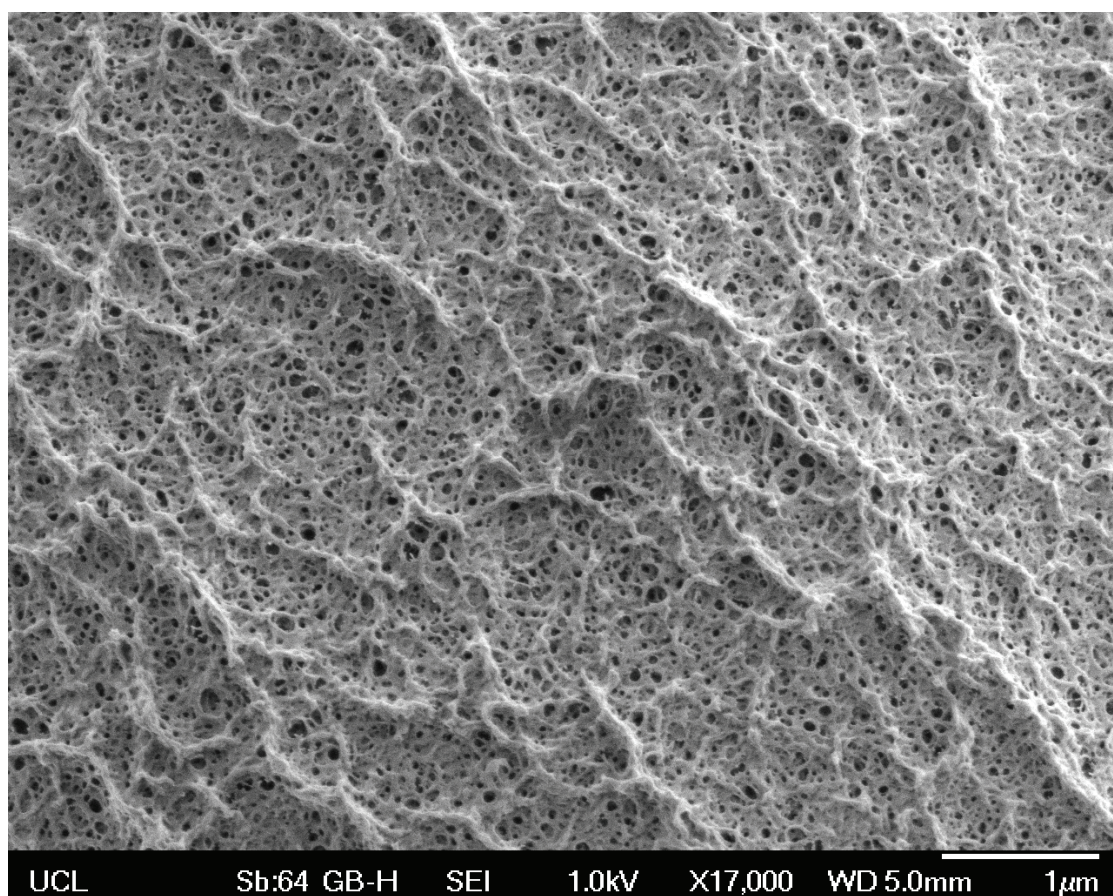


Figure 1-1: Structure of fresh Sepharose[®] Butyl-S 6 Fast Flow resin. (Image produced by scanning electron microscope at X17,000 magnification)

Pressure can build up during a chromatography run, where the resin is compressed because of the combined influence of flow rate, feed stream viscosity and

scale of the column (Joseph et al., 2007). Therefore, if the speed of separation is critical, a more rigid resin with a higher degree of cross-linking between the polymers should be used. In adsorption chromatography, capacity is an important parameter in process design for sizing chromatography system according to demands. While static binding capacity is determined by the ligand type and density, the more process-relevant dynamic binding capacity is further limited by porosity of the resin. Equally important are the product recovery and resin reusability, influenced by chemical properties of the functional group, spacer and resin backbone.

Sepharose[®] (GE Healthcare, Buckinghamshire, UK) is one of the most widely used commercial resins, in which hydrophilic chains of agarose with different degrees of intra-chain cross-linking (Figure 1-1) provide a range of rigid and macroporous base supports, such as 6% agarose highly cross linked in 6 Fast Flow (FF) and 4% in 4 FF. A large selection of functional ligands is available to cater for the specific selectivity requirements. For example, ligands in hydrophobic interaction chromatography (HIC) resins often consist of straight alkyl chains (butyl, octyl, ether, isopropyl), which show a pure hydrophobic character, and aryl group (phenyl), which shows a mixed-mode behaviour of both aromatic and hydrophobic interactions (GE Healthcare, 2010). While the type of ligand is important, the degree of substitution is also determinative to the overall selectivity, thus a selection of high and low substitution resins is also available. Functional ligands are covalently attached to the spacer arms on the beads typically via either an oxygen or a sulphur connector atom. The spacer arm varies in length, for example 13 atom-length in Sepharose[®] 6 FF and 4 atom-length in Sepharose[®] 4 FF, severing to improve accessibility of the ligands.

Figure 1-2 summarises the structures of common HIC ligands and spacer arm in Sepharose[®] 6 FF.

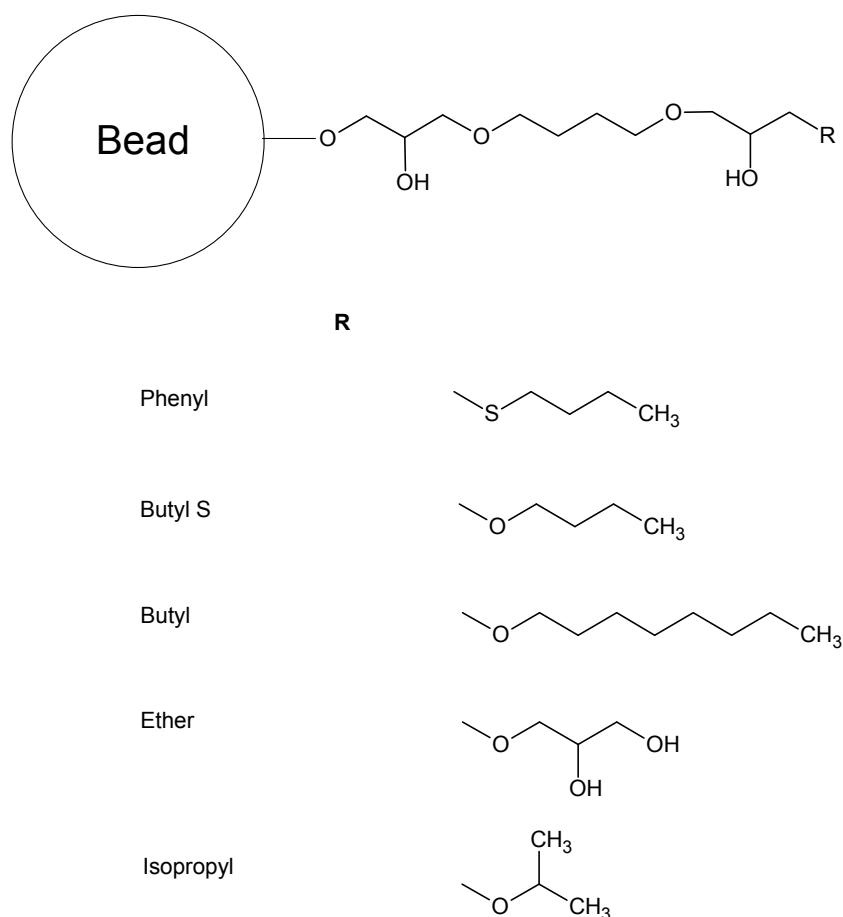


Figure 1-2: General structure of Sepharose[®] 6 Fast Flow (spacer arm) and ligands substituted on HIC resin (GE Healthcare, 2010).

It is, however, important to realise that products can be lost on a very hydrophobic resin due to irreversible binding, hence a reduced product yield. Furthermore, hydrophobic interactions often make cleaning of chromatography resins more difficult. The effectiveness of clean-in-place (CIP) through the use of harsh

cleaning and sanitising agents is of great importance to process economics, as it extends column life and minimises the need to unpack, clean and repack columns.

1.1.4 Techniques

In process chromatography, various techniques are available, covering most aspects of biologics purification. Size exclusion chromatography (SEC), also known as gel filtration, separates through the difference in size and shape between solutes. Small solutes are able to access to larger pore volume in SEC, resulting in a longer travelling distance, hence leaving the column later as opposed to large solutes. It is the only non-adsorptive based chromatography, hence a gentle separation. Ion exchange chromatography (IEX) utilises a resin with either positive (anion-exchange) or negative (cation-exchange) charge groups attached via a spacer arm. Solutes with opposite surface charge are attracted to the resin in a low ionic buffer environment. Elution is accomplished through adding competing ions to the mobile phase. Hydrophobic interaction chromatography (HIC) exploits the hydrophobic effect, where nonpolar solutes are expelled from polar mobile phase to the hydrophobic surface of the resin so that hydrogen bonds can be reformed and the most energetically favoured state can be reached. The adsorption takes place in high-ionic strength mobile phase, which promotes interaction between the solutes and the resin, whereas elution is carried out by decreasing the ionic strength of the mobile phase making the bound solute solvable again in the polar mobile phase. In affinity chromatography (AC), separation is generated from biospecific or group-specific interaction between ligands and solutes. Due to the high selectivity, a high degree of purification can be achieved in a single AC step. In most cases, desorption is carried out by varying the

pH to change the conformation, or alter the surface charge of the solutes or the ligands. However, affinity resins are expensive to produce and generally have short lifespan. Due to the biological nature of the ligands, their activity can gradually decrease through usage, CIP and storage. In addition, sophisticated pretreatments of the feed stream for reducing foulants, such as lipids, are often required to maintain reproducibility of the process. These factors limit the use of AC in large-scale purification to only high-value products, such as antibodies and hormones.

1.1.5 Hydrophobic Interaction Chromatography

HIC is an established and powerful technique that is often used as an orthogonal separation mechanism in combination with other purification techniques, such as IEX. In addition, the hydrophobic interaction phenomenon (the underlying mechanism of HIC) also influences the efficiency of separation and column reusability in other chromatography techniques. However, due to the lack of attention it receives in contrast to the more widely used IEX and AC, HIC is currently limited in the number of applications it finds use, and interactions between many process variables and the observed phenomenon are less well understood. Therefore, a greater understanding of HIC will not only contribute to the realisation of its full potential as a separation technique, but also, often of greater importance, lay down the necessary foundations for process optimisations in the overall chromatography purification scheme, such as improving recovery and reducing fouling.

Retention in HIC is contributed directly from the physical structure of the resin and thermodynamic factors (Equation 1-3). Phase ratio of a solute with a given size is

determined by pore size distribution (PSD), which is a principal property of the resin. Interpretation of the distribution coefficient and thermodynamic retention mechanism, however, is rather complicated and under constant debate. Solvophobic theory (Katti et al., 1987; Melander and Horváth, 1977; Melander et al., 1984; Melander et al., 1989; Szepeszy and Horváth, 1988) and preferential interaction theory (Arakawa, 1986; Arakawa and Timasheff, 1982; Perkins et al., 1997; Timasheff, 1993; Timasheff and Arakawa, 1988; Wu et al., 1986) are most commonly used to relate experimental observations in HIC. According to solvophobic theory, hydrophobic interaction is driven by the unfavourable energy needed for solvation of the hydrophobic solutes in the polar solvent. Thus, the solutes are believed to be forced out of the mobile phase into forming an interaction with the hydrophobic ligand at high ionic strength, rather than actively pulled out of the mobile phase by the ligand, such as the case in IEX (Hagel et al., 2007). Similarly, in the preferential interaction theory, retention is thought to be driven by the release of water molecules from solutes upon adsorption to the resin. Hence, in both theories, retention is linked to free energy of the system and increases with temperature, solute surface area and surface tension resulted from the chemical nature and concentration of the salt in the mobile phase. However, extensive experimental data suggest that a wide range of factors influence retention in HIC, including salt (Oscarsson, 1995a; Rippel and Szepeszy, 1994; Schmuck et al., 1986), ligand type (Benedek, 1988; Berna et al., 1998; Fausnaugh et al., 1984; Gao and Dubin, 1999; Lin et al., 2001; Lina et al., 2000; Schmuck et al., 1986), ligand density (Kato et al., 2002; Wu et al., 1986), pH (Fausnaugh et al., 1984; Fausnaugh and Regnier, 1986; Geng et al., 1990; Heinitz et al., 1988; Schmuck et al., 1986; Wu et al., 1986) and temperature (Benedek, 1988; Chen et al., 2003; Geng et al., 1990; Goheen

and Engelhorn, 1984; Wu et al., 1986). Therefore, both solvophobic theory and preferential interaction theory are insufficient to account for the retention mechanism in HIC and to yield a process optimisation from a combination of these factors in a predictable way.

In addition, it has been shown that proteins undergo conformational changes when they are adsorbed to a hydrophobic surface (Corradini et al., 1994; Oscarsson, 1995b; Tibbs Jones and Fernandez, 2003; Wu et al., 1986; Zoungrana et al., 1997), where the protein unfolds and exposes its internal hydrophobic domains to the resin surface. This complicating factor extends the dependence of retention on protein properties from the simple surface hydrophobicity predication to include additional elements such as heat capacity, a measure of protein stability (Lenhoff and To, 2007; Ueberbacher et al., 2010). More significantly for protein, high degree of unfolding and prolong exposure in such unfolded state can result in the loss of activity and its irreversible binding to the resin as often seen in the case of low recovery and fouling.

In order that such separations are viable in a manufacturing context, it is necessary to maintain product yield and limit fouling over multiple cycles. The fact that hydrophobic materials are often also the most challenging foulants to be removed from chromatography columns in general emphasises the importance of understanding retention mechanisms in HIC, as it will benefit not just HIC, but also the understanding of fouling in all chromatography techniques. Despite recent advances in models to include many of the HIC retention factors, these models are mostly based on retention data obtained from simple one or two component systems. In reality, however, a large number of interacting species exist in the feed stream, and it is still currently not possible to model a process from first principles in such complexity.

Therefore, it is of great importance to study the impact that a real process feed stream has on HIC performance, and to pinpoint the underlying mechanism of retention as well as fouling using novel microscopic techniques, such as confocal scanning laser microscopy (CSLM).

In the HBsAg VLP process examined by Belew et al. (1991), HIC using Butyl-S Sepharose[®] 6 Fast Flow was employed as a primary capture step, thus exploiting the strong hydrophobicity of the VLP. However, due to the hydrophobic nature of lipids, which are co-released with HBsAg VLP in the pretreatment processes, this subsequent HIC step will be particularly susceptible to lipid fouling. Therefore, this provides a realistic industrial scenario for studying foulant interactions in HIC.

1.2 Virus-like particle (VLP)

1.2.1 VLP advantages

Virus-like particles (VLPs) were first isolated and characterised from blood samples of hepatitis B patients (Bayer et al., 1968). As empty 22-nm particles solely composed of the small hepatitis B virus (HBV) surface antigen (HBsAg), they are thought to be mass produced and released from infected cells to trigger host immune responses from the infectious viral offspring (Ludwig and Wagner, 2007). Subsequently, it was used as vaccine against the cognate virus infection (Blumberg et al., 1985).

VLPs are recombinant viral structural proteins that self assemble into particles, typically 25 – 100 nm in size, in a highly repetitive and ordered manner (Noad and Roy, 2003). Being structurally similar, VLPs are antigenically indistinguishable from their parental viruses (Jennings and Bachmann, 2008). Traditional vaccines, which are mostly in the form of soluble viral subunit proteins and inactivated or attenuated viruses, often suffer from weak immunogenicity, instability and risks of viral reversion, recombination or re-assortment (Noad and Roy, 2003).

VLPs offer several clear advantages. They lack viral genetic material that renders them unable to cause infection, hence greater safety (Buckland, 2005). Benefiting from the large number of the same antigen orderly presented on the surface of the particle, they are effective in triggering a rapid and potent humoral and cellular immune response even at low dosage levels. This is further enhanced by its particulate nature and dimensions, resulting in favourable uptake by dendritic cells that are crucial in activating innate and adaptive immune responses (Grgacic and Anderson, 2006). The versatile antigen-displaying platform of a VLP can accommodate a diverse range of foreign molecules via either genetic fusion or surface attachment. Through genetic engineering, VLP chimeras are formed by inserting the gene encoding the foreign epitope into regions of the native gene encoding the polypeptide of the VLP that will be most exposed upon assembly following expression. However, the size and structure of the foreign epitope is limited by the folding constraint of VLP subunit, hence the need for the more robust and flexible modular approach in order to preserve the epitope native conformation. The VLP and foreign epitope are individually produced, both of which are engineered with the addition of reactive groups for covalent attachment or tags for non-covalent attachment. The target epitopes are

subsequently coupled to the surface of VLP *in vitro*. It was shown that more than 150 direct surface attachments can be successfully induced using a single VLP carrier, with epitope size ranging from 6.6 to 63 kDa (Jennings and Bachmann, 2008). Structural stability and tolerance towards manipulation to carry and display heterologous molecules have rapidly established VLP as the platform of paramount importance for the development of new generation vaccines (Ludwig and Wagner, 2007).

1.2.2 VLP applications

To date, several VLP-based vaccines have been successfully developed against some of the world's most common and serious infectious diseases. Recombivax HB[®] from Merck and Co. (1984) and Engerix B[®] from GlaxoSmithKline (GSK) (1988) are licensed as preventive vaccines against hepatitis B virus, which currently has 350 million carriers and causes 1 million deaths each year. Both vaccines are safe and potent, with responder rates above 90% and a long lasting effect for over a decade. They are one of the highest revenue generating vaccines in the world today (Coates et al., 2001; Jennings and Bachmann, 2008). More recently, VLP vaccines against human papillomavirus (HPV) gained market authorisations in most major countries. HPV infection is responsible for the development of nearly all cases of cervical cancer (Walboomers et al., 1999), which has a more than 50% fatality rate and are currently affecting half of million people worldwide (Shikary et al., 2009). Among the 13-15 HPV types identified for causing cervical cancer, type 16 and 18 account for more than 70% of the cases. Gardasil[®] from Merck and Co., containing the recombinant major capsid (L1) proteins of type 6, 11, 16 and 18, was shown close to 100%

effective in trial subjects against infections and cancers caused by those HPV types (Garland et al., 2007). Similarly, Cervarix[®] from GSK, targeting HPV type 16 and 18, also reported strong results from its clinical trial (Paavonen et al., 2007). Since its first approval in 2007, more than 9 million doses have been distributed worldwide in total, and in the UK it was chosen for the National Health services (NHS) HPV vaccination programme with more than 1.4 million doses have been given so far.

Another key disease area for VLP vaccine developments is seasonal epidemics and global pandemics, such as influenza. High mutation rate of the viral surface proteins and genetic shift of influenza viruses from animal to human make the developments of conventional flu vaccine, often in the form of inactivated virions or purified viral proteins, gruelling and require periodic re-evaluations to boost the falling effectiveness. In addition, the current egg-based manufacturing strategy is slow and cannot fulfil the global demand during a pandemic. Owing to its unique and efficient antigen display platform aided by structural stability and potentials for large-scale production in recombinant system, VLP has the promise to address the difficulties in influenza vaccine supply. Clinical trials of several VLP vaccine candidates are currently underway, including the 2009 H1N1 pandemic VLP vaccine and a trivalent seasonal influenza VLP vaccine migrating from the commercially available trivalent inactivated vaccine format.

Furthermore, in addition to combating infectious diseases, the developments of VLP-based therapeutic vaccines for treating chronic diseases are gaining significant momentum. These include cardio vascular and respiratory diseases, diabetes, obesity and cancer, which represent the majority of disease burden in global healthcare (Jennings and Bachmann, 2008).

1.2.3 VLP manufacturing process

VLP vaccines were originally isolated from the blood of the infected donors, such as hepatitis B vaccine HEPTAVAX B[®] (licensed in 1981, Merck), which then go through a vigorous purification process to achieve the required purity. However, the labour intensity of process, which on average take more than a year to manufacture a single batch, and the growing public concern of over AIDS contamination in the already limited supply of human plasma led to the developments of the recombinant VLP product. As mentioned previously, one of the major advantages of VLP is its suitability for large-scale production through recombinant hosts. Although mammalian cells produce authentic virus, the high cost associated with their large-scale culture leads to other eukaryotic systems typically being utilised for VLP production. For example, HPV vaccine Cervarix[®] is synthesized in insect cells. However, a significant portion of the current commercial VLP vaccines are produced from recombinant yeast *Saccharomyces cerevisiae*, including Recombivax HB[®], Engerix B[®] and Gardasil[®]. Yeast is one of the most studied and the best understood organisms at both molecular and genetic levels. It has been well developed into various heterologous expression systems (Hitzeman et al., 1983). The use of yeast fermentations to produce biological products is industrially significant, as they offer the benefits of ease of genetic manipulation, eukaryotic glycosylation, rapid growth, and less stringent requirements for growth as compared to mammalian cells, and hence lower costs (Buckholz and Gleeson, 1991).

In spite of the superiority over traditional vaccines and the versatility for potential therapeutic applications in various fields, the number of licensed VLP

products on the market remains low, mainly due to its complicated and inefficient manufacturing process. The beneficial recombinant nature of VLPs does however require the use of sophisticated downstream processing to achieve a high purity through the elimination of all the host contaminants, while maintaining structural and compositional consistency of the product in order to satisfy regulatory requirements. Furthermore, for future therapeutic VLPs to become successful, an efficient and scalable downstream process is needed to replace the current process, which was originally designed for vaccine supply decades ago and typically in small scale. For example, the current process of commercial VLP products, such as Recombivax HB[®] and Engerix B[®], often deploys density gradient ultracentrifugation for harvesting VLP from the crude lysate. Although a powerful separation tool by itself, it is limited by the size and not scalable. Together these present significant challenges in the VLP process developments (Buckland, 2005). To achieve lower costs in VLP manufacturing and rapid delivery to the market, bioprocess manufacturing research is as critical as the product development itself (Pattenden et al., 2005). As discussed previously, it is the focus of this project to study various means of improving the bioprocessing of VLPs to complement the development of a new generation of novel VLP vaccines in the pipeline.

1.2.4 Hepatitis B virus surface antigen (HBsAg)

HBsAg was the first recombinant VLP vaccine approved for human use (Hilleman, 2001; Hilleman, 2003; McAleer et al., 1984; Valenzuela et al., 1982). It was produced in yeast *Saccharomyces cerevisiae* as a 22 nm lipoprotein particle with highly hydrophobic lipid-rich core, formed through self-assembly of approximately

100 hepatitis B surface antigen protein monomer of P24 (24 kDa) and its glycosylated form GP27 (27 kDa) (Figure 1-3) (Aggerbeck and Peterson, 1985; Ganem and Prince, 2004; Peterson, 1987). Studies have shown that the yeast-derived HBsAg particle has a M_r of 3.5×10^6 composed of 75% protein, 90% of which are P24 and GP27, and 25% host-derived lipid (Dreesman et al., 1972; Gavilanes et al., 1982a). The lipid-protein interactions play a vital role in maintaining the proper helical structure of the HBsAg proteins, hence the antigenicity and immunogenicity of the HBsAg VLP (Gavilanes et al., 1990).

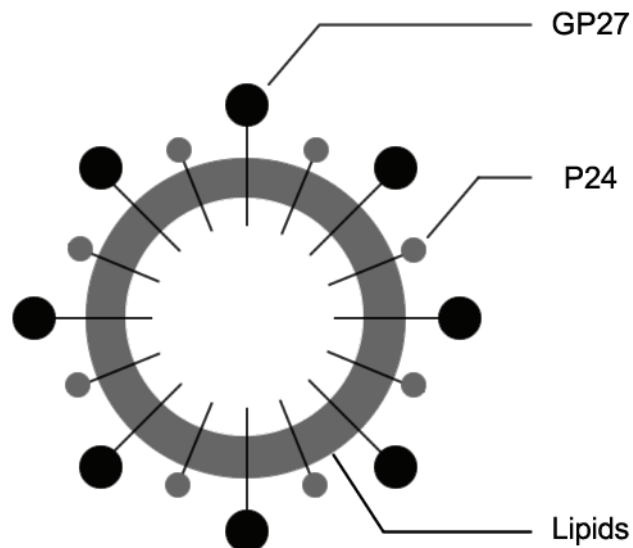


Figure 1-3: Diagrammatic representation of hepatitis B virus surface antigen.

Intra and intermolecular disulphide bonds contribute significantly to overall conformational stability and immunogenicity of HBsAg VLP. The 14 cysteine residues contained in each of the HBsAg monomer provide numerous opportunities for disulphide bond formation (Wampler et al., 1985). In both yeast and humans, the

HBsAg assembly process occurs in the endoplasmic reticulum (ER) membrane, where the disulphide-linked HBsAg protein dimers are rapidly formed in the presence of high levels of protein disulphide isomerase (PDI). However, in humans, these dimers are then translocated through a pre-Golgi compartment, where HBsAg dimers form higher oligomers and assemble into mature VLP particles via extensive disulphide bonds in the absence of PDI and are subsequently secreted (Huovila et al., 1992). Whereas in yeast, the lack of protein transport machinery results in the HBsAg particles being permanently budded into the ER and are held together mainly by noncovalent interactions (Biemans et al., 1992). Upon released from the ER, HBsAg subunits start to be partially disulphide-linked, and this continues throughout the entire purification process. This maturation of the VLP is completed by the addition of ammonium or potassium thiocyanate and storage at elevated temperatures at the end (Zhao et al., 2006).

The typical downstream process for HBsAg is shown in Figure 1-4 (Kee et al., 2008). Yeast cells harvested from fermentation are concentrated and washed with buffer to remove media components and antifoam by microfiltration. After a centrifugation step, cell pellet is suspended in a buffer containing phenylmethylsulfonyl fluoride, a protease inhibitor, which prevents the degradation of the HBsAg. This is followed by a high-pressure homogenisation step to rupture the cells and release the intracellular HBsAg. Non-ionic surfactant, usually Triton X-100, is then added to the homogenate for liberating the HBsAg from tightly associated ER membrane components (Wampler et al., 1985). Cell debris and unbroken cells can be removed by centrifugation (Wampler et al., 1985) or microfiltration (Dekleva, 2002). An optional ultrafiltration step through 100-kDa hollow fibre filter can be introduced

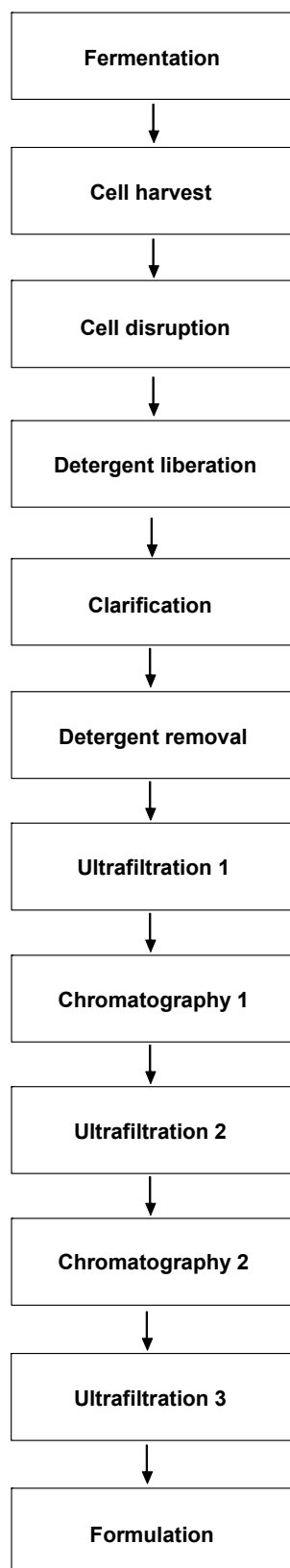


Figure 1-4: Process flow chart of VLP purification (Kee et al., 2008).

to clear small molecular weight contaminants and for product concentration. Residual detergent is then removed by recirculation through polystyrene XAD-4 beads. The capture step is currently performed by gradient centrifugation in the commercial HBsAg products, although chromatography-based operations have been proposed and remains an active research area for process improvements. Both fumed silica, Aerosil, (Dekleva, 2002; Wampler et al., 1985) and hydrophobic Butyl-S Sepharose resin (Belew et al., 1991) have all been reported as adsorption medium for HBsAg VLP, whereas in the final polishing step, hydrophobic interaction (Dekleva, 2002) or gel filtration chromatography are utilised (Belew et al., 1991). Finally, to ensure the maturation of the HBsAg VLP through disulphide bond formation, the purified particles are treated with ammonium or potassium thiocyanate and incubated at 37 °C prior to formulation (Zhao et al., 2006). The product is finally adjuvanted by co-precipitation with aluminium hydroxide (Dekleva, 2002).

At the start of this multistage purification process, the homogenisation and detergent mediated liberation steps usually cause a high level of the intracellular contents such as host lipids to enter the process stream. This can be particularly problematic in terms of the deleterious effects on the performance of the downstream processing steps that follow, such as chromatography (Bracewell et al., 2008). This is further complicated by the fact that HBsAg VLP matures through the purification, which makes it the ideal case where the process of producing the vaccine itself often defines the end product (Buckland, 2005). Unexpected changes in the microenvironment during the process, for example those as result of fouling, can often have a substantial impact on the quality of the product. From a manufacturing perspective, this places a significant burden on process economics, where stringent

regulatory requirement of the purification specification consistency necessitate the frequent replacement of the expensive industrial chromatographic media.

1.3 Fouling in Chromatography

In generally, the manufacturing process for a biopharmaceuticals consists of upstream cell culture, downstream separation and formulation. The separation step is typically divided into two distinct operations: recovery and purification.

Recovery steps usually include product isolation and feed stream clarification, which aims to provide a certain level of purification and are mostly carried out through operations such as cell disruption, centrifugation, filtration, expanded bed adsorption (EBA) and precipitation. The sequence of operations that are deployed will be based on product localisation at the end of fermentation. For example, when product is secreted, only host cell removal, by either centrifugation or filtration, is usually required after harvest. In contrast, for intracellular product, cells needs to be first retained and then ruptured in order to release the product into the process stream and the resulting cell debris is removed prior to next operation (Balasundaram et al., 2009). However, this is sometimes further complicated by the fact that intracellular products are often associated with cellular components that cell disruption alone cannot dissociate, hence an additional liberation step, such as a detergent step, is

required. Consequently, such routes inevitably introduce a higher level of the intracellular contents into the feed stream, and these additional contaminants will adversely affect the performance of the downstream processing steps that follow, such as chromatography. One can argue that the efficiency, hence the economics, of downstream process is directly dictated by its upstream design, of which factors includes product characteristics, choice of expression system, host cellular content and machineries for product secretion.

The subsequent purification steps are designed to remove process and product related impurities, while maintaining structural and functional characteristics of the product. The ability to handle vastly different conditions and an enormous variety of complex and sensitive biological mixtures makes chromatography the dominant force in this purification stage. In the last 20 years, thanks to the maturation in chromatography, the number of chromatography steps in a process has reduced on average from four to three, typically including capture, purification and polishing steps. Today, some companies even push this boundary by presenting processes with just two chromatography steps. Obviously, the major benefit of this reduction in the number of steps is the cost saving on both production overhead and capital investment in chromatography equipments and resins, which could still run up to more than 50% of the total downstream cost (Hagel et al., 2007; Peskin and Rudge, 1992). Hence, there is continuous demand for current chromatography operations to be able to cope with higher level of impurities and last longer. As a result, the ability to counter the deleterious effect from process materials on column performance, generally referred to as fouling, becomes a fundamental challenge in process chromatography.

1.3.1 Type of foulants

From a process design point of view, the difficulty in combating fouling lies in the complexity of the feed stream in modern biopharmaceutical manufacturing. Determined by both the fermentation and pretreatment steps, a large number of impurities exist in the feed stream. Among these, many have the potential to cause fouling in chromatography. Table 1-2 lists common foulants in the feed stream arriving at the capture step chromatography. By their interaction with the column, these materials can be broadly classified into two groups: chemical foulant and physical foulant. For example, lipids or proteins are most likely to interact with the

Table 1-2: Common foulants in the feed stream and possible source.

Foulant	Possible source
Host cell	Fermentation
Host cell debris	Fermentation / Cell disruption
Protein precipitate	High salt conditions
Carbohydrates	Cell disruption
Host cell proteins (HCPs)	Cell disruption
Additives	Fermentation media / detergent step
Lipids	Cell disruption / detergent step
Antifoam	Fermentation media
Nucleic acids	Cell disruption
Endotoxins	Cell disruption
Metal ions	Fermentation media
Salts	Fermentation media

column chemically either via hydrophobic interactions or electrostatic forces, while cell debris particulates will physically affect the hydrodynamics within the column. Thus, it can be considered that chemical fouling is more concerning with foulant-column interaction at a micro-level, while physical fouling is on a macro-level.

1.3.1.1 Proteins

Protein is the most important class of biological macromolecules. They are among the most abundant and have essential roles in virtually every process within the cells. Their versatility in fulfilling a wide range of biological functions makes them the prime target for biopharmaceutical developments. Traditionally, proteins are harvested from natural sources, such as human plasma. However, the limited supply and high risk of lethal impurities gear protein production towards using recombinant systems. To date, recombinant protein products, such as recombinant insulin and antibodies, have dominated the licensed biologics market.

Structural properties are crucial to protein functionalities. Proteins are composed of polypeptide chains, the amino acids sequence of which is called the primary structure. Through intra-molecular hydrogen bonds, these polypeptide chains can be arranged into energetically favourable secondary structures such as alpha helix and beta strands. According to their localisation, proteins are further arranged into a stable conformation through reducing surface energy. For instance, in the case of cytosolic proteins, hydrophobic domains are buried inside the core of the molecule in order to increase protein solubility, whereas in transmembrane proteins, hydrophobic domains are exposed on the surface to allow its association with the hydrophobic

membrane. This compact three-dimensional structure is generally referred to as tertiary structure, which is stabilised by intra-molecular disulphide bonds. As a result, protein surface properties vary significantly in terms of not only physical dimensions, but also hydrophobicity and polarity, the latter of which is highly dynamic to changes in pH. This uniqueness provides the basis for protein separation in all commonly used chromatography techniques.

Due to the purity requirement in biopharmaceuticals, all the non-target protein impurities in the process stream need to be removed during the purification process. They are mostly host cell proteins (HCPs) either originated from cell breakage during fermentation or co-released with target protein in the cell disruption steps. As contaminant and foulant, proteins may affect chromatographic purification in two ways: competitive uptake with target product and modification of resin properties as result of irreversibly binding of the protein.

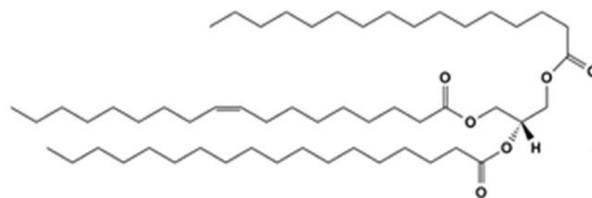
Linden et al. (1999), by using confocal laser scanning microscopy, showed a competitive binding phenomenon on the outer region of the cation exchange resin beads in a two-component system of IgG and bovine serum albumin (BSA) (used to represent a major contaminant in the feed stream during the purification of antibodies). IgG was less concentrated in this region as a result when comparing to the situation where BSA was not presented. Interestingly, BSA co-adsorbed uniformly with IgG on an affinity resin at equilibrium. That is to say, BSA as a foulant, although limited in amount, has higher retention factor due to favourable surface polarity on cation exchange resin than IgG, leading to an apparent reduced capacity for IgG. However, on affinity resin, the interactions between the immobilised protein A and IgG are specific, hence the interference from BSA is less profound.

Under conditions that favour strong interactions, proteins will tend to precipitate out from the mobile phase on to the resin. Prolong exposure under such conditions will often lead to losses of target protein activity and accumulation of protein foulant within the column. Unexpected results from previous studies (Dziennik et al., 2005; Harinarayan et al., 2006; Linden et al., 2002; Susanto et al., 2007) have demonstrated this phenomenon on both cation exchange and hydrophobic resins by showing the diffusion hindrance caused by protein accumulation under fast uptake. Therefore, it is possible that the target protein itself will potentially act as a foulant under certain operating conditions, which will significantly limit the column life. Although the exact mechanism of protein fouling in chromatography is still unclear, analogy may be drawn from the extensive work carried out on protein fouling in the membrane filtration industry (Belfort and Nagata, 1985; Marshall et al., 1993). Kelly and Zydney (1997) proposed that proteins in solution can bind to already-adsorbed protein deposit on an ultrafiltration membrane through intermolecular disulphide bond formation or hydrophobic interactions, giving rise to secondary fouling. The wider implication of these findings is that fouling can involve complex foulant-foulant interactions leading to secondary or even multi-layered adsorption.

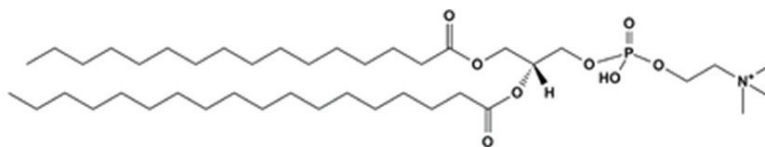
1.3.1.2 Lipids

Lipids are a broad group of chemically diverse compounds that serve important functional roles in areas such as energy reserve, biological membranes and cell signalling. The three major classes of biological lipids are glycerols, sterols and phospholipids (Figure 1-5).

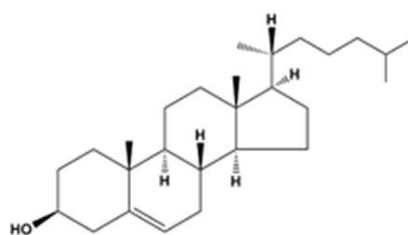
Triacylglycerols are formed from three molecules of fatty acid combined with a single molecule of glycerol. The fatty acid tails vary in length, but typically consist of 16-20 carbons. As a result, triacylglycerols are highly hydrophobic and are stored exclusively as cytoplasmic lipid droplets enclosed by a monolayer of phospholipids and hydrophobic proteins. In addition to serving as energy storage, triacylglycerols also provide structural fatty acids for biosynthesis of other essential lipid compounds.



triacylglycerols



phospholipid



cholesterol

Figure 1-5: Structures of triacylglycerols, cholesterol and phospholipids.

Phospholipids are the key building blocks of lipoprotein assemblies and biological membranes. They are amphipathic molecules containing a glycerol core linked to both hydrophobic fatty acid tails and a hydrophilic phosphate head group. As a result, they will self-aggregate into micelles or bilayer arrangements in a polar solvent via hydrophobic effects. Phospholipids form a bilayer by orienting its polar head groups towards the polar solvent on both cytosolic and extracellular sides while shielding the hydrophobic fatty acid tails internally, thus creating a barrier preventing polar solutes from diffusing across the membrane. Under certain conditions, a micelle is formed from a monolayer of phospholipids, such as in the case of lipoproteins, and it is usually of spherical shape and has a core containing highly hydrophobic neutral lipids, such as triacylglycerols and cholesterol esters. Because of its cylindrical shape, phosphatidylcholine is the key structural elements in biological membranes, often accounting for almost half of the total cellular phospholipid content. One of its two fatty acid tails contains an unsaturated acyl group, which gives a kink in the hydrocarbon chain providing the underlying fluidity on the membrane.

Sterols are a family of polycyclic compounds, among which cholesterol is the most abundant. Cholesterol is mainly located in membranes and functions to modulate the fluidity and permeability of the membranes by interacting with phospholipids and certain membrane proteins. As a neutral lipid, cholesterol associates with membrane mainly via van der Waals forces and hydrophobic interactions. Within membrane bilayer, cholesterol disrupts electrostatic interactions between the polar phospholipid head groups. Thus by minimising the disordered packing resulting from the kinked phospholipid acyl chain, cholesterol is able to reduce the fluidity of the membranes. In

addition, high cholesterol concentrations in membranes reduce their already limited passive permeability to polar solutes.

Due to the hydrophobic nature of lipids, host lipids are often the most challenging type of foulant in chromatography. Lipids interact with resin via their long hydrocarbon tails through hydrophobic interactions and have greater diffusivity and access to the internal areas of the resin beads thanks to their small sizes. Often great emphasis is placed on ensuring that lipids are removed through pretreatments prior to chromatography, as most standard cleaning-in-place (CIP) procedures are relative ineffective in dealing with fouled lipids. However, due to various product and process constraints, pretreatments rarely completely eliminate lipids in the feed stream. The amount of host lipids arriving at the chromatography, particularly the capture step, is still sufficient to have potential to cause significant fouling, particularly after multiple cycles.

As most lipids are either located in the biological membrane or enclosed within intracellular lipid particles, the majority of host lipid impurities are introduced into the feed stream by cell disruption step. A detergent liberation, a step often necessary for recovering membrane bound products, will further release lipid content into the feed stream from membrane debris following cell disruption.

Although lipids are a common problem in most purification processes, studies on the subject are scarce. Recently, Bracewell et al. (2008) reported that lipid fouling could have a major impact on the performance of chromatography by showing an improved protein product capacity in HIC from extensively centrifuge-clarified yeast homogenates. As previously, where analogy in chromatography is drawn from the membrane filtration fouling studies, lipid fouling from lipid-protein mixture caused a

significant increase in membrane hydrophobicity and a severe flux decline (Maartens et al., 1998). This is a strong indication that the lipid fouling in chromatography may be of similar complexity involving multiple foulant-foulant interactions affecting both chemical and physical properties of the resin.

1.3.1.3 Nucleic acids

Nucleic acids, the universal genetic information carrier, are single or double stranded linear polymers of nucleotides. Each nucleotide consists of a nitrogenous heterocyclic base, a pentose sugar and a phosphate group. Depending on the presence of a hydroxyl group in the sugar, nucleic acids can be classified as deoxyribose nucleic acid (DNA) or ribose nucleic acid (RNA). At pH above 4, the phosphate backbone of nucleic acids gives a strong overall negative charge to the molecule. Thus, anion exchange chromatography is routinely used to purify nucleic acids. Although the usage of HIC has been reported, operating conditions are limited to low pH and require a cationic agents to suppress ionisation of the phosphate groups.

It is however important to realise that most nucleic acids are in the form of macromolecules (typically 4-150 kbp) that are significantly larger than proteins. For example the size of a 5.7 kbp plasmid DNA is about 800 nm in open circular and 480 nm if supercoiled. As a result, they will not be able to enter the pores of conventional resins designed for proteins, and only the outer surface of the resin may be available for interaction (Siu et al., 2006b).

As foulants, nucleic acids may enter the feed stream following cell disruption from both cell cytoplasm and nucleus. They have the potentials to not only shield the

binding sites on the surface of the beads, but also give a rise in feed stream viscosity. High viscosity is often undesirable for chromatography, as it limits the operating velocity, i.e. the speed of separation. The use of high velocity with viscous feed streams will otherwise cause packed beds to be compressed and fail. Enzymatic digestion using nuclease, such as DNases, is sometimes adopted as a pretreatment to reduce nucleic acid size and hence the viscosity of the feed stream. However, the relatively high cost of these enzymes for biopharmaceutical use makes it undesirable to scale up to industrial productions.

1.3.1.4 Particulates

Insoluble particulates in the feed stream generally consist of whole cells, cell debris and large aggregates from colloidal materials such as proteins and lipids. Cell debris, mostly fragments of cell walls are the major particulates. It typically originates from cell disruption operation or cell breakage by agitation shear generated during fermentation.

Most particulates will be removed during the pretreatment steps. However, in certain situations, where the speed of recovery is required, or fewer pretreatment operations are available due to capital investment constraints, feeds are clarified to a lesser extent and particulates may still be present at chromatography stages.

Apart from the obvious column blockage caused by accumulation of the particulates, leading to flow resistance and increased operating pressure, particulates will also chemically interfere with adsorption and sometimes act as an adsorbent to withhold protein product. As the cell wall normally associated with all

microorganisms contains a high level of mannoprotein, cell debris usually carries a net negative charge at neutral pH from the phosphate groups in the mannoproteins, which provides the basis for interactions with opposite charged chromatography resin and other materials such as target proteins. Studies have shown that anion exchange resin retained cells and cell debris much more strongly than any other resin (Feuser et al., 1999), and positively charged proteins could bind to cell debris from *Saccharomyces cerevisiae* (Shaeiwitz et al., 1989).

1.3.2 Fouling effects

Chromatography fouling is a direct result of the feed composition and the exposure time the column has experienced under such condition. The detrimental effect of fouling on operating efficiency, depending on the process and type of foulant, may include changes in column capacity and selectivity, mass transfer limitation, increased column pressure drop and loss of bed integrity.

Foulants can preferably bind to chromatography resin through their intrinsic chemical characteristics, such as polarity and hydrophobicity. Once bound, the active binding sites on the resin are shielded from the target solutes, hence a reduced apparent binding capacity is seen. If the irreversibly bound foulants cannot be removed during elution, column cleaning and regeneration steps, the loss in capacity will gradually worsen as the number of cycle increases. Furthermore, the bound foulants on the resin may act as new ligands hence changing the original selectivity of the resin. As a result, the resolution and yield of the process will be adversely affected. A number of industrially significant proteins and peptides have been shown to have

severely reduced static and dynamic binding capacities when culture medium is present due to competitive binding of foulants when compared to binding of the isolated proteins (Staby et al., 1998). However, few studies have been carried out to investigate the effects of foulant accumulation. Siu et al. (2006a) mimicked fouling in a real process by pre-incubating fresh resin with yeast homogenates and showed that breakthrough happened earlier with increased foulant contact time.

Mass transfer in chromatography is a complex multi-stage process. In order to predict and optimise the performance of chromatography separation, various mathematics models have been developed (Section 1.4.1). However, these models are based on data from idealised single or two-component systems. Not to mention, it was not until recently that real time bead-level uptake profiles of solutes could be monitored thanks to the utilisation of confocal laser scanning microscopy in chromatography research. Diffusion hindrance caused by protein accumulation in the resin pores has been observed, through the studies on the uptakes of pure proteins to IEX and HIC resins (Dziennik et al., 2005; Harinarayan et al., 2006; Linden et al., 2002; Susanto et al., 2007). Therefore, all these models fail to address the significant role that fouling plays in limiting mass transfer of the target solute in real processes, where foulants will not only irreversibly bind to the resin but also interact with various materials. For a more accurate model of mass transfer in chromatography, a greater understanding of the detailed fouling mechanism is required.

At the macroscopic level, the development of flow heterogeneity and increased pressure drop due to flow resistance may arise from physical properties of the foulants. Insoluble and colloidal particulates can clog up the frit and flow distributor in column header as well as disrupt the packed bed. The resulting flow channelling will cause

band broadening and insufficient contact time, greatly affecting the separation efficiency. Column pressure drop is determined from a group of factors including feed viscosity, flow velocity, bed porosity, bed height and bead size (Bird and Ross, 2002; Joseph et al., 2007). In cases of severe particulate fouling, deposits of particulates will reduce the porosity of the bed, leading to an increased pressure drop. As most commonly used resins are made of mechanically soft materials such as agarose, the pressure drop caused by fouling will increase the potential for resin compression. Excessive resin compression will shift the pressure-flow correlation to the non-linear region, resulting in flow instability (Mohammad et al., 1992; Soriano et al., 1997; Verhoff and Furjanic, 1983). Expanded bed adsorption (EBA) has been specifically developed to tackle the fouling problem of particulates, where the expansion in bed volume provides large spaces between the beads that allow debris to flow through (Mattiasson and Nandakumar, 2000). Feed is loaded upwards and the particulates flow out from the top while the product binds. Elution is then commenced once the bed is packed. However, EBA is still not readily deployed in most current downstream purification schemes.

1.3.3 CIP and validation

Column cleaning, defined as the removal of soil, debris and particulates from surfaces, is both a regulatory and economic requirement. The risk of carryover between cycles is one of the main concerns of the regulatory agencies in regard to chromatography. This is especially true for columns used early on in a downstream process, such as capture step chromatography. A range of materials, including both active and inactive form of the product, host cell proteins, nucleic acids, lipids

particles and processing additives, e.g. detergents, have the potential to remain in the column even after routine regeneration and re-equilibration steps. Thus, in order to control carryover, development of effective CIP protocol is essential. Hale et al. (1994) showed that without the use of caustic CIP, the cross-contamination level is significantly higher in a multi monoclonal antibody production over 85 cycles.

Cleaning routines should be performed to restore column performance when there is loss of capacity, resolution and recovery or increased backpressure. Typically, cleaning accounts for 20-30% of the total chromatography cycle and 60–80% of the total buffer consumption in the process. The economic benefits of an effective CIP routine are twofold: longer column life and reduced column maintenance cost.

Unlike pretreatments, where product recovery is the priority and care is required in handling product-containing feed, CIP is dedicated for post-operational foulant removals. Therefore, operating parameters can be tailored to specifically target the bound foulants and harsh conditions are often permissible. Parameters of CIP include type of cleaning reagents, concentration, volume, contact time, temperature, flow rate and frequency. Selection of cleaning agent is the most important in the design of cleaning process and will be dictated by effectiveness, compatibility, costs, disposal issues and experience. Foulants and commonly used cleaning agent pairs are listed in Table 1-3. Sodium hydroxide is the most widely used in all of the fouling situations except for lipids, where non-ionic detergents and organic solvents are often required. CIP with 0.5 M NaOH for 12-16 hours was sufficient in restoring column performance following extensive foulant challenges (Levison et al., 1995).

Table 1-3: Foulants and commonly used cleaning agents (Hagel et al., 2007).

Foulant	Cleaning agents
Soluble proteins	NaCl, low ionic strength buffer, water
Precipitated proteins	NaOH, HAc, NaCl, water
Hydrophobic proteins	NaOH
Lipids	Non-ionic detergents, ethanol, isopropanol, acetonitrile
Nucleic acids	NaOH, NaCl, DNase
Endotoxins	NaOH
Viruses	NaOH

However, it should be cautioned that overexposure of the resin to harsh clean agents will be more likely to cause harmful effects. For instance, hydrophobic resin butyl Sepharose tolerated caustic cleaning agents better than acidic ones, where functional deterioration was observed for even moderate contact time (Berggrund et al., 1994). Over the last decade, resin manufacturers have put considerable effort into making materials more resistant to cleaning agents, especially sodium hydroxide. Morrow et al. (2006) reported that while conventional Protein A resin loses binding capacity when treated with 0.1 M NaOH for 15 min, a new Protein A resin enhanced by replacing alkali-sensitive amino acid residues could maintain binding capacity up to 149 cycles with 0.1 M NaOH and 60 cycles even with 0.5 M NaOH.

Due to the complexity of foulant materials in real feed streams and the lack of detailed understanding of the fouling process, it would be extremely difficult to develop cleaning protocols by simply choosing compatible cleaning agents and a

suitable frequency without lengthy screening and validation studies. Certain feed characteristics, such as high lipid content, are particularly problematic, as conventional caustic CIP is relative ineffective. While detergents and organic solvents are often used in such case, the complete removal of the cleaning agents themselves from the column presents a formidable challenge. Further, organic solvent will significantly increase the viscosity of the solution. As a result, there is a realistic limit as to how high the concentration of the organic solvent can be used without causing resin compression, hence the limited effectiveness for columns severely fouled with lipids. Therefore, through better understanding of the fouling mechanism and identification of the key foulants, the screening and validation of cleaning protocols can be based on a great degree of process understanding.

1.4 Confocal and Electron Microscopy

1.4.1 The study of mass transfer in chromatography

The basis of using porous beads in chromatography is the mechanical rigidity under flow and the vast internal surfaces they provide for interaction in addition to those on the outer surface. However, this requires solutes to be transported into the beads from the mobile phase. Therefore, the separation power of chromatography, under a given set of experimental conditions, is a direct function of the rate of the mass transfer. Consequently, there have been extensive studies on the kinetics of mass transport in porous resin in attempt to improve efficiency. The general understanding

is that three phenomena govern the overall rate of the mass transfers in chromatography: the external film mass transfer resistance, the intra-particle pore diffusion, and the kinetics of adsorption-desorption (Guiochon et al., 2006; Ruthven, 1984).

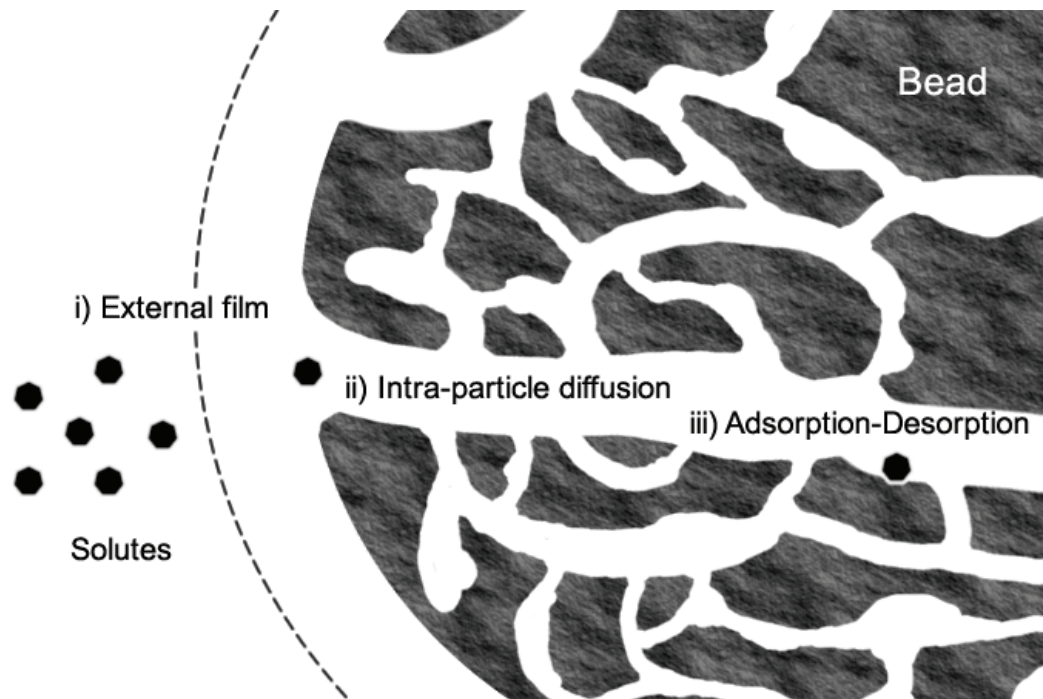


Figure 1-6: Schematic illustration of solute mass transport into a chromatography bead. The three steps that solutes need to overcome are i) external film; ii) the intra-particle pore diffusion and iii) adsorption-desorption.

Figure 1-6 illustrates this process in a simplified fashion. In adsorption, the solute must firstly traverse the laminar sub-layer surrounding the bead by molecular diffusion. The thickness of this layer, hence the mass transfer coefficient, is determined by hydrodynamic conditions, such as flow velocity. Having arrived at pore openings, solute must then travel into the resin via intra-particle diffusion, which is

composed of pore and surface diffusion. Finally, the solute can be adsorbed to the internal binding sites. In the desorption process, the steps are almost identical but in the opposite direction. In practice, as the kinetics of adsorption-desorption are relatively fast, the overall rate of mass transfer is predominately determined by the resistance from external film and intra-particle diffusion.

Although the effects of fouling in chromatography may vary, fundamentally it is the changes that fouling has on mass transfer that result in the deterioration of column performance. Therefore, the study of mass transfer of solutes under the influence of foulants is crucial in understanding the underlying fouling mechanism in chromatography. Mass transfer studies are traditionally limited to finite bath or frontal analysis where the amount of adsorbed solutes is measured indirectly by the depletion of solutes in the fluid phase. Interpretation of the dependencies and mathematical modelling can then be commenced (Arve and Liapis, 1987; Chang and Lenhoff, 1998; Johnston and Hearn, 1991; Lewus et al., 1998; Yoshida et al., 1994). However, it is apparent in contrast to common understanding that transition between pore and homogeneous diffusion models can occur at different conditions (Chang and Lenhoff, 1998) (This will be discussed in Chapter 4). Thus, either model alone is not sufficient to account for the actual mass transfer events within the beads. The experimental verification of the mode of transport and adsorption profiles is therefore an inevitable prerequisite for the understanding, modelling, and utilisation of the adsorption and transport phenomena (Hubbuck et al., 2003).

1.4.2 Confocal Microscopy in chromatography research

Confocal scanning laser microscopy (CSLM) has become an increasingly important tool in chromatography research, as a result of its ability to acquire fluorescent images from sections of thick specimen, such as beads.

The technique was first introduced by Marvin Minsky in 1958 (Minsky, 1961; Minsky, 1988). However, it was not until 1996, Ljunglöf and Hjorth (1996) published the first chromatography study deploying CLSM for the visualisation of intra-particle solute profiles. Since then, chromatography data generated by CLSM has flourished, and Hubbuch et al. has compiled a comprehensive list of publications on the analysis of intra-particle processes in chromatographic resins by CLSM (Hubbuch and Kula, 2008). The uptake profile study of lysozyme and hIgG onto SP Sepharose[®] FF and SP Sepharose[®] XL established the correlation between the detected fluorescence intensity within the bead and the traditional fluid phase measurements (Ljunglöf and Thömmes, 1998). Using two fluorescent dyes, Linden et al., (1999) first investigated the competitive behaviour in adsorption of a multi-component protein mixture. In a second publication, Linden introduced a multi dye approach, which in contrast to earlier studies allowed resolving the time-dependent movement of adsorbed protein within the bead during protein uptake (Linden et al., 2002). While all the above investigations were based on finite bath studies, Hubbuch et al. (2002) and Dziennik et al. (2003) pioneered the use of a miniaturised flow cell and thus mimicking uptake profiles in a packed bed chromatography.

1.4.3 Principles of CLSM

In contrast to a conventional light microscope, where the entire specimen is bathed in light, illumination in a confocal microscope is confined to a single, diffraction-limited, point by scanning one or more focused beams of laser across the specimen. An objective lens focuses the laser into the specimen. Reflected laser or emitted fluorescent beams from this single point are refocused by a second objective lens at a second pinhole, which has the same focus as the first pinhole, i.e. it is confocal with it (Figure 1-7). The second pinhole prevents beams from out-of-focus planes from reaching the detector. Thus, such system provides a non-invasive method to section the specimen allowing automated collection of the three-dimensional data in the form of Z-series. This ability of CLSM, generally referred to as optical sections, is the key to the confocal approach. In modern CLSM, rather than moving the specimen station, the imaging plane is driven by computer-controlled oscillating mirrors for faster scanning rates.

The synthesis of novel fluorescent probes continues to influence the development of confocal (Haugland et al., 2005). Fluorochromes have been introduced over the years with excitation and emission spectra more closely matched to the wavelengths delivered by the lasers supplied with most commercial CLSMs. Comprehensive reviews and protocols for fluorescent labelling can be found in Haugland et al. (2005) and Hermanson (2008) or are given by the respective manufacturers.

However, heterogeneity of the resulting target–dye conjugates has already been reported (Dismer and Hubbuch, 2007; Kasche et al., 2003; Teske et al., 2006; Teske et al., 2007). Therefore, control studies needs to be performed to evaluate the

suitability of the dye by examining the artefacts of labelling. Controls commonly include the monitoring of dye to protein ratio (D/P) during an uptake rate measurement in finite bath. If the ratio is constant, there is no preferable binding to either the labelled or the unlabelled species.

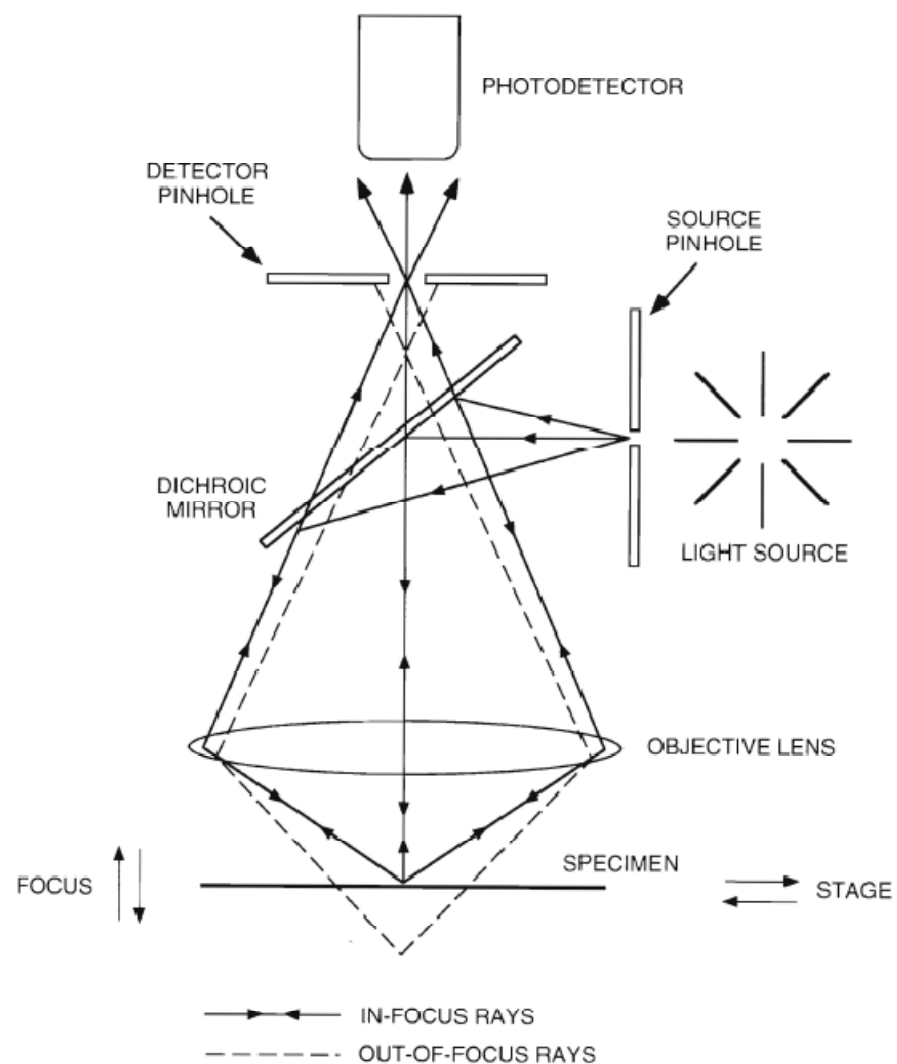


Figure 1-7: Light paths in a confocal scanning laser microscopy (Paddock, 1999).

Dealing with the variety of resin material is another major difficulty in the application of CLSM in chromatography research due to the light attenuation effects caused by material and structure of the respective resin (Dziennik et al., 2003; Kasche et al., 2003; Susanto et al., 2006; Susanto et al., 2007; Susanto et al., 2006). Since light is attenuated as a function of its three-dimensional coordinate within the bead, fluorescent intensity data needs to be corrected prior to any analysis concerning the true distribution of target–dye conjugates within the bead (Susanto et al., 2006). The complexity of the mathematical approaches to solve the attenuation problem seriously limits their applications (Heinemann et al., 2002; Margadant et al., 1996; Susanto et al., 2006; Susanto et al., 2007; Yang et al., 2006). A simplification of the model was introduced by Heinemann et al. (2002, 2004) and extended by Susanto et al. (2006). In their model, the conical light shape is generalised into one-dimensional light path, thus making the model calculation as well as the correction of the confocal scans simpler. The correction for light attenuation effects and thus conversion of the raw data has been shown to be an essential tool for the identification of heterogeneous protein distribution within the beads (Susanto et al., 2007; Susanto et al., 2006). Therefore, this methodology should be considered as routine in CLSM studies on chromatography.

1.4.4 Scanning electron microscopy (SEM)

The highest resolution achievable by CLSM is limited by the visible light wavelengths (about 0.5 μm). Thus, by using electrons with wavelengths much less than 0.1 nm, scanning electron microscope (SEM) is capable of producing high-resolution images of specimen surface morphology. The principle of a SEM is very

simple. An accelerated fine beam of electrons is scanned across the surface of the specimen and a detector monitors the intensity of a chosen secondary signal, namely secondary electrons or backscattered electrons, from the specimen. The intensity data are then translated into images on screen, where holes appear dark and hills have both a bright and a shadowed side, as shown in Figure 1-1.

Furthermore, it is possible to label target molecules in SEM through association of electron-rich elements, typically heavy metals, that is different from the one used in the sample coating. Osmium tetroxide has been used in staining cellular lipid components. As a strong oxidant, it cross-links lipids mainly by reacting with unsaturated carbon-carbon bonds (Kuo, 2007). Because osmium atoms are extremely electron dense, the detector can easily pick up the resulting high-energy secondary backscattered electrons, revealing the distribution of the lipids. Immunogold labelling is also widely used. Gold particles are electron dense, non-hazardous to biological samples and have a wide range of sizes (1 - 40 nm) for imaging at different magnifications (de Harven et al., 1984). Gold particles can be conjugated to either primary or secondary antibodies for targeting antigens and the protocols are identical to those in the standard immunolabeling applications.

The power of resolution, however, comes at a cost. In order to preserve the specimen from the high-energy electron radiation required by the magnification (typically 1 – 25 keV in SEM), sample preparation for SEM can often be elaborate and tedious, involving multiple fixing, rinsing, freeze drying and silver coating steps. Generally, it is not used in live imaging. Also the operational window of conditions is very narrow. For example, the specimen is often required to be stored in ethanol or water in order to prevent the artefacts from forming during sample preparation, such

as salt crystals (Hajibagheri, 1999). As a result, SEM images are often complementary to the quantitative images produced on other more versatile platforms, such as CLSM.

1.5 Research Aims

The goal of this project is to develop a mechanistic understanding of lipid fouling in process chromatography, more specifically through the investigation of a capture step hydrophobic interaction chromatography (HIC) in the yeast-derived HBsAg VLP process. Emphasis is placed on the systematic approach and the use of novel analytical techniques in order to achieve the following objectives:

1.5.1 Quantification of the deterioration in column performance from lipid fouling

Quantification of the fouling impact lipids have on column performance is essential in establishing the difficulty in dealing with feedstocks containing high levels of host lipids, such as those obtained from yeast fermentations. The identification of the major foulant species is a prerequisite for not only the investigation on the underlying fouling mechanism but also the subsequent process optimisation aiming to reduce its impact. For the comparative analysis, a control feedstock with lower level of lipid foulant is required to provide the basis for measuring the deterioration in column performance. In order to be more industrial

relevant, fouling studies are performed over multiple cycles. Thus, the immediate and long-term effects of lipid fouling can both be addressed.

1.5.2 Investigation of the lipid fouling mechanism

Lipid fouling in chromatography most likely originates from the deviations in both the adsorption and diffusion process. Although essential, traditional investigation tools, such as adsorption isotherms and batch uptake rates, do not reveal conclusive evidences on the mechanism of such complex phenomenon. For this reason, the recent development of microscopy applications, such as CLSM and SEM, in chromatography research may prove to be invaluable. By using these techniques, this study is able to investigate the intra-particle material uptake in the presence of lipid fouling and the resulting foulant build-up during the column life-time. Therefore, findings from this study can contribute to a better understanding of the fouling mechanism in process chromatography.

1.5.3 Investigation lipid removal strategies

Results from the preceding investigations are able to provide valuable insights for the design of an effective strategy in reducing lipid fouling. For a thorough investigation, options screened should therefore not be limited to the operating conditions in the current downstream process, but also dedicated lipid removal steps. By measuring the improvement on product capacity and robustness in column performance, the efficacy of each strategy in limiting both the short and long-term impacts of lipid fouling can be evaluated.

1.6 Organisation of this thesis

The first chapter introduces the project and discusses the fundamentals and challenges in process chromatography. The relevance of fouling studying is addressed by examining the various deleterious effects it has on chromatography performance. The novel confocal and electron microscopic investigation platform is introduced. In addition, a literature review on the history, biology and downstream processing of VLPs in general and specifically the HBsAg particle were also presented.

The second chapter provides a compilation of the materials, equipments and experimental methods employed in this study.

The third chapter reports on the comparative analysis of HIC performance deterioration (binding capacities and recoveries) under successive cycles of challenges from lipid-rich and lipid-depleted feedstocks. In addition, full mass balance on lipids is performed to identify the lipid class that has the highest fouling potential.

The fourth chapter first investigates the immediate effect of fouling by examining the material adsorption isotherms and batch uptake profiles, followed by the CLSM confirmation on the mode of intra-particle diffusion and adsorption. The investigation then proceeds onto the inspections on resin conditions at different stages during the column life-time, where high-resolution images of the fouled bead surfaces are also obtained using SEM. Finally, in-column spatial distribution and progression of lipid fouling are examined. From the results, potential lipid fouling mechanism is proposed.

The fifth chapter explores the pretreatment options for improving feed quality. Operating conditions in the current downstream process and dedicated lipid removal steps are examined. The efficacy of each strategy in limiting both the short and long-term impacts of lipid fouling is then verified by measuring the improvement on product capacity and robustness in HIC performance.

The sixth chapter summarises the findings from this study and concludes on the contributions of this thesis. Areas of focus for future work are also outlined here.

The final chapter contains the inventory of references accessed in this thesis.

Chapter 2

Materials and Methods

This chapter provides a compilation of the materials, equipments and experimental methods employed in this study.

2.1 Materials

2.1.1 Chemicals

All chemicals were purchased from Sigma-Aldrich (Dorset, UK) and were of analytical grade unless stated otherwise.

2.1.2 HBsAg VLP cell line

The recombinant *Saccharomyces cerevisiae* used to produce the hepatitis B surface antigen (HBsAg) VLP was donated by Merck & Co Inc (West Point, PA, USA). It contains a Leu⁺ gene insertion, thus allowing the use of a leucine-free selective media for fermentation. Additionally, expression of the HBsAg gene is controlled the GAL-10 operon, which is activated when the glucose is depleted and the utilisation of galactose starts.

2.2 Analytical

2.2.1 Optical density measurements

Optical densities (OD) of samples from fermentation were determined by measuring the absorbance at 600 nm on a BioMate3 spectrophotometer (Thermo

Spectronic, Rochester, NY, USA). Dilution was required for samples with OD values above 1 Au.

2.2.2 Dry cell weight measurements

Dry cell weight was measured by filtering a known volume of sample through a pre-weighed 0.7 µm glass microfibre Filter (Whatman, Maidstone, UK) and rinsed with de-ionised water. The filter was then dried at 100 °C in an oven overnight and re-weighed.

2.2.3 Glucose & galactose measurements

Sample glucose and galactose concentration were measured using a YSI bioanalyser[®] (YSI Life Sciences, Yellow Springs, Ohio, USA). Dilution was required for samples with glucose and galactose concentrations above the linear detection range (0-5 g/L).

2.2.4 Enzyme Linked ImmunoSorbent Assay (ELISA) for VLP

To quantify HBsAg, a HBsAg version 3 microplate-based sandwich ELISA kit from Abbott-Murex (Dartford, Germany) was used. The calibration curve was produced from HBsAg standard purchased from Serotec (Oxford, UK). Following the recommended protocol, samples were pre-diluted 512-fold in order to lie within the optimal detection range. Absorbance measurements were performed using a Tecan Safire[®] II microplate reader (Tecan, Reading, UK).

2.2.5 Lipid quantitation by HPLC

A Jordi Gel Glucose-DVB 500 A column (Grace, Lancashire, UK) was set-up for identification and quantification of lipids. It functions in a mixed mode of size exclusion and hydrophobic interaction chromatography, for which the mobile phase comprises of chloroform, methanol and 0.15% TFA (in water) in a ratio of 50: 43: 7. 70 μ L of sample was added to 970 μ L of extraction solution, which is made from the same mobile phase composition but without the aqueous portion. The mixture was then allowed to settle for 30 minutes and centrifuged to remove the precipitates. The sample injection volume was set to 50 μ L. The column was operated with a flow rate of 1 mL/min and thermal stabilised at 20°C. The chromatogram was recorded using an Evaporative Light Scattering Detector 3300 (ELSD) (Grace, Lancashire, UK) at 39.8°C, gas flow 1.4 L/min and gain of 1. The analysis was automated on an Agilent 1100 HPLC system (Agilent, Cheshire, UK). Calibrations were performed using standards of triacylglycerol, Triton X-100, ergosterol and phospholipids at various concentrations.

2.2.6 Protein quantitation

Protein levels were quantified using the Pierce BCA (bicinchoninic acid assay) assay RAC (reducing agent-compatible) version (Thermo Fisher Scientific, Leicestershire, UK). The RAC version of the assay provides accurate determinations of protein concentration in samples that contain high levels of detergents and lipids. Calibration curve was produced from bovine serum albumin (BSA) standard. Following the recommended protocol, samples were pre-diluted 8-fold in order to lie

within the optimal detection range. Absorbance measurements at 562 nm were performed using a Tecan Safire[®] II microplate reader (Tecan, Reading, UK).

2.2.7 Scanning electron microscopy (SEM)

The two-step sample preparation for SEM imaging consists of freeze drying and carbon coating. To prevent salt crystal formation during the freeze drying process, column was washed with 2 CV Millipore water for 5 times (flow rate 0.5 mL/min) at the end of the chromatography operation and conductivity in the eluents was monitored to ensure no salt was remaining. The resin was then pushed out as described in Section 2.2.8.3 and stored in Millipore water. A thin layer of the bead solution was then pipetted on to a coated glass slide, where the excess liquid was carefully adsorbed using a filter paper without contacting the beads. The glass slide was quickly immersed in liquid nitrogen, before the frozen samples were transferred onto a copper block. During the procedure, the copper block was constantly kept immersed in liquid nitrogen in a polystyrene container, thus preventing the condensation of moisture onto the sample. The copper block was thereafter transferred to an Edwards Modulyo vacuum pump (Edwards, Crawley, UK), where the drying process continued for 2 days before the temperature reached to room temperature steadily. The freeze-dried samples were then ion-sputtered to avoid the charge effect. This was achieved through coating with 2–3 nm carbon layer in a high resolution ion beam coater (Gatan Model 681, Oxford, UK) at an angle of 45°. Argon ion beam sputter was operated at 6 mA at an acceleration voltage of 10 keV. Coated surfaces were subsequently imaged with a JEOL JSM-7401F scanning electron microscope (JEOL Ltd., Tokyo, Japan) at 1 keV accelerating voltage.

In the case where osmium labelling was required, an additional staining step was incorporated before freeze drying. After a 30 minute incubation with the 2% osmium tetroxide solution, the bead sample was then washed with Millipore water for 3 three time prior to the freeze-drying process.

2.2.8 Confocal laser scanning microscopy (CLSM)

2.2.8.1 Description of equipment

The image acquisition was performed on an inverted confocal laser scanning microscope (Leica TCS SPEinv, Leica Microsystems GmbH, Mannheim, Germany) equipped with krypton/argon ($\lambda = 488 \text{ nm}$ and $\lambda = 568 \text{ nm}$) and helium/neon ($\lambda = 633 \text{ nm}$) lasers. Using a 40x oil immersion objective, the images (1024x1024) were captured (3 averages) through the Leica Application Suite (LAS) software (version 2.0) (Leica Microsystems GmbH, Mannheim, Germany). In order for the result to be comparable, all settings (laser intensity, emission detection range and signal gain) on the microscope were kept constant for each dye throughout the study.

For live imaging of the intra-particle material uptake within a packed bed, a miniaturised flow cell was fabricated according to the specifications used by Siu et al. (2006b) (Figure 2-1). Four horizontal channels (length: 10 mm, diameter: 1 mm) were drilled through a Pyrex block, with 45° inlets on both sides. A small viewing window was created by fixing a cover slip was on the face of the block with epoxy glue Araldite® (Huntsman Advanced Materials, Cambridge, UK) to seal the channel. The

resulting effective column volume was 0.066 mL (total length of 22 mm and a diameter of 1 mm).

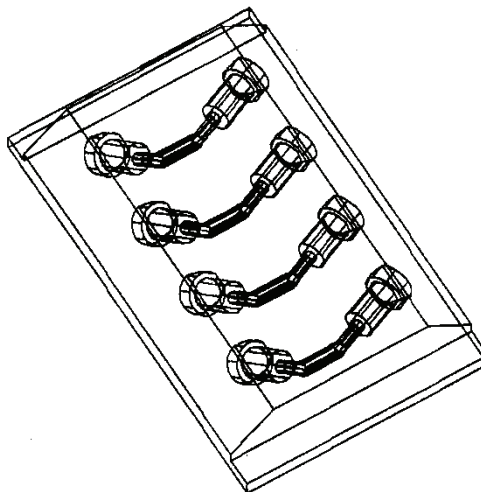


Figure 2-1: Flow cell used in CLSM live imaging. Each column has a volume of 0.066 mL (total length of 22 mm and a diameter of 1 mm).

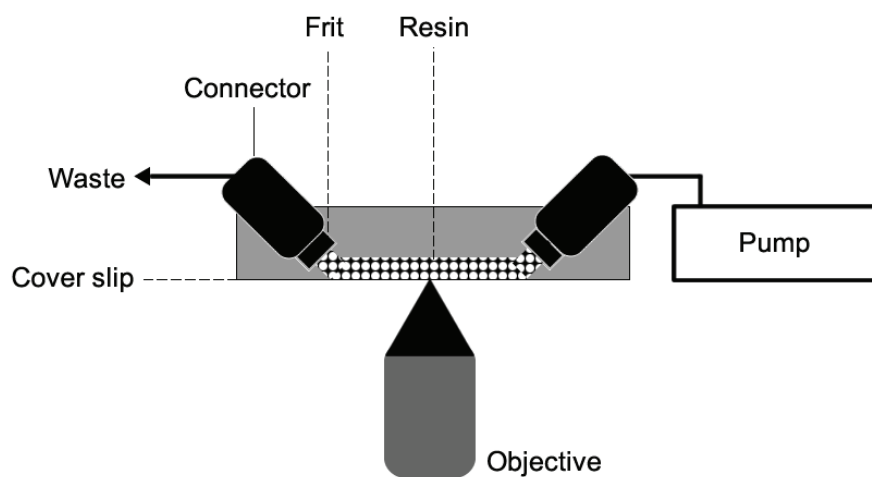


Figure 2-2: Flow cell setting within a confocal microscope.

By using a syringe and manually applying pressure, the resin was packed into each channel in the flow cell. Great care has to be taken to avoid over-pressurising the flow cell channel thus causing air bubbles or even rupture of the glass cover slip. Frits were placed at both sides of the channel, which was then connected to a P6000 pump (GE Healthcare, Buckinghamshire, UK). Washing was carried out with 0.5 mL of 0.2 mM phosphate buffer pH 7.0 at 200 cm/h before equilibrating with the corresponding mobile phase in each experiment. The setting of flow cell within the inverted confocal microscope is shown in Figure 2-2.

2.2.8.2 Fluorescent labelling

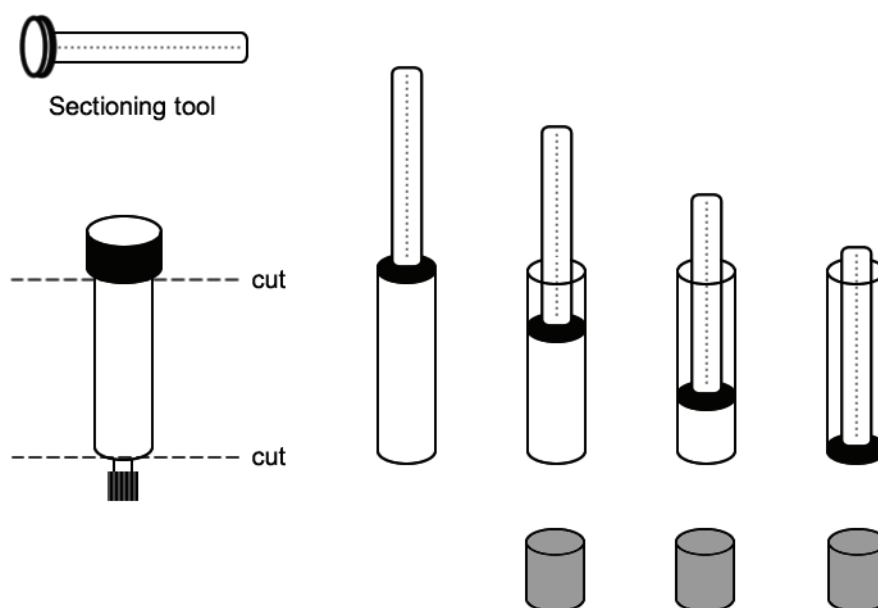
In order to specifically label the neutral lipids in the feed, lipophilic Bodipy[®] 493/503 ($E_{x_{max}}/E_{m_{max}}$: 493/503 nm) (Invitrogen, Paisley, UK) and Nile red ($E_{x_{max}}/E_{m_{max}}$: 552/636 nm) (Invitrogen, Paisley, UK) were used. 1 mL of 4 μ M dye solution was added to 100 mL of chromatography feedstock, giving a final ratio of approximately 8 μ M dye per gram of lipids. The mixture was incubated at 20°C overnight before use. Samples were protected from light by being wrapped in aluminium foil throughout the preparation.

2.2.8.3 Column sectioning tool

A simple tool (Figure 2-3) was designed to vertically section the matrix in a fouled 1 mL Hitrap[®] column. With 2 mm divisions, matrix can be pushed out and collected evenly across the length of the column, allowing offline microscopic examination of the bead conditions.



(a)



(b)

Figure 2-3: (a) Column sectioning tool. (b) Procedures of column sectioning.

2.3 Experiments in Chapter 3

2.3.1 Fermentation

4.2 litres of inoculum was prepared using a leucine-free liquid medium, containing (per litre): 8.5 g Difco yeast nitrogen base without amino acids and ammonium sulphate; 0.2 g adenine; 0.2 g uracil; 10 g succinic acid; 5 g ammonium sulphate; 80 g glucose; 0.25 g L-tyrosine; 0.1 g L-arginine; 0.3 g L-isoleucine; 0.05 g L-methionine; 0.2 g L-tryptophan; 0.05 g L-histidine; 0.2 g L-lysine and 0.3 g L-phenylalanine. This was adjusted to pH 5.5 with 4 M NaOH prior to sterilization in an autoclave. After growing on a rotary shaker (250 rpm) for 24 hours at 28°C, the inoculum was transferred to a 75L fermenter (Inceltech High Containment fermenter, Maidenhead, UK) with a working volume of 45L. The previous inoculum medium compositions were used again, but were now supplemented by (per litre) 40 g galactose and 0.3 mL LB-625 antifoam. This medium was then adjusted to pH 5.5 with 4 M NaOH prior to sterilization in an autoclave. The fermentation was operated at 28 °C for 72 hours, using a sparge rate of 45 L of air per minute and an impeller speed of 250 rpm. The fermenter was monitored by off-line glucose (YSI glucose analyzer, YSI Life Sciences, Ohio, USA), OD₆₀₀ and dry cell weight measurements as well as on-line mass spectrometry (Prima δB, Thermo Fisher Scientific Inc, Massachusetts, USA). The culture was harvested and centrifuged at 19118 g and a flow rate of 1 litre per minute using a tubular bowl centrifuge (CARR Powerfuge P6, Pneumatic Scale Corporation, Florida, USA). The cell paste was then stored at -80 °C.

2.3.2 Primary recovery

The process was adapted from the work of Kee et al. (2008) and is shown in Figure 2-4. Frozen cell paste was re-suspended in PBS at 25% (w/w), to which the protease inhibitor phenylmethylsulfonyl fluoride was added up to a final concentration of 2 mM. The suspension was then homogenised at 1200 bar for 3 passes (Gaulin Micron Lab 40, APV Gaulin GmbH, Lubeck, Germany). Triton X-100 was added in order to liberate VLP from endoplasmic reticulum membranes. Crude feed extract was diluted with an equal volume of 10 mM phosphate buffer containing 0.8% (v/v) Triton X-100 detergent, and incubated in a rotary shaker at 20 °C 150 rpm for 4 hours. Cell debris was then removed by centrifugation at 3000 g for 5 minutes (Beckman CS-6R centrifuge, Buckinghamshire, UK). To remove Triton X-100, 0.5 g of polystyrene beads XAD-4 per g of Triton X-100 was added to the supernatant obtained after centrifugation, incubated in a rotary shaker at 20 °C 150 rpm for 2 hours. This was followed by a two step filtration in order to remove XAD-4 and finally to clarify the feed. The first step used a single 1.0 µm glass microfibre filter (Whatman, Kent, UK), whilst the second step used a two-layer filter consisting of a 1.0µm filter on top of a 0.7 µm filter. The feed was adjusted to the chromatography starting buffer conditions of 0.6 M ammonium sulphate by dilution with concentrated ammonium sulphate stock (3 M).

2.3.3 Preparation of low lipid feedstock

In order to prepare a low lipid feed for comparative study, a modified (from Section 2.3.2) process (Kee et al., 2010) was used, including a reduced homogenisation pressure at 400 bar and two additional centrifugation steps. The first

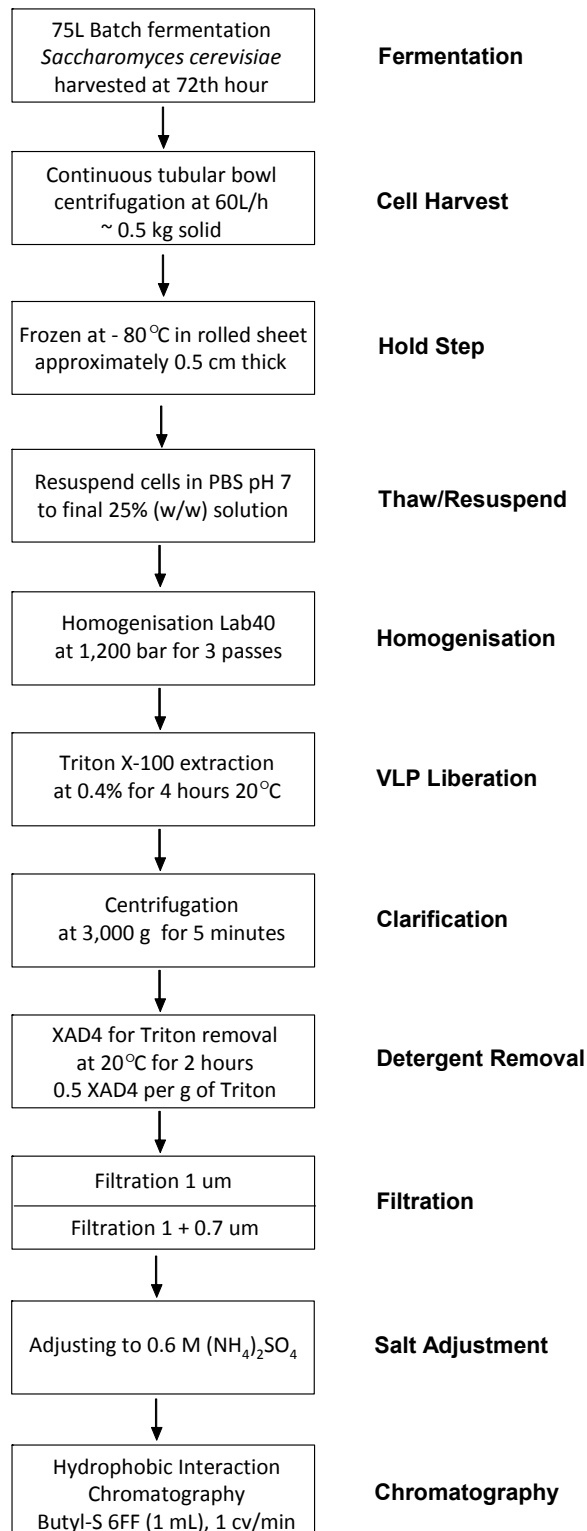


Figure 2-4: Process flow chart for HBsAg VLP purification.

centrifugation was carried out after homogenisation at 3000 g for 10 minutes to remove cytosolic contaminants, followed by re-suspension of the resulting pellet in Triton X-100 solution (0.4% v/v). The second centrifugation was after the salt adjustment step at 10000 g for 1 hour, where the supernatant was collected. It should be noted that in order to avoid the floating lipid layer 50 mL centrifuge tubes were used and supernatants were carefully taken up using disposable syringes without disrupting the lipid layer.

2.3.4 Hydrophobic interaction chromatography (HIC)

HIC was used as a capture step for the HBsAg VLP. The media was Butyl-S Sepharose[®] 6 Fast Flow from (GE Healthcare, Buckinghamshire, UK) in a 1 mL HiTrap[®] prepacked format. Following the recommended method Belew et al. (1991), the following buffer compositions were employed: Buffer A, 20 mM sodium phosphate, 0.6 M ammonia sulphate, pH 7.0; Buffer B, 10 mM sodium phosphate, pH 7.0; Buffer C, 30% isopropanol dissolved in Buffer B. The chromatography system used was an AKTA Explorer[®] controlled via Unicorn version 4.0 (GE Healthcare, Buckinghamshire, UK). The flow rate was set at 1 mL/min (156 cm/h).

The column was first equilibrated with 2 column volumes (CV) of Buffer A (0.6 M ammonium sulphate), followed by loading 2 CV of sample solution onto the column and then washing with Buffer A. The elution was carried out with 2 CV Buffer B (0.1 mM phosphate buffer) to desorb most of the bound fraction followed by 2 CV Buffer C (30% isopropanol) to desorb the most tightly bound material. The column was then regenerated with a further 2 CV of Buffer C followed by 3 CV of de-

ionized water, and finally equilibrated with 2 CV of Buffer A. After every 5 cycles, CIP using 2 CV of 0.5 M NaOH was performed to remove contaminants, which was followed by 3 CV of de-ionized water and finally the column was equilibrated with 2 CV of Buffer A.

2.4 Experiments in Chapter 4

For improved reliability and precision, liquid handling in all microplate-based experiments were carried out by Tecan Freedom EVO[®] robot equipped with a T-vac unit (Tecan, Reading, UK).

2.4.1 Adsorption isotherm measurements

A set amount of Sepharose[®] Butyl-S 6 Fast Flow resin was first allowed to settle by gravity. After measuring the settled volume, the resin was washed with ultra-pure Millipore water to remove the storage ethanol solution and equilibrated with either 0.6 M or 0.3 M (NH₄)₂SO₄ pH 7.0 buffer, giving a final concentration of 80% (v/v). 50 µL of this slurry was then aliquoted to each well in a 96-deep-well plate. Considering the void volume of a typical small packed bed with spherical particles (Brauer et al., 1971), the exact resin volume in each well was calculated to be approximately 25 µL. Up to seven different dilutions were prepared from the process feed labelled with Bodipy[®] 493/503. Each well was subsequently filled with 500 µL

of the feed solution and shaken at 1000 rpm 20 °C for either two or four hours on an Eppendorf Thermomixer[®] (Eppendorf, Cambridge, UK). The plates were shielded from lights during the process. At the end, 200 µL of the solution was transferred from each well to a MultiScreen_{HTS} filter plate (Millipore, Watford, UK) and vacuum-filtered to an opaque receiver plate. The filtrates were further diluted four times into UV-transparent receiver plates, where the material levels were then examined.

The levels of Bodipy[®] 493/503 labelled neutral lipids were measured at 550 nm emission wavelength after excitation at 488 nm, and they were then confirmed in the HPLC quantitation (Section 2.2.5). Protein concentrations were determined using the BCA method described in Section 2.2.6, and the levels of HBsAg VLP were quantified using ELISA.

2.4.2 Uptake rate measurements

Sepharose[®] Butyl-S 6 Fast Flow resin was prepared and aliquoted in a 96-deep-well plate as previously in the adsorption isotherm measurements (Section 2.4.1). 500 µL of the Bodipy[®] 493/503 labelled feed solution was added to every well in the plate. Immediately afterwards from each well in the first column on the plate, 200 µL of the solution was transferred to a MultiScreen_{HTS} filter plate (Millipore, Watford, UK) and vacuum-filtered to an opaque receiver plate. This procedure was repeated every five minutes at the next column of wells until the last column was reached. During the experiment, the 96-deep-well plate was constantly shaken at 1000 rpm 20 °C except for during solution transfers from the plate. The filtrates were further diluted four times into an UV-transparent receiver plate, where the levels of neutral

lipids, proteins and HBsAg VLP were then quantified as previously (Section 2.4.1).

The experiment was repeated with two other feed volumes: 200 μ L and 100 μ L.

2.4.3 Effect of salt concentrations on diffusion profile (flow cell)

A set amount of Sepharose[®] Butyl-S 6 Fast Flow resin was first allowed to settle by gravity. After measuring the volume of the resin, it was washed with ultra-pure Millipore water to give final 80% (v/v) resin slurry. By using a syringe and manually applying pressure, the slurry was then packed into three channels in the flow cell. Once packed, each channel was then equilibrated with 3 mL of one of the three perspective running buffers (0.6 M, 0.3 M (NH₄)₂SO₄ buffer pH 7.0 and 20 mM phosphate buffer pH 7.0) at a flow rate of 400 cm/h. Bodipy[®] 493/503 labelled feed solutions were adjusted to the required salt concentrations and pH in the running buffers and loaded onto the equilibrated beds at a flow rate of 200 cm/h. Confocal images were recorded at set time intervals for each channel with excitation at 488 nm and emission detection in range 520 - 550 nm.

2.4.4 Effect of lipid fouling on protein diffusion (flow cell)

BSA-Alexa[®] 555 conjugate (Invitrogen, Paisley, UK) was re-suspended in unlabelled BSA solution at a ratio of 1:20 to a final BSA concentration of 2 mg/mL, which is similar to the protein concentration in the process feed. Same amount of BSA-Alexa[®] 555 conjugate were also added to the Bodipy[®] 493/503 labelled feed. Both solutions were then adjusted to 0.6 M (NH₄)₂SO₄ pH 7.0 prior to loading.

Two channels in the flow cell were packed with Sepharose[®] Butyl-S 6 Fast Flow resin and equilibrated with 3 mL of 0.6 M (NH₄)₂SO₄ buffer pH 7.0. At a flow rate of 200 cm/h, the BSA solution was loaded to the first channel in the flow cell. Krypton/argon 568 nm laser was used to excite the Alexa[®] 555 fluorophore, while the emission detection range was set at 600 - 650 nm. Confocal images were recorded at set time intervals. For the second channel, the BSA-containing process feed mixture was loaded at the same flow rate. At predetermined time intervals, the two dyes were imaged in succession: the flow cell channel was first excited at 488 nm and the image was recorded in emission detection range 520 - 550 nm, which is seamlessly followed by excitation at 568 nm and the imaging in emission detection range 600 - 650 nm.

2.4.5 Lipid displacement (flow cell)

To show the displacement of the adsorbed lipids by the new incoming lipids, process feed was labelled with Bodipy[®] 493/503 and Nile red (Invitrogen, Paisley, UK) individually. A single channel in the flow cell was packed with Sepharose[®] Butyl-S 6 Fast Flow resin and equilibrated with 3 mL of 0.6 M (NH₄)₂SO₄ pH 7.0 buffer at a flow rate of 400 cm/h. The Nile red labelled feed was first loaded to the channel at a flow rate of 200 cm/h for 10 minutes. It was then switched to the Bodipy[®] 493/503 labelled feed, and the loading continued for another 10 minutes. At predetermined time intervals throughout the 20 minute period, image recordings in both emission detection ranges of 503 - 500 nm and 600 - 650 nm were carried out in succession with 488 nm and 568 nm excitation respectively.

2.4.6 Lipid foulant distribution within the column

Process feed was labelled with Bodipy[®] 493/503 and adjusted to 0.6 M (NH₄)₂SO₄ pH 7.0. The feed solution was incubated at 25 °C, shielded from light and kept agitated during the experiment. Butyl-S Sepharose[®] 6 Fast Flow in a 1 mL HiTrap[®] prepacked format was used (GE Healthcare, Buckinghamshire, UK). Following the method described in Section 2.3.4, the columns were operated for various numbers of cycles (1, 10 and 40 cycles). Similarly, the columns were also protected from lights during the process. At the end of each operation, resin in the column was pushed out in three equal portions (top, middle and bottom) using a column sectioning tool (Section 2.2.8.3). Attempting to divide the column into more sections would not have been feasible due to the small size of the column. Each portion of the resin was then re-suspended in ultra-pure Millipore water and immediately imaged under CLSM. No less than 100 qualified beads, with a size between 90 – 110 µm, were imaged for each portion. The same bead samples were also examined under SEM (Section 2.2.7).

2.4.7 Progression of lipid fouling within the column

In order to visualise the progression of lipid fouling within the column, process feed was labelled with Bodipy[®] 493/503 and Nile red (Invitrogen, Paisley, UK) individually, and adjusted to 0.6 M (NH₄)₂SO₄ pH 7.0. The feed solution was incubated at 25 °C, shielded from light and kept agitated during the experiment. Butyl-S Sepharose[®] 6 Fast Flow in a 1 mL HiTrap[®] prepacked format was used. The Bodipy[®] 493/503 labelled feed was used for the first 10 cycles of operation, after

which the operation commenced with the Nile red labelled feed for the next 10 cycles. At the end, the resin in the column was pushed out, sectioned and imaged under CLSM as previously (Section 2.4.6).

2.5 Experiments in Chapter 5

2.5.1 Homogenisation pressure and centrifugation

Homogenisation were carried out at four different pressures (100, 400, 800 and 1200 bar) at 3 passes with an undisrupted control sample following the primary recover process described in Section 2.3.2. An additional centrifugation step, reported to be beneficial in lipid removal (Kee et al., 2010), was also included as an option. Both homogenates and the re-suspended sediments from centrifugation were then diluted with an equal volume of 10 mM phosphate buffer containing 0.8% (v/v) Triton X-100 detergent, and incubated in a rotary shaker at 20 °C 150 rpm for 4 hours. Cell debris was then removed by centrifugation at 3000 g for 5 minutes (Beckman CS-6R centrifuge, Buckinghamshire, UK). 0.5 g of polystyrene beads XAD-4 per g of Triton X-100 was added to the supernatant obtained after centrifugation, incubated in a rotary shaker at 20 °C 150 rpm for 2 hours. This was followed by a two step filtration in order to remove XAD-4 and finally to clarify the feed. The first step used a single 1.0 µm glass microfibre filter (Whatman, Kent, UK), whilst the second step used a two-layer filter consisting of a 1.0 µm filter on top of a 0.7 µm filter.

2.5.2 Triton X-100 concentrations

Triton X-100 concentrations were screened in the range between 0.1% and 7% (v/v). Prior to the detergent step, samples were prepared by following the primary recover process described in Section 2.3.2. The feedstocks were incubated with Triton X-100 at 8 different concentrations within the range in a rotary shaker at 20 °C 150 rpm for 4 hours. Cell debris was then removed by centrifugation at 3000 g for 5 minutes (Beckman CS-6R centrifuge, Buckinghamshire, UK). Corresponding XAD-4 (0.5 g of polystyrene beads XAD-4 per g of Triton X-100) amount steps were then added to the supernatant obtained after centrifugation and incubated in a rotary shaker at 20 °C 150 rpm for 2 hours. This was followed by a two step filtration in order to remove XAD-4 and finally to clarify the feed. The first step used a single 1.0 µm glass microfibre filter (Whatman, Kent, UK), whilst the second step used a two-layer filter consisting of a 1.0 µm filter on top of a 0.7 µm filter.

2.5.3 Additional lipid removal steps

The options examined included ammonium sulphate precipitation, LRA (Lipid Removal Agent) treatment, XAD-4 treatment and CUNO Zeta Plus[®] Delipid filtration. The starting feed material was the pre-HIC feed, prepared from the primary recover process described in Section 2.3.2.

In ammonium sulphate precipitation, saturations up to 35% were screened. 10 mL of the process feed was adjusted to each of the required (NH₄)₂SO₄ concentrations by mixing with small volume of the (NH₄)₂SO₄ stock while keeping the overall volume constant for all samples. After brief mixing, the samples were incubated at 20

°C for 30 minutes. Centrifugation was then carried out at 3000 g for 30 minutes. At the end, the supernatant was filtered by a single 1.0 µm glass microfibre filter (Whatman, Kent, UK) to remove the floating material layer and subsequently analysed for HBsAg VLP and lipid level. Similarly, LRA (Advance Minerals Corp, California, USA) was added to 10 mL of the starting feed at concentrations up to 80 mg/mL. Mixing, incubation, centrifugation and filtration were all carried out as previously. The resulting filtrates were analysed for HBsAg VLP and lipid level. This same protocol was again used in the XAD-4 screening, where the starting feed was treated with XAD-4 concentrations up to 500 mg/mL.

CUNO Zeta Plus[®] BC25 capsule filters (Cuno 3M, Bracknell, UK) were used as an alternative method of lipid removal strategy. Three flow rates (6.5mL/min, 20mL/min and 65mL/min) were screened on an AKTA Cross-flow[®] system controlled via Unicorn version 4.0 (GE Healthcare, Buckinghamshire, UK). The filters were first rinsed with Millipore water in order to stabilise the pressure, and this was followed by the filter flux tests at the corresponding flow rate. After equilibration with 200 mL of 0.6 M ammonium sulphate pH 7.0, 120 mL of the feed was allowed to pass through filter. A new filter was used at each flow rate. The filtrates were collected and subsequently analysed for its HBsAg VLP and lipid level.

Chapter 3

Quantification of the deterioration in column performance from lipid fouling

This chapter reports on the comparative analysis of HIC performance deterioration under successive cycles of challenges from lipid-rich and lipid-depleted feedstocks. In addition, full mass balance on lipids is performed to identify the lipid class that has the highest fouling potential.

3.1 Introduction

Virus-like particles (VLPs) represent a platform for a new generation of vaccines, and offer several clear advantages over traditional vaccines. They are potent in triggering an immune response even at low dosage levels, benefiting from their structural similarity to real viruses, yet providing greater safety as they lack viral genetic material that renders them unable to cause infection (Buckland, 2005). Yeast expression systems have been well developed and are the preferential host for the production of recombinant VLP vaccines (Hitzeman et al., 1983). The use of yeast fermentations to produce biological products is industrially significant, as they offer the benefits of eukaryotic glycosylation, rapid growth, ease of genetic manipulation and less stringent requirements for growth as compared to mammalian cells (Buckholz and Gleeson, 1991). For example, Hepatitis B Surface Antigen (HBsAg) VLP-based vaccine has been produced successfully in *Saccharomyces cerevisiae* (Bitter et al., 1988). The HBsAg VLPs self assemble and permanently bud into the endoplasmic reticulum (ER) membrane as a 22 nm (3.5 MDa) lipoprotein particle with a highly hydrophobic lipid-rich core. In the purification process, a homogenisation step is required to rupture the cells and then a detergent mediated liberation step is used to release the VLPs from the ER membrane. These steps cause a high level of the intracellular contents such as host lipids to enter the process stream. This can be particularly problematic in terms of the deleterious effect on the performance of the downstream processing steps that follow, such as chromatography (Bracewell et al., 2008). As with all biopharmaceuticals, chromatography is the core operation about which the downstream processing of VLPs is centred due to the unparalleled

resolution it is capable of achieving (Hagel et al., 2007). Nevertheless, it is also prone to fouling by components in process feed streams under repeated or prolonged exposure (Siu et al., 2006a), and although standard clean-in-place (CIP) conditions will help to restore most column types toward their original states, the fouling caused by certain types of material such as lipids is far more challenging to remove (Bracewell et al., 2008; Hagel et al., 2007; Siu et al., 2006a). Although using harsher CIP conditions will remove the lipids, this will adversely affect the ligand and thus reduce binding capacity in subsequent loading steps. To minimise their impact on the cost of goods, industrial columns typically need to last for hundreds of cycles (Hagel et al., 2007), so the loss of capacity caused by harsh CIP would necessitate more frequent column replacement and so place a substantial constraint on process economics. To date, only a very limited number of studies have been conducted to address fouling effects during packed bed chromatography (Feuser et al., 1999; Shepard et al., 2000; Staby et al., 1998). The majority of studies have focused on the clogging of solids within the column, which results in uneven distribution and channelling of the flow (Fernandez-Lahore et al., 1999). Findings on how fouling affects the capacity and breakthrough characteristics in ion exchange chromatography (IEX) (Siu et al., 2006a), and a later study (Siu et al., 2006b) to visualise matrix fouling on individual beads using confocal scanning laser microscopy have laid down a solid foundation in terms of utilising these techniques to study other process feeds and matrices. However, these previous studies focused on protein and nucleic acid fouling from an artificial and hence vastly simplified feed stream.

In the HBsAg VLP process examined by Belew et al. (1991), hydrophobic interaction chromatography (HIC) using Butyl-S Sepharose[®] 6 Fast Flow was

employed as a primary capture step, thus exploiting the strongly hydrophobic nature of the VLP. Most host proteins and other low molecular weight solutes do not bind to this mild hydrophobic adsorbent (Belew et al., 1991). Conversely, Bracewell et al. (2008) reported that lipid fouling can have a major impact on the performance of chromatography. Due to the hydrophobic nature of lipids, which are co-released with HBsAg VLP in the upstream process, this subsequent HIC step will thus be particularly susceptible to lipid fouling. In the extreme case, it can be envisaged that lipid fouling might be so acute as to render a whole process economically unfeasible. This scenario provided the impetus for the current study which was set up to investigate the nature and extent of lipid fouling on HIC steps during the processing of a yeast-derived VLP. Efforts were directed to characterise the nature of the foulant-matrix interaction and to identify the type of lipids as well as how the properties of the matrix altered as a result of lipid fouling. Comparative binding capacity, recovery and purity data between lipid-rich (conventional) and lipid depleted feeds were used to study chromatography performance differences over repeated cycles of operation. By delivering an enhanced understanding of lipid fouling, this study therefore lays down the necessary foundations for introducing pre-treatment steps designed to remove these foulants, hence extending the life of the column and achieving a concomitant improvement in process economics.

3.2 Results and Discussions

3.2.1 Fermentation

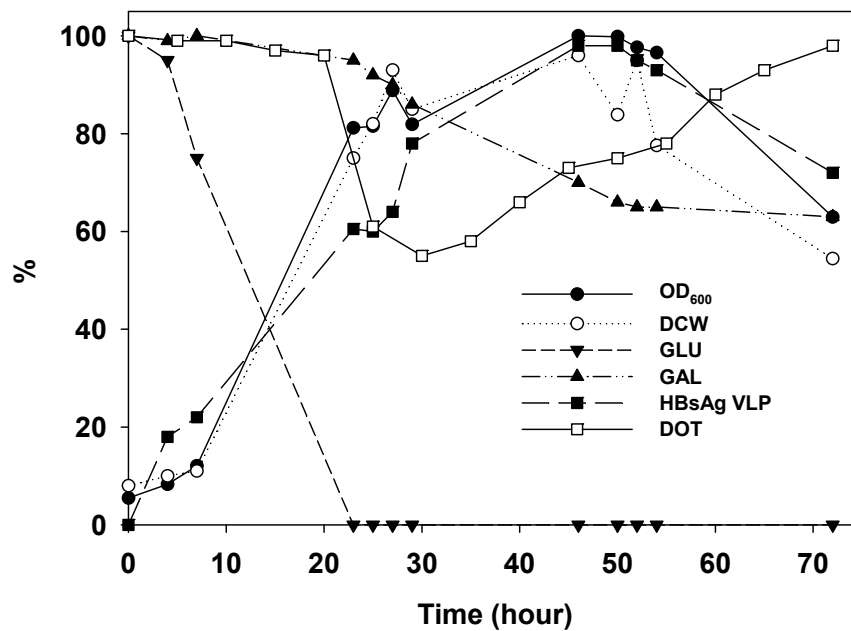


Figure 3-1: Recombinant *Saccharomyces cerevisiae* HBsAg VLP fermentation (75 L). Media and operating conditions are adopted from Kee et al. (2008). Percentage profiles of the 72 hour period shown are OD₆₀₀ (●), dry cell weight (DCW) (○), Glucose concentration (GLU) (▼), Galactose (GAL) (▲), HBsAg VLP (■) and dissolved oxygen tension (DOT) (□).

In order to generate feedstock for the subsequent fouling studies, 75 L recombinant *Saccharomyces cerevisiae* HBsAg VLP fermentations were carried out. The media and operating conditions (Section 2.3.1) were adopted from Kee et al. (2008). The result shows the induction started when glucose went to completion at

around 20th hour. The level of HBsAg VLP peaked at around 50th hour, and the drop afterwards was primarily due to cell death, which could be seen from the decreases in both OD₆₀₀ and dry cell weight measurements towards the end of the 72 hour period. This does suggest HBsAg VLP yield can be improved if the cells are harvested at 50th hour. Nevertheless, approximately 400 g of wet cells were harvested at the end (72 hour) and the HBsAg VLP titre was estimated to be 75 mg/L. These were considered to be sufficiently close to those in the industrial process (Kee et al., 2008), hence the relevance of fouling studies performed on such feedstock.

3.2.2 HIC chromatogram

HIC was used as a capture step for the HBsAg VLP. The media was Butyl-S Sepharose[®] 6 Fast Flow from (GE Healthcare, Buckinghamshire, UK) in a 1 mL HiTrap[®] prepacked format. Using the recommended method (Belew et al., 1991), the following buffer compositions were employed: Buffer A, 20 mM sodium phosphate, 0.6 M ammonia sulphate, pH 7.0; Buffer B, 10 mM sodium phosphate, pH 7.0; Buffer C, 30% isopropanol dissolved in Buffer B. The chromatography system used was an AKTA Explorer controlled via Unicorn version 4.0 (GE Healthcare, Amersham, Buckinghamshire, UK). The flow rate was set at 1 mL/min (156 cm/h). Feed loading volumes were varied for conventional and low lipid feed in order to match the VLP to adsorbent ratio used by Belew et al. (1991). A typical chromatogram from the method described in Section 2.3.4 is shown in Figure 3-2. After loading, the elution was carried out with Buffer B to desorb most of the bound fraction followed by Buffer C to desorb the most tightly bound materials. It should be noted that isopropanol is highly destructive to the HBsAg VLP (Belew et al., 1991), so no measurement of VLP

level is possible for this fraction. The column was then regenerated with a further Buffer C followed by washing with de-ionised water.

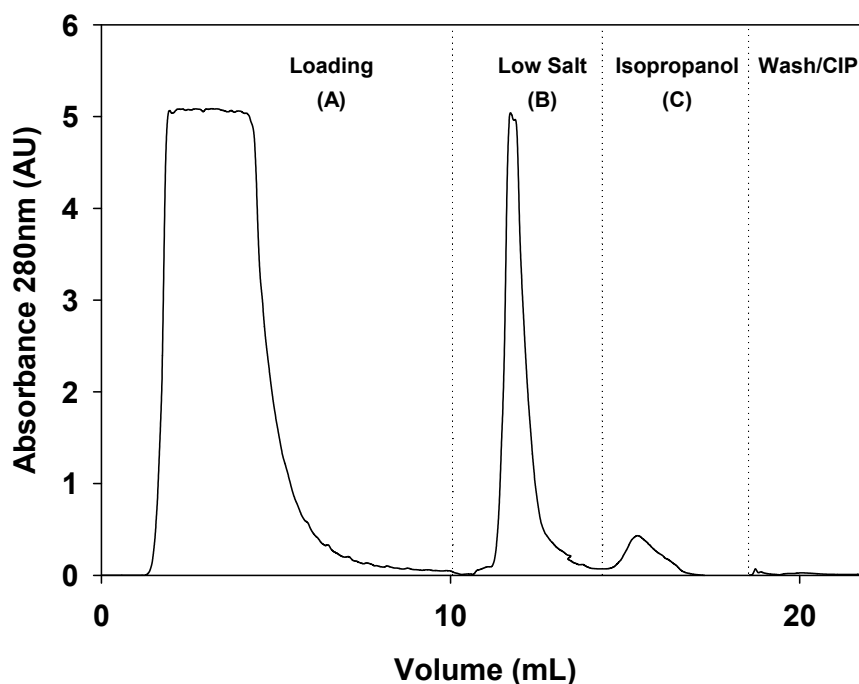


Figure 3-2: The HIC loading and elution profile. The column was first equilibrated with 2 CV of Buffer A, and the 2 CV of sample solution was applied to the column followed by washing with Buffer A. The elution was carried out with 2 CV Buffer B to desorb most of bound fraction followed by 2 CV Buffer C to desorb the most tightly bound proteins. The column was regenerated by washing with a further 2 CV of Buffer C followed by 3 CV of de-ionized water and finally equilibrated by 2 CV of Buffer A. Buffer compositions are given in the text.

3.2.3 Lipid composition in the feed

The total lipid content in *Saccharomyces cerevisiae* ranges from 3.5 to 14.7 % of dry cell weight depending on the growth stage and cultivation conditions (Ramsay

and Douglas, 1979; Rattray, 1988; Sajbidor et al., 1994). Triacylglycerols and ergosterol esters, serving as lipid reserves, are highly hydrophobic and stored almost exclusively in lipid particles within the yeast cells (Clausen et al., 1974). Ergosterol is an essential membrane component along with different classes of phospholipids (Natter et al., 2005). The pre-chromatography feed materials were analysed in order to determine major lipid classes and their levels. The results from HPLC (Figure 3-3) showed three major peaks at 8.2 minutes, 8.8 minutes and 9.6 minutes, along with one minor peak at 14 minutes. From the retention profile of lipid standards, the four peaks were identified respectively as triacylglycerol, Triton X-100, ergosterol and phospholipids. The significant levels of Triton in the feeds could result from the ineffectiveness of XAD-4 in removing micellised Triton (Rigaud et al., 1998a), or perhaps the loss of XAD-4 capacity in the presence of lipids. Overall, neutral lipids accounted for the majority of the lipid content of the feeds (Table 3-1). This is very different to the lipid composition of the cytoplasmic yeast cells themselves (Blagović et al., 2005), but rather similar to that of lipid particles within the cell (Clausen et al., 1974). Lipid particles play an important role in the formation of VLP in yeast and result in their close proximity to the VLP embedded in the ER membrane (Roingeard et al., 2008). The Triton X-100 mediated liberation step for releasing VLPs from ER will most likely co-release the contents of the lipid particles at the same time, giving rise to the lipid profiles observed in the feeds used in this study. The mechanism of detergent liberation involves the interaction between the Triton X-100 molecules (molecular structure shown in Figure 5-2) and the VLPs, and the subsequent formation of stable water soluble micelles. However, since both VLP and neutral lipids are able to form micelles simultaneously with Triton (Dahim et al., 1998), any

attempt to remove the lipid-Triton micelle by centrifugation will inevitably also take out a significant portion of the VLP-Triton micelle. This was exactly what occurred when forming the lipid-depleted feed, which served as a control for quantifying the fouling effect from the conventional feed (lipid-rich). The lipid-depleted feed was prepared from a selective method examined by Kee et al. (2010), which incorporates a reduced homogenisation pressure and an additional centrifugation step to remove cytosolic contaminants. Although the VLP to lipid ratio improved (the VLP to protein ratio remained approximately the same), the 50% reduction in lipids that was achieved came at a cost of 30% VLP loss (this will be further investigated in Chapter 5).

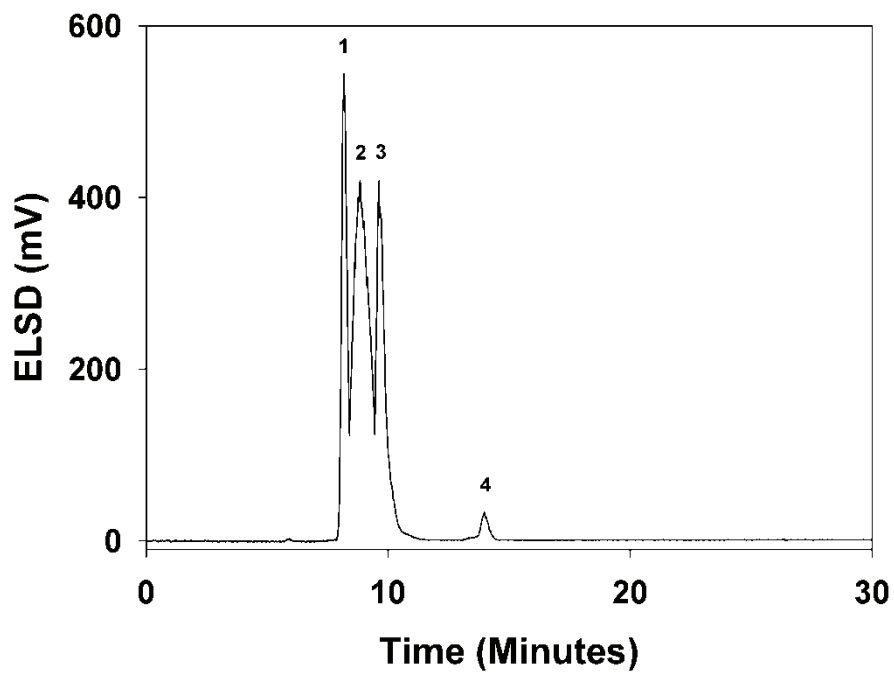


Figure 3-3: Chromatogram of the lipids composition in the feed: The results from HPLC-ELSD show three major peaks at 8.2 minutes, 8.8 minutes, 9.6 minutes, and one minor peak at 14 minutes. Using the lipid standards the following peaks were identified: Peak 1: triacylglycerol; Peak 2: Triton X-100; Peak 3: ergosterol and Peak 4: phospholipids.

Table 3-1: Lipid compositions in the conventional HIC feed, the low lipid HIC feed, Saccharomyces cerevisiae cells (literature values) (Blagović et al., 2005) and S.C. lipid particles (literature values) (Clausen et al., 1974). All measurements were made in triplicate and all values were found to lie within $\pm 5\%$ of each other.

	Conventional HIC feed		Low lipid HIC feed		<i>S. cerevisiae</i>	S.C. Lipid particles
	Concentration (mg/ml)	(% of Total)	Concentration (mg/ml)	(% of Total)	(% of Total)	(% of Total)
Triacylglycerol	4.14	(61.6)	1.71	(51.5)	(4.1)	(51.0)
Ergosterol/ester	1.72	(25.6)	1.06	(31.9)	(23.4)	(47.8)
Phospholipids	0.26	(3.9)	0.08	(2.4)	(67.0)	(1.2)
Triton X-100	0.60	(8.9)	0.47	(14.2)	-	-

3.2.4 Lipid deposition into the column

In order to estimate the level of lipids irreversibly bound to the column, the amount of lipids leaving the column in the flow through, elution, washing and CIP fractions was measured against the total lipids loaded into the column. The results are shown in Table 3-2, for both the conventional and low lipid feeds at the end of the first cycle. 3.25 mg (24.2%) and 0.74 mg (4.8%) of lipids remained within the column respectively and in both cases, triacylglycerol was the major contaminant. CIP appeared to have little effect in reversing the build up. This lipid accumulation was further confirmed by confocal microscopy. Neutral lipids in the feed were labelled specifically (green) with Bodipy[®] 493/503 dye (Invitrogen, Paisley, UK). As the number of cycles increased, a lipid ring was found to develop on the outer surface of the bead (Figure 3-4) (this will be further discussed in Chapter 5).

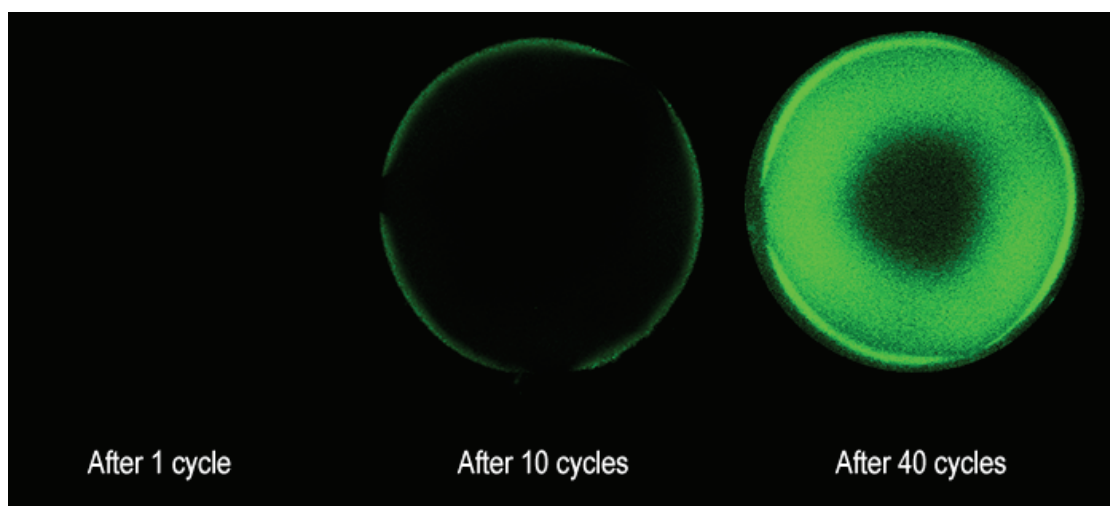
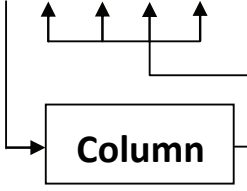


Figure 3-4: Confocal laser scanning microscopy image of Sepharose[®] Butyl-S 6 FF beads after repeated loading cycles. Neutral lipids in the feed were labelled specifically (green) with Bodipy[®] 493/503 dye (Invitrogen, Paisley, UK). As the number of cycles increased, a lipid ring was found to develop on the outer surface of the bead.

Table 3-2: Lipid mass balance for conventional and low lipid feed in the first HIC cycle. All measurements were made in triplicate and ranges are shown in the table. (N.D. not determined.) The compositions of Buffers A-C are given in the text.



	Triacylglycerol (mg)	Ergosterol (mg)	Phospholipids (mg)	Triton X-100 (mg)	Total (mg)
[In] Total	8.28 ± 0.03	3.44 ± 0.09	0.52 ± 0.01	1.20 ± 0.03	13.44
A	2.39 ± 0.04	1.39 ± 0.04	0.07 ± 0.01	0.26 ± 0.08	4.11
B	2.29 ± 0.05	1.14 ± 0.11	0.09 ± 0	0.55 ± 0.05	4.07
C	0.45 ± 0.04	0.52 ± 0.08	N.D.	0.18 ± 0.03	1.15
Wash/CIP	0.37 ± 0.01	0.37 ± 0.05	N.D.	0.11 ± 0.02	0.85
[Out] Total	5.51	3.43	0.16	1.09	10.19
Conventional	[In] – [Out]	0.01	0.36	0.11	3.25
HIC feed	% loss of lipid	0.3	68.5	8.9	24.2
Low lipid	[In] – [Out]	0.00	0.18	0.02	0.74
HIC feed	% loss of lipid	0.0	56.1	1.0	4.8

3.2.5 Column performance with lipid fouling

Among the many performance parameters used to judge the effectiveness of a chromatography separation, binding capacity, recovery and purity are the most likely to be affected by the chemical properties of the foulants. To estimate the binding capacity of VLP, the amount of VLP in the flow through was subtracted from the amount in the feed loaded. For the conventional feed, only 0.22 mg (33%) of the VLP was bound to the matrix during loading in the first cycle (Figure 3-5). However, this number rose gradually to 0.40 mg towards the end of the 40 cycles. In contrast, 0.46 mg (70%) of the VLP was able to bind to the matrix in the first cycle for the low lipid feed, and the capacity stayed constant and did not rise until the 20th cycle. These results suggest that lipids in the feed may influence HIC capacity in two ways. Firstly, lipids in the feed compete or shield the binding surface for VLP, so that when the lipid feed content was reduced, a larger percentage of the binding surface was available for VLP, resulting in an improved VLP capacity. Capacities of up to 0.70 mg of VLP per ml of Butyl-S Sepharose[®] absorbent have been reported by Zhou et al. (2007), where the VLP was captured first by an ion exchange column and which therefore reduced the lipid content significantly prior to the HIC step (Zhou et al., 2007). Secondly, as lipids accumulated within the column, the binding properties of the matrix might have been altered causing an apparent increase in VLP capacity. CIP appeared to be ineffective in reversing the lipid build-up for the conventional feed, but performed better for the low lipid feed.

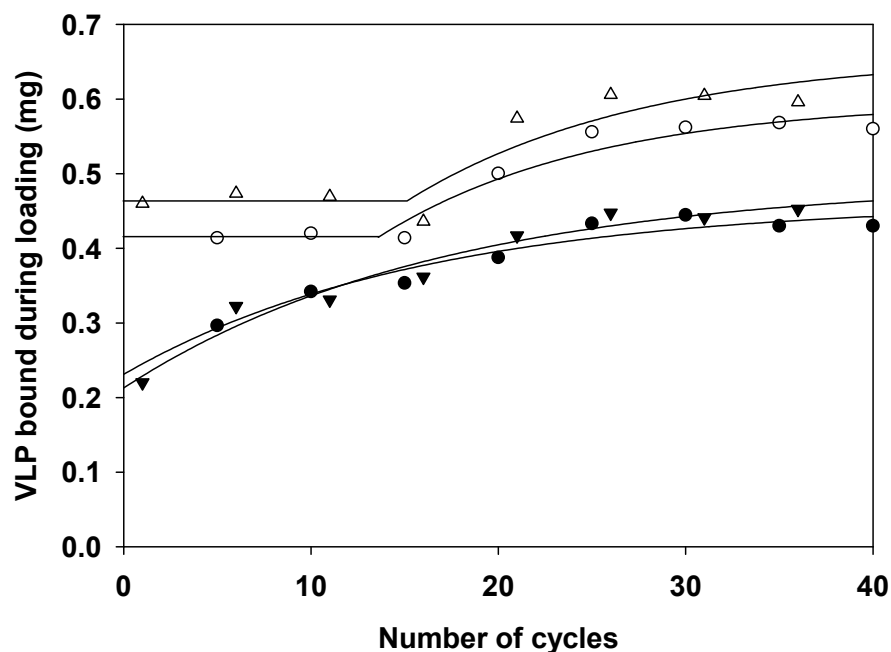


Figure 3-5: Percentage of VLP bound during loading. Conventional feed: pre-CIP cycle (●) and new and post-CIP cycle (▼); Low lipid feed: pre-CIP cycle (○) new and post-CIP cycle (Δ). For the conventional feed, there was only 20% of VLP bound to the matrix during loading in the first cycle. However, this number gradually rose to 40% towards the end of the 40 cycles. In contrast, 75% of the VLP was able to bind to the matrix in the first cycle for the low lipid feed, with the capacity staying constant and not rising until the 20th cycle.

In order to confirm whether there was a change in property of the matrix, the total quantity of compounds eluting from the column from each cycle was compared. Peak areas of UV absorbance at 280 nm from the recorded chromatogram were measured using a method adapted from Belew et al. (1991). The amount of total material bound to the matrix during loading stayed relatively constant throughout the 40 cycles (data not shown). Thus the overall binding capacity did not vary significantly. However, as shown in Figure 3-6 over successive cycles, the level of

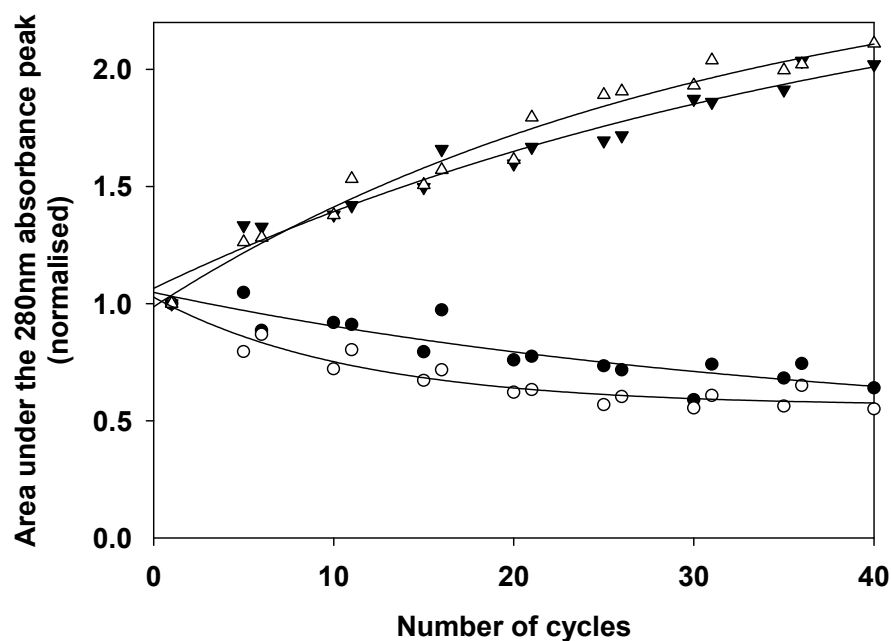


Figure 3-6: Comparison of amount of total materials during low salt and 30% isopropanol elutions (normalised from the values of the first cycle). Conventional feed: low salt elution (●) and 30% isopropanol elution (▼); Low lipid feed: low salt elution (○) and 30% isopropanol elution (Δ). Values for the areas of the 280 nm absorbance peaks from the recorded chromatogram were determined by manual integration. As the number of cycles increased, the level of eluted material during the low salt elution fell, while more was eluted during the 30% isopropanol elution.

elutents during the low salt elution fell, while more was eluted during the stronger 30% isopropanol strip. This shift gives a strong indication that the binding affinity of the matrix towards feed components was increasing. As a result the VLP recovery, defined as the amount of VLP recovered in the low salt elution step divided by the VLP captured by the column during loading, was affected significantly (Figure 3-7). For the conventional (lipid-rich) feed, the recovery dropped from more than 90% to 30% during the first 20 cycles and stayed low thereafter. For the low lipid feed, where

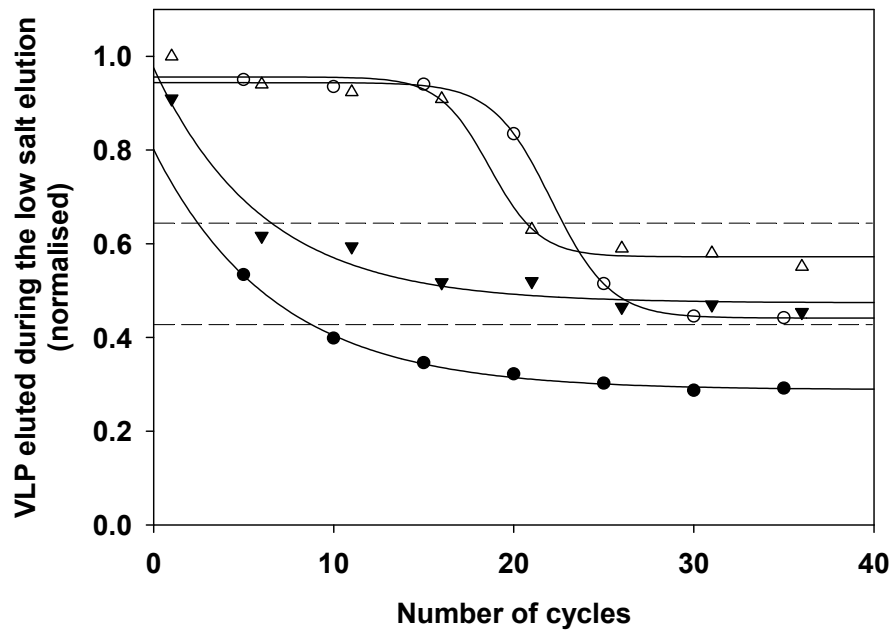


Figure 3-7: Percentage of VLP eluted during the low salt elution of total VLP bound. Low lipid feed: pre-CIP cycle (○) new and post-CIP cycle (Δ); Conventional feed: pre-CIP cycle (●) and new and post-CIP cycle (▼). For the conventional feed, the recovery dropped from more than 90% to 30% during the first 20 cycles and stayed low thereafter. For the low lipid feed, where lipid fouling was less severe, high recovery (more than 90%) was maintained until the 20th cycle, after which recovery fell to around 40%. A 20% rise in recovery was observed in later post CIP cycles, while a minimal rise was seen in early ones.

the resulting fouling was less severe, a high recovery (more than 90%) was maintained until the 20th cycle, after which recovery fell to around 40%. It is interesting to note that in this instance the effect of CIP only became noticeable with the higher degree of lipid fouling. A 20% rise in recovery was observed after 10 cycles, while only a minimal rise was seen in the earlier ones. However, the effect of CIP was not significant enough to prevent the overall trend of decline in VLP recovery. On the other hand, it is no surprise to see that the VLP purity remained relatively unaffected

(data not shown), as the reduction in the quantity of VLP was coupled to a decrease in total materials eluted during the low salt elution step.

A potential mechanism to explain these effects is proposed below, based on results presented previously in the literature. For example, Belew et al. (1991) observed increased binding capacities and lowered product recoveries using matrices with elevated ligand concentrations. Furthermore, according to the investigation by Lenhoff et al. (2007), the retention characteristics in HIC depend on a number of factors including the molecular mass, the flexibility of the solute, the physical structure of the matrix, the ligand type and density and the type and concentration of the salt in the mobile phase. Hence, since lipid fouling is most likely to have an impact on the binding properties of the ligand, it is proposed that as more lipids accumulated, effectively they formed a lipid layer covering the surface of the absorbent. Furthermore, most lipids consist of much longer hydrocarbon chains compared to the intrinsic ligand (Butyl-S: C_4H_9S , Triacylglycerol: $C_{55}H_{98}O_6$), which if anchored on the absorbent, could act as highly hydrophobic ligands themselves. Zhou et al. (2007) have shown that a custom-made Butyl-S absorbent with a three-carbon spacer arm achieved a VLP recovery that was 30% higher than the Butyl-S Sepharose[®] absorbent with its ten-carbon spacer arm, possibly as a result of the differences in hydrophobicity. Therefore in this study, it is proposed that both the ligand density and type may have been altered as a result of lipid fouling. As lipids start to saturate the whole column, VLP binds increasingly to the lipid layers that provide stronger interactions across a larger number of binding sites than the ligand on its own. Cycle number twenty marks a transition point where no more intrinsic binding sites are available for VLP, resulting in a sudden change in capacity and recovery during that

period. The processing implications of this means that further bead level studies are warranted in order to study this phenomenon.

Comparing the conventional and low lipid feeds, there was a difference in their VLP fouling profiles, but their OD₂₈₀ area fouling profiles were well matched. The reason for this could lie in the size difference between VLP and cellular proteins, the latter contributing most to the absorbance at 280 nm. The relatively small size of host cell proteins means that they are able to penetrate the beads equally in both lipid-rich and lipid-depleted feeds, resulting in equivalent 280 nm fouling profiles. Conversely, with a diameter of 22 nm, VLPs are at least one order of magnitude larger than most cellular proteins. Based upon data from GE Healthcare, VLP is on the edge of the 4 MDa exclusion limit for Sepharose[®] adsorbents (GE Healthcare, 2010), while Lenhoff et al. (2007) indicates that the phase ratio (i.e. the accessible area per unit accessible mobile phase volume) for VLP is at least 30 times less than an average cellular protein. Both of these facts help to explain why VLP capacity is so low compared to other values in the literature e.g. GE Healthcare report that Butyl Sepharose exhibits a binding capacity of 38 mg/mL for β -lactoglobulin (GE Healthcare, 2010). Hence, VLP can only bind to a highly confined outer region of the bead, which is also where the greatest amount of lipid fouling was observed by confocal microscopy. This helps to explain why the differences in lipid content of the feed altered the VLP fouling profiles. Therefore, the observation that VLP binding was not affected to the same extent in the low lipid feed appeared to suggest that the rate of lipid build-up at the surface of the bead is related to the initial lipid concentration in the feed. Taken together with the possible competition between VLP and lipids for available adsorbent binding sites, along with the comparative ineffectiveness of the strong CIP conditions

employed in this study, these results suggest that it would be more beneficial to incorporate lipid removal strategies earlier in the process, rather than to screen for better CIP conditions.

3.3 Conclusion

The results from this study demonstrate clearly the difficulties in chromatographic purification when dealing with high lipid content feeds. In the examined yeast derived HBsAg VLP process, HPLC data showed that neutral lipids accounted for the majority of the lipid content in the feed stream, a composition resembled yeast lipid particles (Clausen et al., 1974). Both mass balance and confocal data confirmed lipid accumulation within the column over time with more than 24% of the lipids being permanently retained in the first cycle alone, and triacylglycerol was identified as the major foulant. Comparative analysis of HIC performance showed that the HBsAg VLP binding capacity was particularly poor and more susceptible to changes when high levels of lipid foulant were present. Where the lipid-rich feedstock was used, its capacity more than doubled towards the end of the 40 cycles. In contrast, only a small improvement in binding capacity was seen for the lipid-depleted feedstock after 40 cycles, and it had remained constant until the half-way point. This observation was in agreement with the findings from Siu et al. (2006a), who reasoned the rising capacity was a result of the nonspecific binding from hydrophobic foulants in the yeast homogenate. However, over the 40 cycles VLP recovery from elution

dropped by more than half for both lipid-rich and lipid-depleted feedstocks, only that in the latter case the decline was again not apparent until the 20th cycle. Overall, the column appeared to be more hydrophobic as lipid fouling progressed, and the harsh isopropanol regeneration and caustic CIP proved to be ineffective in reversing either of the rising capacity or falling recovery. In terms of compliance with stringent regulatory requirements, this therefore could result in a very short column life-time, undesirably raising the manufacturing costs. Hence, this study has laid down the foundations for carrying out further microscopic investigations (Chapter 4) in order to gain a better understanding of detailed lipid fouling mechanisms.

Based on the results of such studies, improvements to adsorbent design and operating protocols could then be explored, such as by optimising the ligand density and spacer arm length, or by using stronger CIP conditions. In this study, however, the relatively harsh CIP was shown to be ineffective and improvements to the regenerating buffer alone would be unlikely to tackle the problem of reduced column capacity caused by the presence of competing lipids. Alternatively and of potentially greater utility could be the introduction of feed pre-treatment steps to reduce the lipid level prior to chromatographic purification. Chapter 5 will demonstrate the potential benefits of these operations in terms of improving product capacity and prolonging product recovery over a larger number of loading cycles, thus helping to maintain column performance and so improve the cost-effectiveness of VLP manufacture.

Chapter 4

Investigation of lipid fouling mechanism

This chapter first investigates the immediate effect of fouling by examining the material adsorption isotherms and batch uptake profiles, followed by the CLSM confirmation on the mode of intra-particle diffusion and adsorption. The investigation then proceeds onto the inspections on resin conditions at different stages during the column life-time, where high-resolution images of the fouled bead surfaces are also obtained using SEM. Finally, in-column spatial distribution and progression of lipid fouling are examined. From the results, potential lipid fouling mechanism is proposed.

4.1 Introduction

Confocal scanning laser microscopy (CSLM) has become an increasingly important tool in chromatography research, due to its ability to acquire fluorescent cross-sectional images from within relative transparent specimens, such as chromatography beads.

The technique was first introduced by Marvin Minsky in 1958 (Minsky, 1961; Minsky, 1988). However, it was not until 1996, Ljunglöf and Hjorth (1996) Ljunglof and Hjorth published the first chromatography study deploying CLSM for the visualisation of intra-particle solute profiles. Since then, chromatography data generated by CLSM has flourished, and Hubbuch et al. has compiled a comprehensive list of publications on the studies of intra-particle uptake processes in chromatographic resins by CLSM (Hubbuch and Kula, 2008). The uptake study of lysozyme and hIgG onto SP Sepharose[®] FF and SP Sepharose[®] XL established the correlation between the detected fluorescence intensity within the bead and the traditional fluid phase measurements (Ljunglöf and Thömmes, 1998). Using two fluorescent dyes, Linden et al. (1999) first investigated the competitive behaviour in adsorption of a multi-component protein mixture. In a second publication, Linden introduced a multi-dye approach, which in contrast to earlier studies allowed resolving the time-dependent movement of adsorbed protein within the bead during protein uptake (Linden et al., 2002). While all the above investigations were based on finite bath studies, Hubbuch et al. (2002) and Dziennik et al. (2003) pioneered the use of a

miniaturised flow cell and thus mimicking uptake profiles in packed bed chromatography.

Fouling causes deviations in the uptake process over time, which is clearly evident from the effects on column performance by the high level of lipids in the process feed during the purification of HBsAg VLP described in the previous chapter. Therefore, understanding of the fouling mechanism is of great importance to bioprocess developers and resin manufacturers. Microscopic techniques, such as CLSM, provide a powerful means of visualising intra-particle diffusion and adsorption, the effect on which by fouling ultimately leads to the deterioration in column performance. Siu et al. (2006b) report such studies on protein and nucleic acid fouling, however it used an artificial and hence vastly simplified feed stream. The lack of systematic studies in literature on process chromatography fouling from real feed stream motivated this study, of which the fundamental goal is an enhanced mechanistic understanding of lipid fouling through the investigation of a capture step HIC. Although the study is focused on lipid fouling in HIC from the purification of HBsAg VLP, it is hoped that the findings can be beneficial to other chromatography techniques, as hydrophobic interaction is the basis for majority of the foulant-column interactions and lipids are one of the most challenging foulants. More importantly, the systematic approach and novel analytical techniques employed in this study can create an investigation platform for fouling studies on other materials and in other systems.

4.2 Theory

4.2.1 Fluorescence

Fluorescent dye or fluorophore is one of the most powerful tools in modern research. By using fluorescent probes, concentration levels and localisation of the targets can be visualised within specimens on an advanced microscopic platform, such as CLSM.

Fluorescence is the intrinsic process of photon emission from fluorophores (generally polyaromatic hydrocarbons or heterocycles) after the adsorption of light, of which the three stages are illustrated by the simple electronic-state diagram (Jablonski diagram) shown in Figure 4-1.

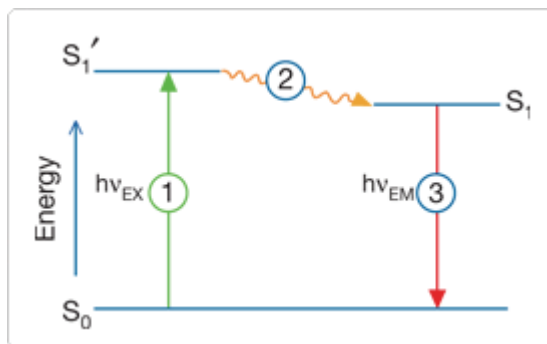


Figure 4-1: Jablonski diagram illustrating the processes involved in the creation of an excited electronic singlet state by optical absorption and subsequent emission of fluorescence (Invitrogen, 2010).

Stage 1: Excitation

From an external source such as a laser, a photon of energy $h\nu_{\text{EX}}$ is supplied to and rapidly absorbed (10^{-15} seconds) by the fluorophore, giving rise to a transitional excited electronic singlet state (S_1'). The marked difference between fluorescence and chemiluminescence is that the excitation in the latter case is via chemical reactions.

Stage 2: Excited-State lifetime

During the short-lived (typically 10^{-9} seconds) excited state, the fluorophore undergoes conformational change, partially dissipating the energy of S_1' to form a relaxed singlet excited state (S_1). It should be noted that some molecules instead of returning to the ground state (S_0) may stay in an alternative excited state for a prolonged period, a process known as photobleaching (Section 4.3.1.1).

Stage 3: Fluorescence Emission

As the fluorophore returns to its ground state S_0 , a photon of energy $h\nu_{\text{EM}}$ is emitted. Due to energy dissipation during the excited state, $h\nu_{\text{EM}}$ is always lower than $h\nu_{\text{EX}}$, and therefore of longer wavelength. The difference in wavelength, known as Stokes shift, is fundamental to the sensitivity of fluorescent imaging as it allows the detection of the emitted photons from ones used in excitation.

In optimum conditions with minimised photobleaching, fluorophore can repeat the entire three-stage fluorescence process for thousands of times, providing relative reproducible results.

The diversity in the excitation and emission spectrums of modern fluorescent dyes permits the simultaneous imaging of multiple fluorophores. Multicolour labelling has major applications in flow cytometry, DNA sequencing, *in situ* hybridisation and fluorescence microscopy (Haugland et al., 2005). In CLSM chromatography research, several studies have been carried out using multicolour-labelled proteins to observe the competitive adsorption behaviour within the beads (Hubbuck et al., 2002; Linden et al., 1999; Linden et al., 2002). In practice, it is important to choose the appropriate combination of dyes. Generally, dye candidates should have the largest possible separation in both excitation and emission spectrums, to avoid the unintended fluorescence resonance energy transfer (FRET) and cross-talk between different detector channels. Additionally, although not ideal, it is advisable to image different dyes in succession to further prevent cross-talk.

Autofluorescence, usually originating from aromatic amino acids, is an intrinsic property of biological specimens and certain materials. It will, however, undesirably raise background noise during imaging. A low laser power should be used at excitation to reduce this background fluorescence, since autofluorescence is normally very weak.

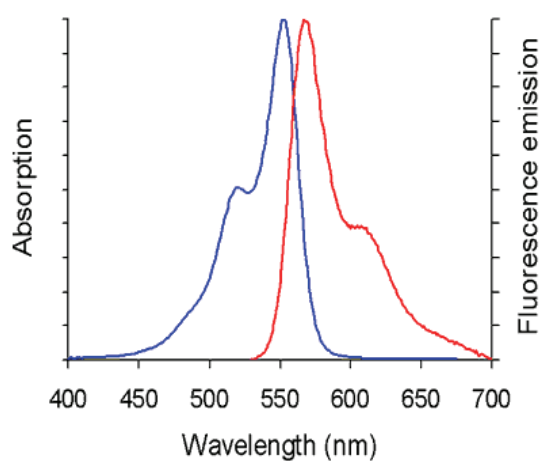


Figure 4-3: Excitation and emission spectra of Alexa Fluor[®] 555. Ex_{max}/Em_{max} (nm): 555/572.

4.2.2.2 Lipophilic dyes

Bodipy[®] is an intensely fluorescent dye which is intrinsically lipophilic. As a result, lipids labelled with this dye are less likely to deviate significantly from the properties of natural lipids. Bodipy[®] 493/503 has a molecular formula of $C_{14}H_{17}BF_2N_2$ ($M_r = 262.11$).

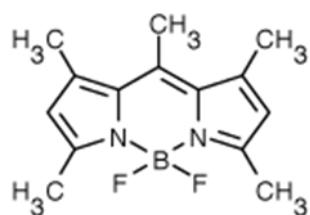


Figure 4-4: Molecular structure of Bodipy[®] 493/503 (Invitrogen, 2010).

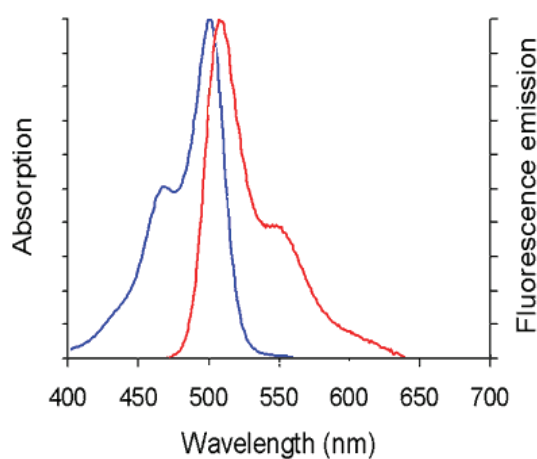


Figure 4-5: Excitation and emission spectra of Bodipy[®] 493/503. Ex_{max}/Em_{max} (nm): 493/503.

Nile red is a lipophilic dye that stains lipid to produce a bright red fluorescence. It is almost nonfluorescent in water but becomes intensely fluorescent in a lipid-rich environment. Nile red has a molecular formula of $C_{20}H_{18}N_2O_2$ ($M_r = 318.37$).

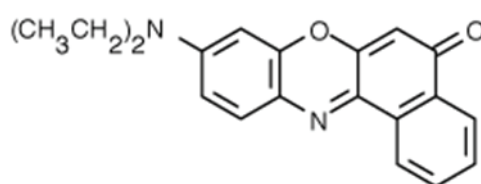


Figure 4-6: Molecular structure of Nile red (Invitrogen, 2010).

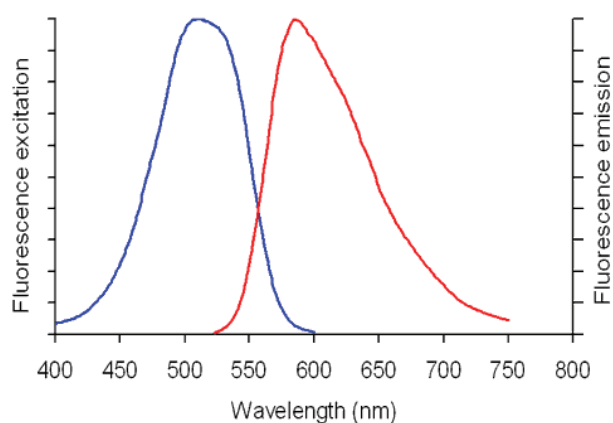


Figure 4-7: Excitation and emission spectra of Nile red. Ex_{max}/Em_{max} (nm): 552/636.

4.2.3 CLSM data processing

4.2.3.1 Light attenuation correction

Visualisation of the intra-particle distribution of fluorescently labelled materials using CLSM without mechanical sectioning of the bead requires careful data analysis in order to obtain quantitative information. The fluorescence intensity profiles measured direct from the confocal images often require correction in order to compensate for light attenuation effects.

Attenuation happens when light is passing through mediums with different refractive indices, such as the case between the internal pore liquid phase and the adsorbent solid phase (Bromley and Hopkinson, 2002; Malmsten et al., 1999; Tallarek et al., 2003). In the current experiment setup, the reduction in fluorescence intensity is two-fold as both light of excitation and emission are subjected to the same attenuation. Without having to use chemical additives to adjust the refractive index of the liquid

phase and causing potential interruptions in the chromatography system, a correction factor approach, such as those described by Heinemann, Visser and Margadant (Heinemann et al., 2004; Heinemann et al., 2002; Margadant et al., 1996), is required. Due to the conical shape of light path between the objective lens and focal point, the physical models of light attenuation are generally very complex, which prompts the need for a simplified model for routine use. In the model proposed by Heinemann et al. (2002), the light path was simplified into the vertical distance between the bead surface and focal point, thus making the correction factor a function of the focal coordinates. Susanto et al. (2006) provided a generalisation of the simplified model as the following

$$I_{corr} = I_{em} \cdot \exp[\varepsilon_{resin} \cdot \text{light path}] \quad (4-1)$$

where I_{corr} is the corrected fluorescence intensity (arb. unit), I_{em} is the emission fluorescence intensity (arb. unit) and ε_{resin} is the extinction coefficient of resin (cm^{-1}).

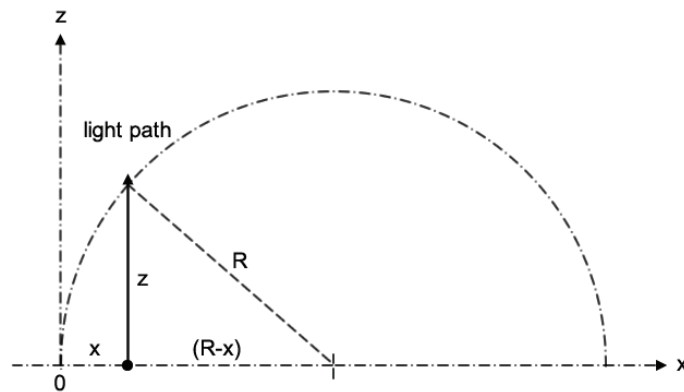


Figure 4-8: Coordinate system in the cross-section at the centre of a bead.

By selecting only cross-section images at the centre of the bead with a radius R and using the coordinate system illustrated in Figure 4-8, the light path z can be given as

$$z = \sqrt{R^2 - (R - x)^2} = \sqrt{2Rx - x^2} \quad (4-2)$$

Thus,

$$I_{corr}(x, z) = I_{em}(x, z) \cdot \exp[\varepsilon_{resin} \cdot \sqrt{2Rx - x^2}] \quad (4-3)$$

The extinction coefficient of the Sepharose[®] resin was referenced to be 61.4 cm^{-1} (Susanto et al., 2006).

In addition, it is worth mentioning that under certain conditions the loss of emitted fluorescence will also occur due to the reabsorption by the dye molecules residing along the light path. The severity of the light attenuation as such, however, greatly depends on the dye concentration. And it is often negligible at very low dye concentration (Susanto et al., 2006), which was the case in the current experiment ($\sim 0.04 \text{ mM}$). Therefore, it was sufficient to correct the light attenuation effect caused by the Sepharose[®] resin alone.

4.2.3.2 Relative capacity calculation

In order to account for the variations in particle size and produce comparable values, calibration of the corrected intensity profiles by converting them into the relative capacity was carried out following the method outlined by Hubbuch et al.

(2002). The overall fluorescence intensity of the particle was considered to be the sum of intensity from the individual shell segmented by the number of pixels along its radius. Thus, intensity of a shell could be calculated from the directly measured volumetric intensity, I_{pv} , of the corresponding pixel.

$$I_{\text{shell}} = I_{pv} \left[\frac{4}{3} \pi (r_a^3 - r_i^3) \right] \quad (4-4)$$

where I_{shell} is the intensity of shell (arb units); r_a and r_i represent the respective outer and inner radii of a pixel within the cross-section of the particle. The final relative capacity could, therefore, be obtained from the overall intensity and volume of the particle.

$$Q_{\text{rel}} = \frac{\sum I_{\text{shell}}}{V_p} \quad (4-5)$$

where Q_{rel} is the relative capacity (intensity/ μm^3) and V_p is the volume of particle (μm^3). The assumption of this calculation is the symmetry in fluorescence intensity profile across the entire bead, which is often however not the case for particles within a packed bed. As evidenced by the current study (Section 4.3.6.1) and others, there was severely restricted mass transport at the contact point between two particles, which invalidated the assumption of symmetry (Hubbuck et al., 2002). As a result, only beads with minimal or no contact points were included in the calculations.

4.2.4 Pore and surface diffusion

Intra-particle diffusion is usually the rate-limiting step in the overall adsorption process in porous particles. Fouling has the potential of affecting column performance through changes in the characteristics of diffusion. Thus, it is essential to understand the mechanisms of diffusion and be able to identify the mode of diffusion in the system studied.

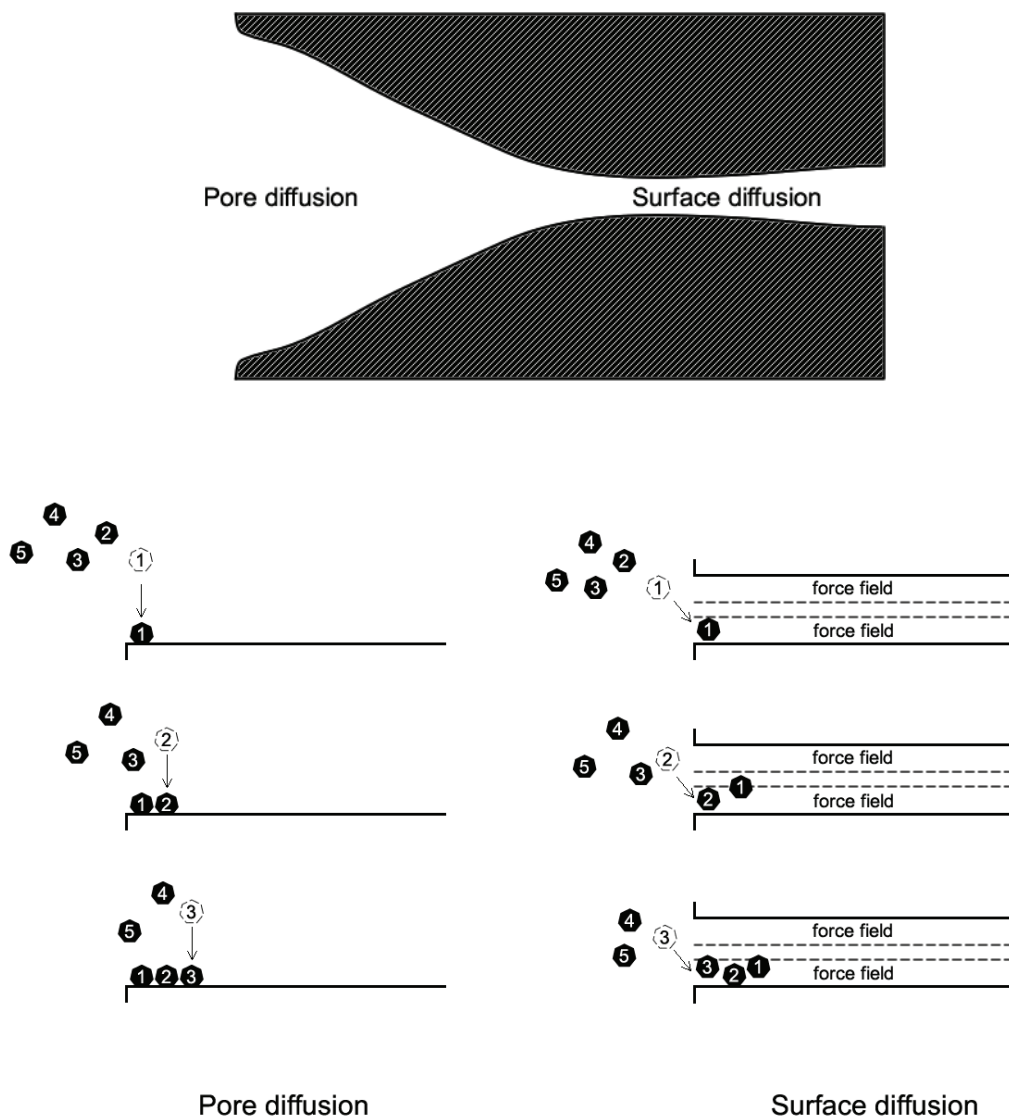


Figure 4-9: Illustrates of pore and surface diffusions in porous particles.

There are two modes of diffusion within the beads: pore and surface diffusion. In pore diffusion, solutes move along in the mobile phase driven by its concentration gradient within the macropore space, which are sufficiently large to allow the solutes to escape from the electromagnetic field on the solid surface. Depending on the adsorption condition, solute molecule may adsorb and desorb to and from the resin surface many times along its transportation path or be permanently adsorbed. However, in either case, only desorbed molecules can undergo transport. In contrast, surface diffusion takes place through the adsorbed layer along the solid surface by an activation process involving jumps between adsorption sites. This is possible only when the activation energy needed for lateral movement is lower than the desorption energy. The pores in such case are sufficiently small that the diffusing solute never escapes the electromagnetic field of the solid surface. Hence, the driving force is the concentration gradient of the species in its adsorbed state (Green and Perry, 2007).

However, it is worth pointing out that in most cases both pore and surface diffusions contribute to the overall intra-particle diffusion into porous particles simultaneously. Suzuki (1990) has derived overall inter-particle diffusion coefficient, D_e , as

$$D_e = D_p + \rho_k K D_s \quad (4-6)$$

where D_p is the pore diffusion coefficient, D_s is the surface diffusion coefficient, ρ_k is the particle density, and K is the Henry constant of adsorption under linear conditions. Furthermore, in conditions that demote adsorption, the surface diffusion coefficient of

weakly retained molecules is approximately 50% lower than their pore diffusivity, possibly caused by steric diffusion hindrance from the distended layer of resin ligands through which surface diffusion must take place (Miyabe and Guiochon, 2001). While in conditions that promote adsorption, strongly retained molecules are laterally immobilised on the solid surface where surface diffusion can be so small as to become practically negligible. Thus, the two phenomena are not fundamentally different from each other.

It is often difficult to identify any changes of diffusion and their respective causes, especially when dealing with multi-component process feed as there are a large number of complicating factors involved. For instance, competitive diffusion, multilayered adsorption and irreversible binding could all be the results from foulants and their deleterious effects. Therefore, it is important to have advanced real-time microscopic experimental platform, such as CLSM and electron microscopy, when investigating fouling phenomena.

4.3 Results and Discussion

4.3.1 Experimental errors

4.3.1.1 Photobleaching

Photobleaching is the irreversible loss of fluorophore activity resulting from intensive illuminations. Instead of returning to ground state, the relaxed singlet excited state can transition to a triplet excited state in energetic favourable conditions, the relaxation of which is among one of the slowest. The negative impact of photobleaching is the unsystematic decrease in emitted fluorescence intensity over time, which may obnubilate the comparability between samples.

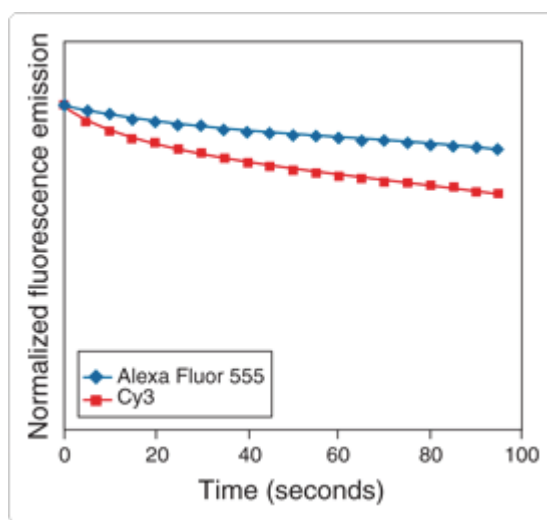


Figure 4-10: Photobleaching profiles of Alexa[®] Fluor 555 and Cy3 dyes (Invitrogen, 2010).

In order to minimise photobleaching, preference has been given to fluorophores with greater photostability. For example, BSA-Alexa[®] 555 conjugate was chosen, as it is more photostable than the Cy3 alternative (Figure 4-10), providing more time for imaging. While Bodipy[®] dyes also showed superior resistance to photobleaching over traditional dyes (Hinkeldey et al., 2008). Precautions have also been taken for the preservation of fluorophores, which include the use low laser power, shortened exposure, low-light CCD camera and high-numerical aperture objectives. Additionally, all samples and apparatuses that were in contact with the dyes were wrapped with aluminium foil for protection against surrounding light.

4.3.1.2 Particle size distribution

Sepharose[®] Fast Flow resin has a wide distribution of particle sizes between 45 and 165 μm in diameter (GE Healthcare), which was evident during the CLSM imaging. However, depending on the dominant mode of diffusion, the rate of material uptake may be a function of particle size (Ruthven, 1984). Ideally, only particles of the same size should therefore be selected for analysis. Nevertheless, this was often not practically possible. As a result, particles within a narrow size range, preferably around the stated mean particle size of 90 μm , were chosen instead. This variation in particle sizes, although small, may still provide a source of error in system studied.

4.3.2 Experimental controls

4.3.2.1 Fluorescent labelling effects on adsorption

Deviations in the adsorption characteristics of proteins by the attachment of dye molecules have been reported (Teske et al., 2005). The preferential binding of the dye-labelled proteins over their native form resulted in a concentration overshoot at the centre of the beads. The hypothesis was the significant alternation of surface net charge to the protein by the dye molecules, hence the profound effects in ion exchange chromatography. Although in theory labelling effect should be less significant in the current hydrophobic interaction chromatography system (Susanto et al., 2007), nevertheless the reservation due to the lack of confirmations in literature regarding the dyes, targets and conditions used in the current study warranted control experiments to be carried out.

When there is preferential binding between the dye-labelled and native targets, the difference in the respective batch uptake rates will yield a change in the external fluid phase molar dye to protein or dye to lipid ratio (generalised as D/P) over time. Thus by monitoring this D/P ratio, deviations, if there is any, from the labelling effect can be evaluated.

During the batch uptake experiments (Section 2.4.2), the monitored D/P ratios of the three dyes, Bodipy[®] 493/503, Nile red and Alexa[®] 555, remained constant at 0.0065 ± 0.0003 , 0.0055 ± 0.0003 and 0.0515 ± 0.0022 respectively for the duration of the experiments. Thus from the results, it was satisfied that the effects on material adsorption from the artefacts of labelling were negligible.

4.3.2.2 Material autofluorescence and cross-talks

The following control experiments have been performed.

Table 4-1: Control experiments performed for CLSM.

Control experiment	Purpose	Results
Fresh Sepharose [®] Butyl-S 6 Fast Flow beads in 0.6 M (NH ₄) ₂ SO ₄ .	To verify the resin and reagents do not autofluorescence.	No fluorescence detected under current laser power.
Sepharose [®] Butyl-S 6 Fast Flow beads incubated with process feed in the absence of any fluorescent dye at 0.6 M (NH ₄) ₂ SO ₄ .	To verify process feed does not autofluorescence.	No fluorescence detected under current laser power.
Sepharose [®] Butyl-S 6 Fast Flow beads incubated with Bodipy [®] 493/503 in the absence of process feed at 0.6 M (NH ₄) ₂ SO ₄ .	To verify Bodipy [®] 493/503 does not binds to the resin.	Uniformly low level of fluorescence, laser power to be reduced.
Sepharose [®] Butyl-S 6 Fast Flow beads incubated with Nile red in the absence of process feed at 0.6 M (NH ₄) ₂ SO ₄ .	To verify Nile red does not binds to the resin.	Uniformly low level of fluorescence, laser power to be reduced.
Sepharose [®] Butyl-S 6 Fast Flow beads incubated with Alexa [®] 555 in the absence of process feed at 0.6 M (NH ₄) ₂ SO ₄ .	To verify Alexa [®] 555 does not binds to the resin.	No fluorescence detected under current laser power.
Flow cell channels in pure water.	To verify no fluorescence from leftover contaminants	No fluorescence detected under current laser power
Repeated scans of all fluorescent dyes used	To check for photobleaching effects	No noticeable reduction in fluorescence intensity for the duration of experiment.

Table 4-2: Control experiment performed to eliminate cross-talks of Bodipy[®] 493/503.

Excitation wavelength (nm)	Emission wavelength (nm)		
	520 - 550	560-590	600-650
488	+++	+	-
543	-	-	-
633	-	-	-

Note: +++ 100% saturation, ++ 50% saturation, + 20% saturation, - Not Detectable.

Table 4-3: Control experiment performed to eliminate cross-talks of Nile red.

Excitation wavelength (nm)	Emission wavelength (nm)		
	520 - 550	560-690	600-650
488	-	-	-
543	-	-	+++
633	-	-	-

Note: +++ 100% saturation, ++ 50% saturation, + 20% saturation, - Not Detectable.

Table 4-4: Control experiment performed to eliminate cross-talks of BSA-Alexa[®] 555.

Excitation wavelength (nm)	Emission wavelength (nm)		
	520 - 550	560-690	600-650
488	-	-	-
543	-	++	+++
633	-	-	-

Note: +++ 100% saturation, ++ 50% saturation, + 20% saturation, - Not Detectable.

4.3.3 Thermodynamic characterisation of process material uptake

4.3.3.1 Adsorption isotherms

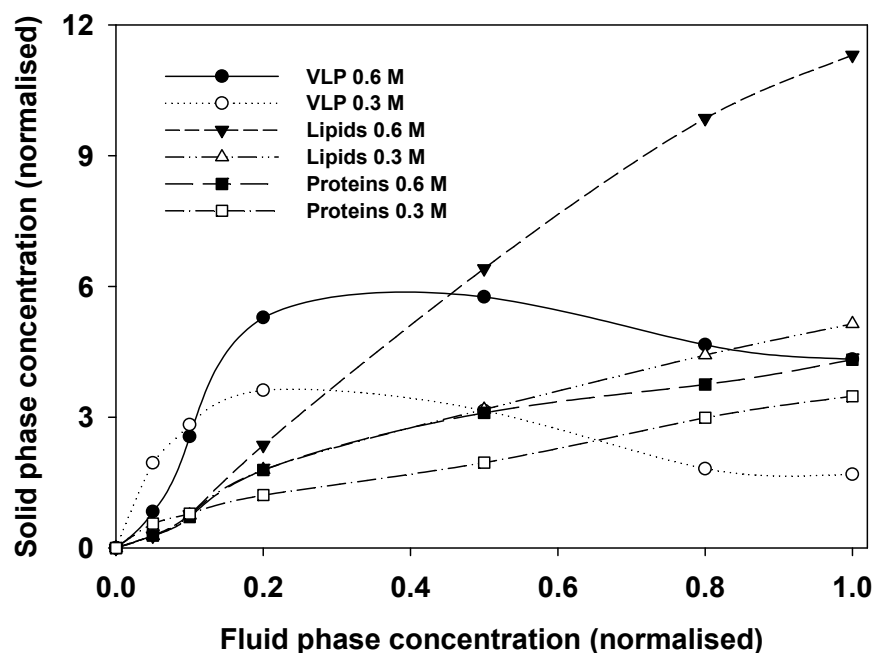


Figure 4-11: Adsorption equilibriums of HBsAg VLP, neutral lipids and proteins in process feed by Sepharose® Butyl-S 6 Fast Flow at 0.6 M (dark) and 0.3 M (light) $(\text{NH}_4)_2\text{SO}_4$. Feed to resin volume ratio was 20:1. Both solid and fluid phase material concentrations were normalised against their respective concentrations in the process feed (HBsAg VLP: 0.28 mg/mL; neutral lipids: 5.1 mg/mL; proteins: 2.3 mg/mL). Standard deviations of all data (triplicate samples) were within 10%.

Adsorption isotherms of HBsAg VLP, neutral lipids and proteins in the process feed were produced as described in Section 2.4.1 (Figure 4-11). To allow easy comparison, isotherm data for each material was normalised against its respective concentration in the undiluted process feed, thus the presented values could be seen as

the factorial difference between concentrations in the solid phase and initial process feed. For example, a value of 3 would indicate the concentration of the adsorbed material is three times of that in the feed used by the capture step HIC. In addition, using a standard Langmuir model (Langmuir, 1916) the values of maximum adsorption capacity (Q_{\max}) and equilibrium dissociation constant (K_d) were estimated for each isotherm and listed in Table 4-5. There are several assumptions that the Langmuir model is based on, which are 1) adsorption cannot proceed beyond monolayer, even at the maximum adsorption capacity; 2) the homogeneity of all adsorbent surface, hence the same mechanism under which all adsorptions occur; 3) no interaction between materials, i.e. the ability to adsorb or desorb at a given site is independent of the occupation of neighbouring sites. The validity of these assumptions under current experimental conditions was, however, arguable as seen in the later results. Therefore, the calculated parameters are strictly presented as a general reflection of trends.

Table 4-5: Estimated values of maximum adsorption capacity (Q_{\max}) and equilibrium dissociation constant (K_d) using standard Langmuir isotherm model.

(NH ₄) ₂ SO ₄ concentration	HBsAg VLP		Neutral lipids		Proteins	
	Q_{\max}	K_d	Q_{\max}	K_d	Q_{\max}	K_d
0.6 M	1.64	0.03	481.4 (p)	36.5 (p)	16.9 (p)	1.7 (p)
	[1.64]	-	[59.1]	-	[9.9]	-
0.3 M	1.02	0.01	59.2 (p)	6.6 (p)	15.4 (p)	2.3 (p)
	[1.02]	-	[30.2]	-	[7.8]	-

Units: Q_{\max} (mg/mL of resin) K_d (mg/mL), (p): projected value, [value]: observed maximum

The maximum HBsAg VLP adsorption (1.64 mg/mL of resin) was reached relatively early at high salt concentration, after which point the adsorption level started to fall. This indicates preferential binding of certain materials in the process feed displacing the adsorbed HBsAg VLP. In comparison, there was an approximately 40% reduction in the maximum adsorption capacity achieved at the low salt concentration, but nevertheless the decreases after maximums were similar in both cases. However, considering the large error (~10%) generally associated with the HBsAg VLP ELISA arisen from the relative manual procedures, the significance of these changes as indications of competitive binding remains to be validated, preferably through a secondary HBsAg VLP (Section 6.5.1). For neutral lipids, isotherm was linear and showing capacities disproportionally higher than that of HBsAg VLP, reaching more than 30.2 mg/mL of resin and 59.1 mg/mL of resin (6 and 11 times of the concentration in process feed) at the low and high salt concentration respectively. For proteins, linear isotherms were again observed, but with significantly lower capacities than neutral lipids. In addition, the increased salt concentration could yield only a moderate gain on protein adsorption (from 7.8 mg/mL of resin to 9.9 mg/mL of resin) at the process feed concentration, suggesting protein capacity was less responsive than those of HBsAg and neutral lipids to the more favourable binding condition exerted under the high salt concentration.

The marked differences in capacities of the three feed components were also reflected from the estimated Q_{\max} , showing at least an order of magnitude between each other (Table 4-5) (Modifications on the adsorption model used may be required to account for the large discrepancies found between the projected and observed maximum capacities, but this is beyond of the scope of current investigation). At the

high salt concentration, neutral lipids had the highest capacity (481.4 mg/mL of resin, projected), followed by proteins (16.9 mg/mL of resin, projected). HBsAg VLP was only able to reach an apparent Q_{\max} of 1.64 mg/mL of resin, which is the lowest of all. This is expected from the significant differences in molecular size between the three. HBsAg VLP, being the largest at 3.5 MDa, is right on the edge of the Sepharose[®] exclusion limit (Lenhoff and To, 2007), hence the lowest phase ratio. It can only bind to the outer surface of the bead with essentially little or no intra-particle diffusion involved, whereas the smaller proteins (average 70 kDa) and lipids (average 1 kDa) can diffuse into the beads to further utilise the internal binding surfaces. It is also possible that the slow adsorption observed for neutral lipids and proteins can be due to the additional intra-particle diffusion process. In order to further examine the competitive effect on VLP binding and the possible influence of lipid fouling on diffusion, material uptake rates were studied.

4.3.3.2 Material batch uptake rates

Batch uptake experiments were performed, and the uptake rates of the three major feed components were measured and shown in Figure 4-12. At high salt concentration, VLP uptake peaked at around 20 minute, after which it dropped slightly. This confirms competitive binding, possibly from lipids or lipid aggregates, was replacing the adsorbed VLP over time. This competitive effect was less noticeable at the low salt condition. For neutral lipids, the adsorption quickly rose to steady levels within 20 minutes, after which although slower, it continued to rise at high salt concentration. No such observation was seen at the low salt concentration. Thus, departures from the standard single-component adsorption isotherm and uptake

profiles appeared to be less frequent under the low salt condition. This indicates there is a strong correlation between the extent of fouling and adsorption strength.

Conversely, considering the substantially increased uptake for both VLP and neutral lipids at higher salt concentration, it was surprising to see that the levels of protein uptake were almost comparable at both salt concentrations. Nevertheless, this was consistent with the result from the adsorption isotherm. Possible explanations for such phenomenon may include competitive binding from lipids due to their higher hydrophobicity and some sort of diffusion hindrance caused by elevated build-up of materials at the high salt concentration. On account of the reported large difference in

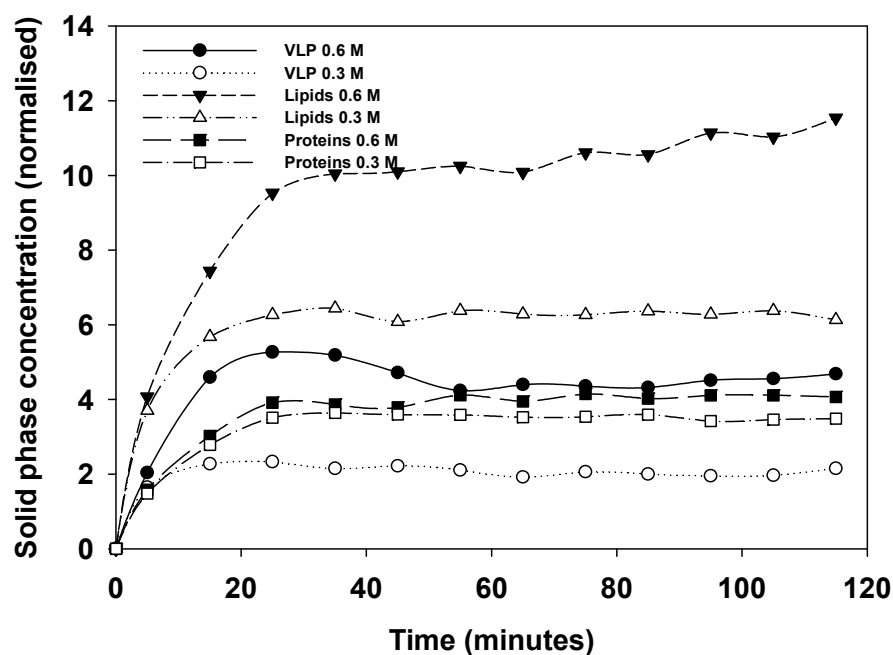


Figure 4-12: Batch uptake curves of HBsAg VLP, neutral lipids and proteins in process feed by Sepharose® Butyl-S 6 Fast Flow at 0.6 (dark) and 0.3 M (light) $(\text{NH}_4)_2\text{SO}_4$. Feed to resin volume ratio was 20:1. Both solid and fluid phase material concentrations were normalised against their respective concentrations in the process feed (HBsAg VLP: 0.28 mg/mL; neutral lipids: 5.1 mg/mL; proteins: 0.23 mg/mL). Standard deviations of all data (triplicate samples) were within 10%.

HIC binding capacity for pure protein at various salt concentrations (Hahn et al., 2003), the low increase in protein uptake was most likely to be resulted from the combination of the two effects.

4.3.3.3 Effects of material interactions on uptake rates

As discussed previously, material concentration gradient is the main driving force for diffusion and adsorption in porous media (Section 4.2.4). In the batch uptake experiment, total material available for interaction will increase if higher feed to resin volume ratio is used. Thus, by keeping material concentrations constant, i.e. diffusion and adsorption potentials, deviation in uptake profiles resulted from material interactions would be made more apparent. Batch uptake experiment (Section 2.4.2) was repeated at two other feed to resin volume ratios, 4:1 (4x) and 8:1 (8x), in addition to the pervious 20:1 (20x). Amounts of materials in both the adsorbed and free fractions at the end of the two-hour uptake experiments were also calculated and listed in Table 4-6.

Results obtained at the high salt concentration were first examined. Figure 4-13 and Table 4-6 show that after being completely taken up at 4x neutral lipids appeared to have saturated the adsorbent at 8x, as indicated by the presence of free lipids. However, even though the adsorption potential (concentration) remained unchanged, a further 30% increase in capacity was seen at 20x, when more lipids were available. This is consistent with the linearity observed in the isotherm, thus strongly suggesting that a significant portion of the additional capacity achieved at 20x was due to the elevated lipid-lipid interactions and the resulting multilayer adsorption.

Table 4-6: The amounts of material in the adsorbed and free state at the end of the two-hour batch uptake. Three feed to resin volume ratios (4x, 8x, and 20x) were tested. Values in bracket indicate the corresponding percentages of the initial material amount. (a) 0.6 M (NH₄)₂SO₄; (b) 0.3 M (NH₄)₂SO₄. Standard deviations of all data (triplicate samples) were within 5%.

(a)

Feed to resin ratio	HBsAg VLP		Neutral Lipids		Proteins	
	Adsorbed	Free	Adsorbed	Free	Adsorbed	Free
4	1.1 (99.5%)	0.0 (0.5%)	20.4 (100.0%)	0.0 (0.0%)	7.1 (77.0%)	2.1 (23.0%)
8	1.2 (54.5%)	1.0 (45.5%)	38.0 (93.1%)	2.8 (6.9%)	10.4 (56.4%)	8.0 (43.6%)
20	1.3 (23.4%)	4.3 (76.6%)	58.9 (57.7%)	43.1 (42.3%)	9.8 (21.4%)	36.2 (78.6%)
Unit: mg/mL of resin						

(b)

Feed to resin ratio	HBsAg VLP		Neutral Lipids		Proteins	
	Adsorbed	Free	Adsorbed	Free	Adsorbed	Free
4	0.9 (78.2%)	0.2 (21.8%)	20.0 (98.2%)	0.4 (1.8%)	5.4 (59.2%)	3.8 (40.8%)
8	0.7 (31.5%)	1.5 (68.5%)	27.7 (67.8%)	13.1 (32.2%)	6.4 (35.0%)	12.0 (65.0%)
20	0.5 (9.8%)	5.1 (90.2%)	31.2 (30.6%)	70.8 (69.4%)	8.0 (17.4%)	38.0 (82.6%)
Unit: mg/mL of resin						

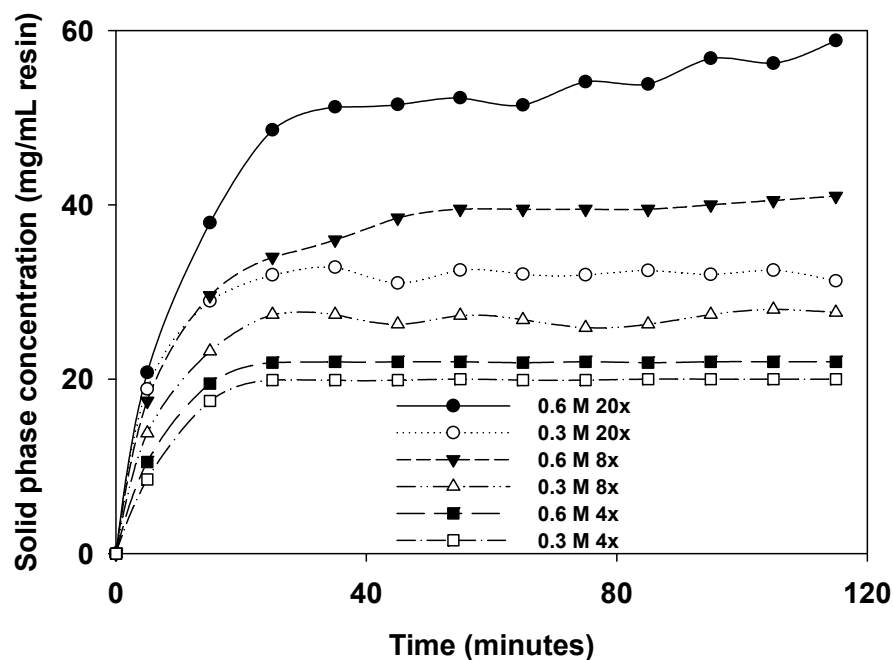


Figure 4-13: Batch uptake curves of neutral lipids in process feed by Sepharose® Butyl-S 6 Fast Flow at 0.6 (dark) and 0.3 M (light) $(\text{NH}_4)_2\text{SO}_4$. Feed to resin volume ratios tested were 20:1(20x), 8:1(8x) and 4:1(4x). Standard deviations of all data (triplicate samples) were within 5%.

Capacity contributed by such nonspecific interactions may even be present at 8x or 4x, further study is required though in order to confirm this. As for both HBsAg VLP and proteins, the overall adsorption levels were not significantly varied at all the three ratios tested (Figure 4-14 and Figure 4-15), suggesting a lower degree of nonspecific interactions between themselves or with the lipids. Nevertheless, the displacement effect of the adsorbed HBsAg VLP previously seen at 20x was again observed at 8x but not at 4x (Figure 4-14), which was most likely due to the depletion of competing lipids. Interestingly, there were small but noticeable increases in HBsAg VLP adsorption towards the end of the two hour period at both 8x and 20x, an effect also seen in heavily fouled column during the previous fouling experiment (Chapter 4).

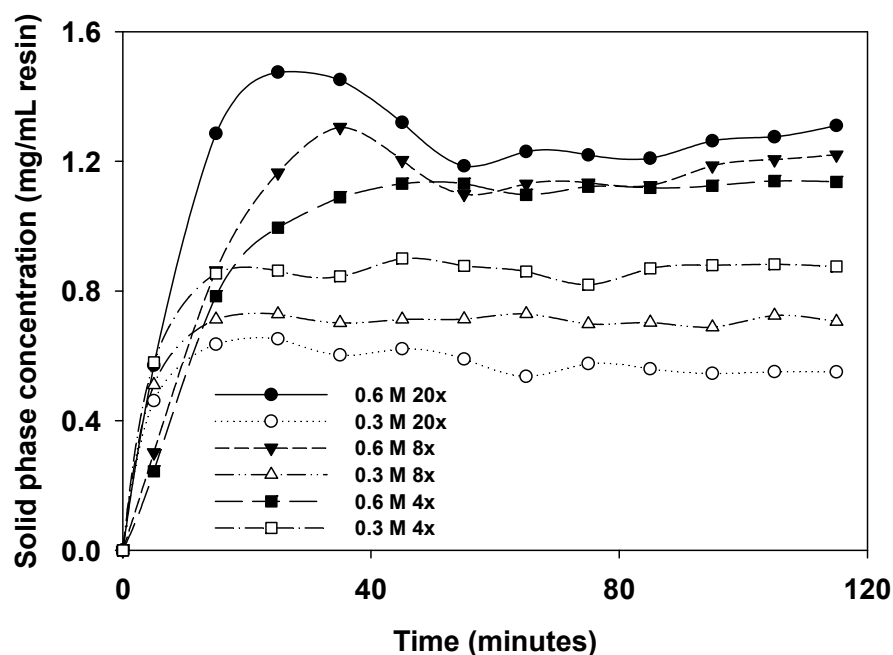


Figure 4-14: Batch uptake curves of HBsAg VLP in process feed by Sepharose® Butyl-S 6 Fast Flow at 0.6 (dark) and 0.3 M (light) $(\text{NH}_4)_2\text{SO}_4$. Feed to resin volume ratios tested were 20:1(20x), 8:1(8x) and 4:1(4x). Standard deviations of all data (triplicate samples) were within 10%.

At the low salt concentration, no significant rise in the levels of adsorbed lipids was seen from 8x to 20x. This suggests that at lowered hydrophobic condition either the lipid binding capacity was reduced and saturation was reached earlier, or the lipid-lipid interaction was weakened so that it was insufficient to yield further capacity. In contrast to the high salt condition, the level of HBsAg VLP adsorption appeared to be adversely affected by the feed to resin volume ratio and no delayed displacement of the adsorbed VLP was observed. As discussed previously, VLPs can bind to only the outer surface of the beads due to their size, thus the reduced adsorptions may indicate a build-up of lipid foulants in this region, occupying VLP binding sites. Further, as

lipid saturation occurred very early at the low salt condition, it is very likely that the effect of such competitive binding was immediate after adsorption had began, whereas at the high salt condition due to the vastly increased capacity it took longer for lipids to reach saturation, thus its competitive effect on adsorbed HBsAg VLP was delayed. It is, therefore, possible that the competitive effect on VLP binding escalated only after lipid adsorption had achieve certain degree of saturation at the outer surface of the beads. Unfortunately, the adsorption isotherm and batch uptake data does not provide information on the progression and characteristics of material uptake at the microscopic level, such as localised concentrations or multilayer adsorption. Therefore, CLSM was utilised to further examine the lipid fouling phenomena.

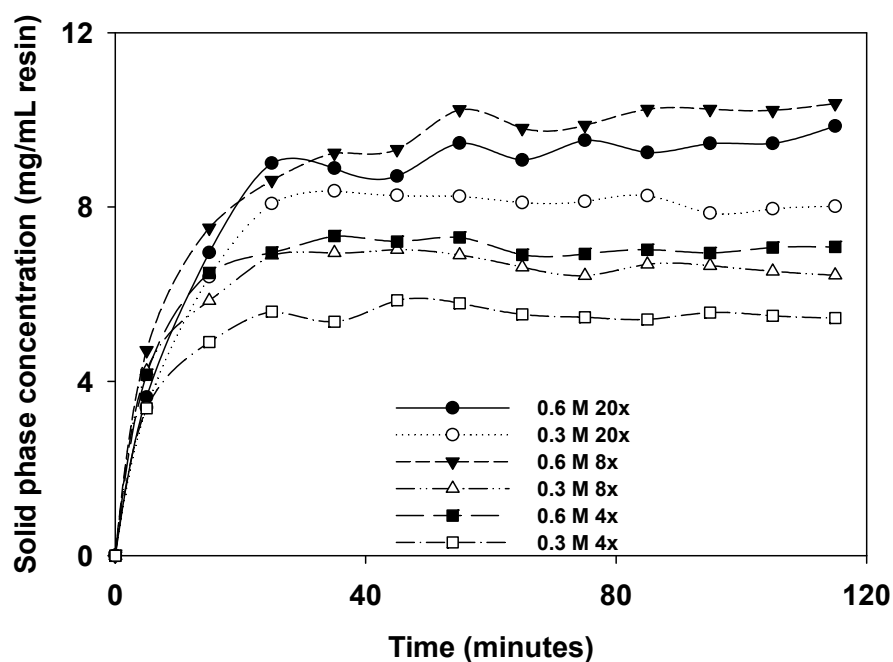


Figure 4-15: Batch uptake curves of proteins in process feed by Sepharose® Butyl-S 6 Fast Flow at 0.6 (dark) and 0.3 M (light) $(\text{NH}_4)_2\text{SO}_4$. Feed to resin volume ratios tested were 20:1(20x), 8:1(8x) and 4:1(4x). Standard deviations of all data (triplicate samples) were within 5%.

4.3.4 Investigation of material uptakes under the effect of fouling by CLSM

In order to visualise the lipid foulant build-up, intra-particle concentration profiles of fluorescently labelled neutral lipids in the process feed were followed in a miniaturised flow cell under CLSM.

4.3.4.1 Effect on mass transport by salt concentrations

Previous results showed that adsorption isotherms and batch uptake rate differed significantly between the high and low salt conditions. Thus, to further explore the effect of adsorption conditions on lipid fouling, three mobile phases of various salt concentrations (0.6 M, 0.3 M and no ammonium sulphate) were included in the flow cell experiment (Section 2.4.3). The measured intra-particle fluorescence intensity has been corrected for light attenuation effect using the same method described by Susanto et al. (2006) (Section 4.2.3.1). Control experiments were also performed (Section 4.3.2.1), and the result showed that the effects on material adsorption from the artefacts of labelling were negligible.

The CLSM data showed a distinct change in the uptake profiles from a sharp to diffuse front at the decreasing salt concentrations, indicating a shift in the dominant mode of mass transport from pore to homogenous diffusion (described in Section 4.2.4). Even though hydrophobic interaction was the strongest at 0.6 M $(\text{NH}_4)_2\text{SO}_4$, lipid diffusion appeared to be the slowest, where the build-up of lipids was primarily concentrated in the area adjacent to the rim of the bead (Figure 4-16). In contrast, at the intermediate salt concentration lipids were able to diffuse further and faster into

the beads (Figure 4-17). In the absence of ammonium sulphate, lipids reached the centre of the bead instantly achieving saturation under two minutes (Figure 4-18).

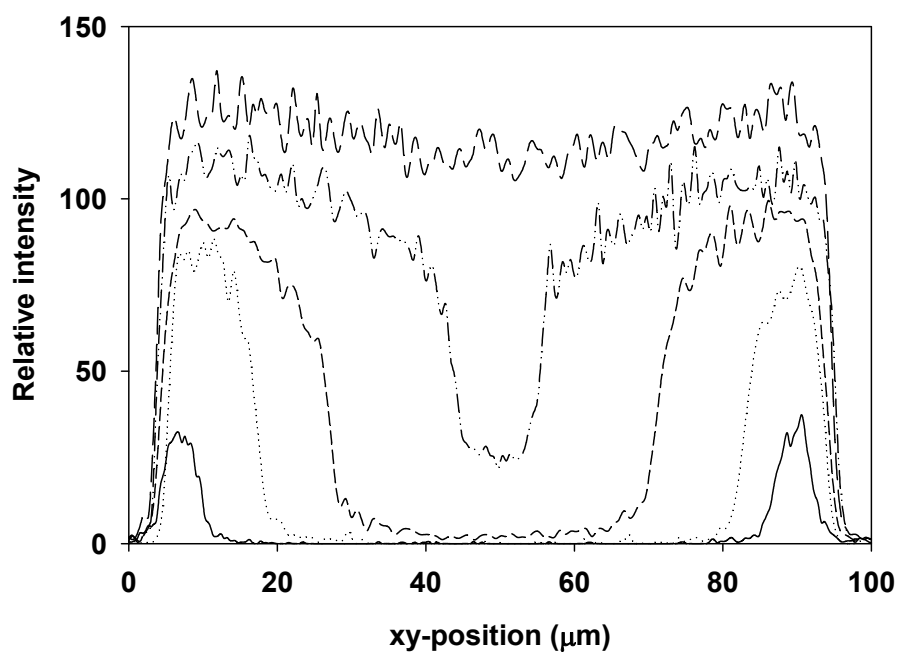
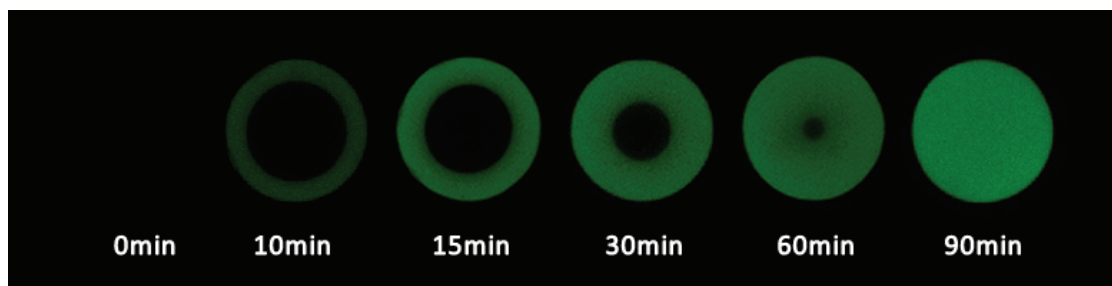


Figure 4-16: Time series of bead cross-sections (10, 15, 30, 60, and 90 min) during the uptake of Bodipy[®] 493/503 labelled lipids from process feed to fresh Sepharose[®] Butyl-S 6 Fast Flow beads at 0.6 M (NH₄)₂SO₄ concentration, pH 7.0 and flow rate of 200 cm/h.

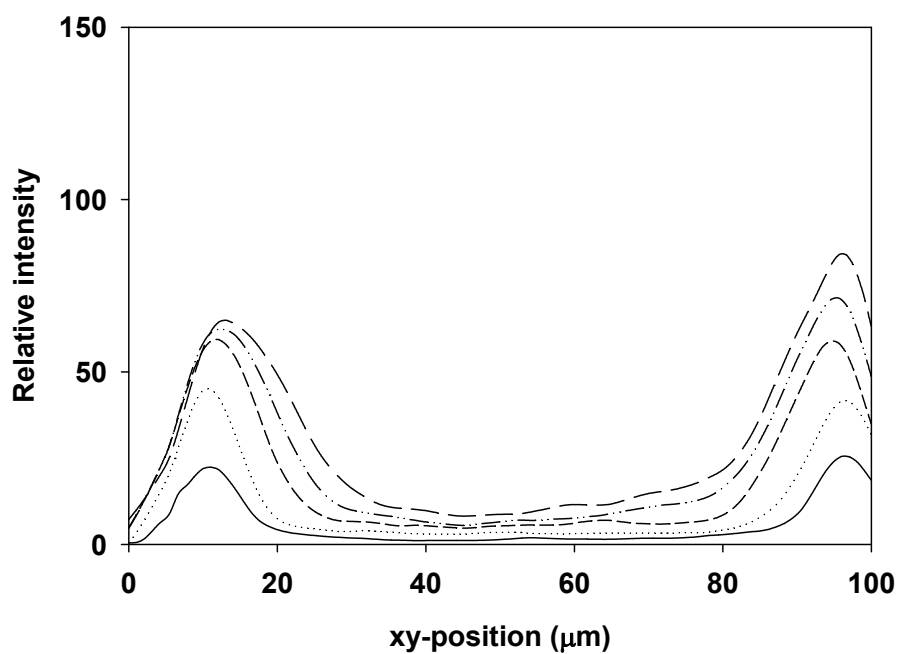
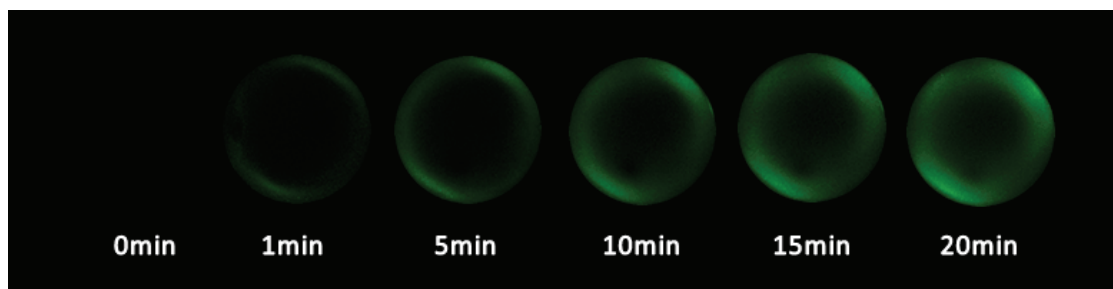


Figure 4-17: Time series of bead cross-sections (1, 5, 10, 15, and 20 min) during the uptake of Bodipy[®] 493/503 labelled lipids from process feed stream to fresh Sepharose[®] Butyl-S 6 Fast Flow beads at 0.3 M (NH₄)₂SO₄ concentration, pH 7.0 and flow rate of 200 cm/h.

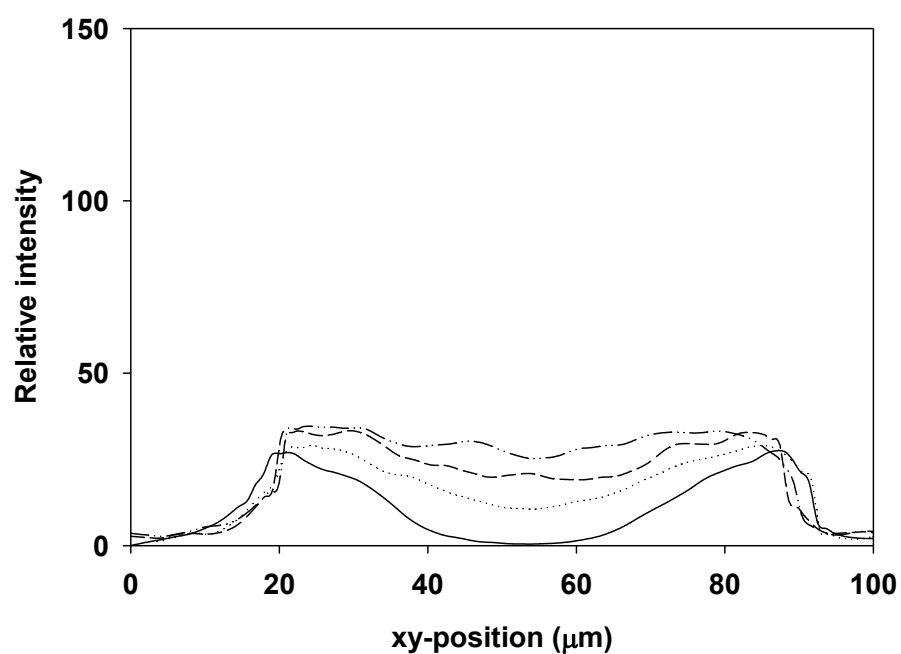
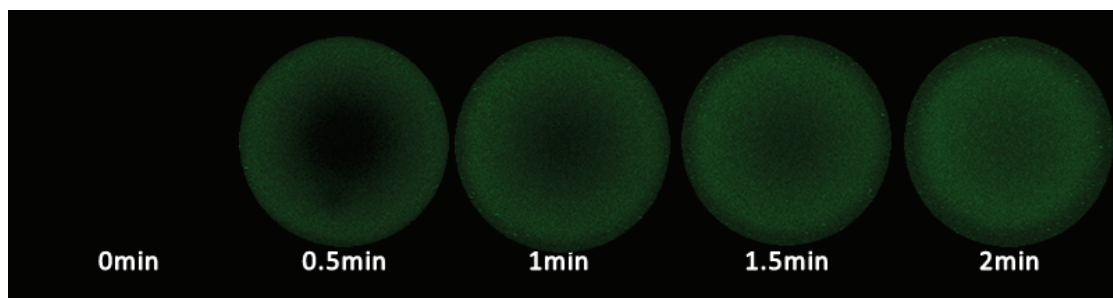


Figure 4-18: Time series of bead cross-sections (0.5, 1, 1.5, and 2 min) during the uptake of Bodipy[®] 493/503 labelled lipids from process feed to fresh Sepharose[®] Butyl-S 6 Fast Flow beads in the absence of $(\text{NH}_4)_2\text{SO}_4$, pH 7.0 at flow rate of 200 cm/h.

This exact phenomenon has also been reported by several other studies (Dziennik et al., 2005; Harinarayan et al., 2006; Linden et al., 2002), all of which showed a transition from pore to homogenous diffusion during the uptake of pure protein solution on an ion-exchange resin using mobile phases with increasing ionic strengths. Harinarayan et al. (2006) suggested that the slow diffusion was due to the hindrance posed by the electrostatic repulsion from the adsorbed protein layer to the incoming charged proteins at the particle boundary. However, the occurrence of such phenomenon on the current HIC resin strongly indicates that although the suggested protein–protein electrostatic interaction is not entirely negligible, diffusion hindrance should primarily originate from the steric resistance to intra-particle diffusion, more specifically, pore blockage resulted from the multilayer adsorption as suggested by Susanto et al. (2007).

4.3.4.2 Effects of diffusion hindrance

To visualise the possible diffusion hindrance caused by lipid build-up, a protein probe is required, as HBsAg VLP is most likely to be excluded from the beads due its size even in the absence of pore blockage. Thus, fluorescently labelled BSA as a probe was added in the process feed, and its intra-particle diffusion profile was examined under CLSM (Section 2.4.4). Although it is preferable to directly label the yeast proteins, the specificity of labelling was difficult to achieve in such complex feed stream. Additionally, there is no effective means of removing the unbound dye molecules without significantly altering the feed property. For example, the most commonly used SEC method will at the same time unavoidably eliminate feed

components that are of similar size to the dye molecule. Thus, alternatively pure BSA-Alexa[®] 555 probe was employed.

In the control experiment, the diffusion of pure BSA displayed a typical homogenous profile at 0.6 M (NH₄)₂SO₄ (Figure 4-19). As mentioned previously (Section 4.2.4), homogenous diffusion, in contrast to pore diffusion, generally occurs at weak adsorption strength, where surface diffusion is significant. The intrinsic surface polarity of BSA resulted in a loose binding between itself and the hydrophobic resin, providing sufficient mobility for the adsorbed BSA to undergo surface diffusion, hence the homogenous diffusion profile. Further, the currently employed Butyl-S resin is the weakest in the HIC series, thus BSA adsorption is unlikely to cause diffusion hindrance as confirmed by the rapid diffusion observed.

At the beginning of the actual experiment (Figure 4-20), BSA in the process feed was able to rapidly diffuse to the centre of the bead the same way as that in the control experiment, while lipids first built up at the rim of the bead and moved inward slowly. However, as the accumulation of lipids rose, external BSA was apparently not able to pass through this adsorbed lipid layer. Thus, this is a clear evidence of diffusion hindrance caused by lipid build-up.

On account of the physical and chemical properties of lipids and BSA, two possible mechanisms are proposed. First, the multilayer adsorption of lipids reduced size of the pores and might lead to complete pore blockage in the acute case. This steric hindrance was specific for BSA because the hydrodynamic radius of an average protein is at least an order of magnitude larger than that of lipids. Thus, while external lipids might still be small enough to pass through, BSA could not. Second, due to the

hydrophobic effect, the intrinsic surface polarity of BSA may prevent it from entering a passage surrounded by highly hydrophobic materials such as lipids.

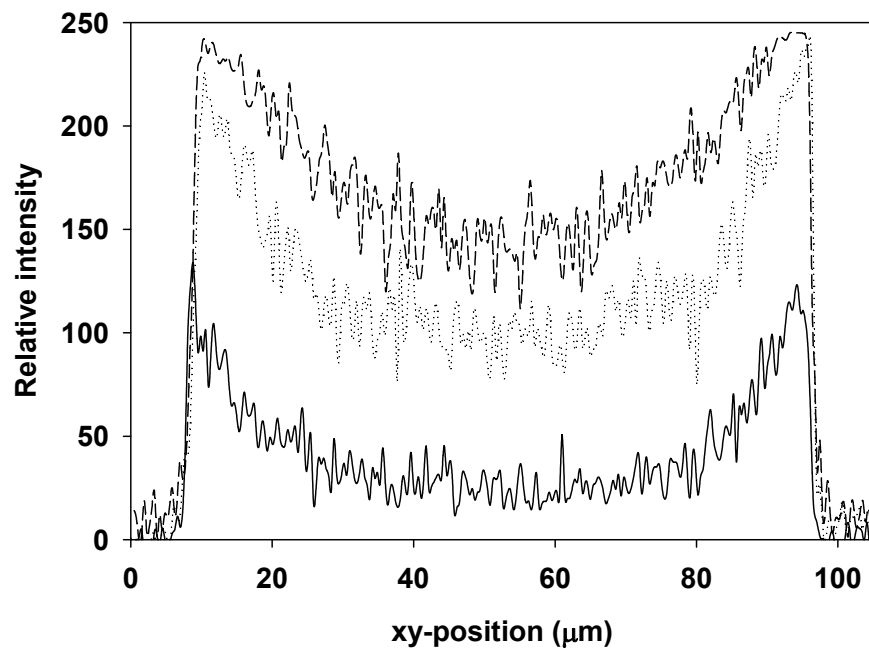
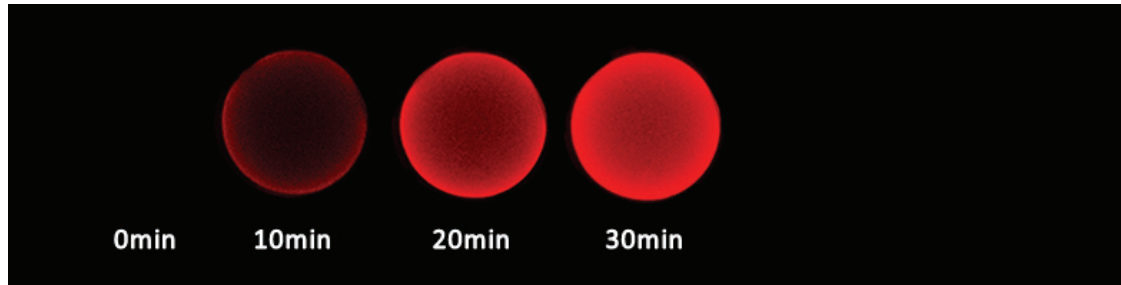


Figure 4-19: Time series of bead cross-sections (10, 20, and 30 min) during the uptake of pure BSA-Alexa[®] 555 to fresh Sepharose[®] Butyl-S 6 Fast Flow beads at 0.6 M (NH₄)₂SO₄, pH 7.0 and flow rate of 200 cm/h.

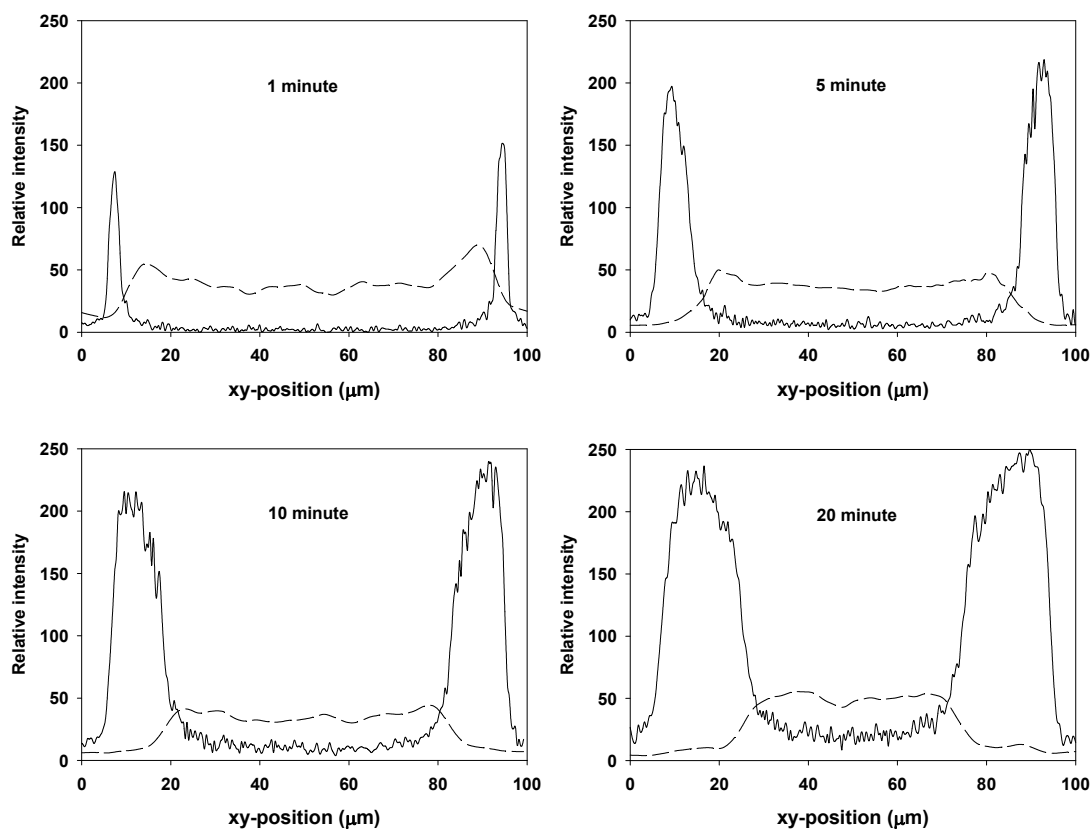
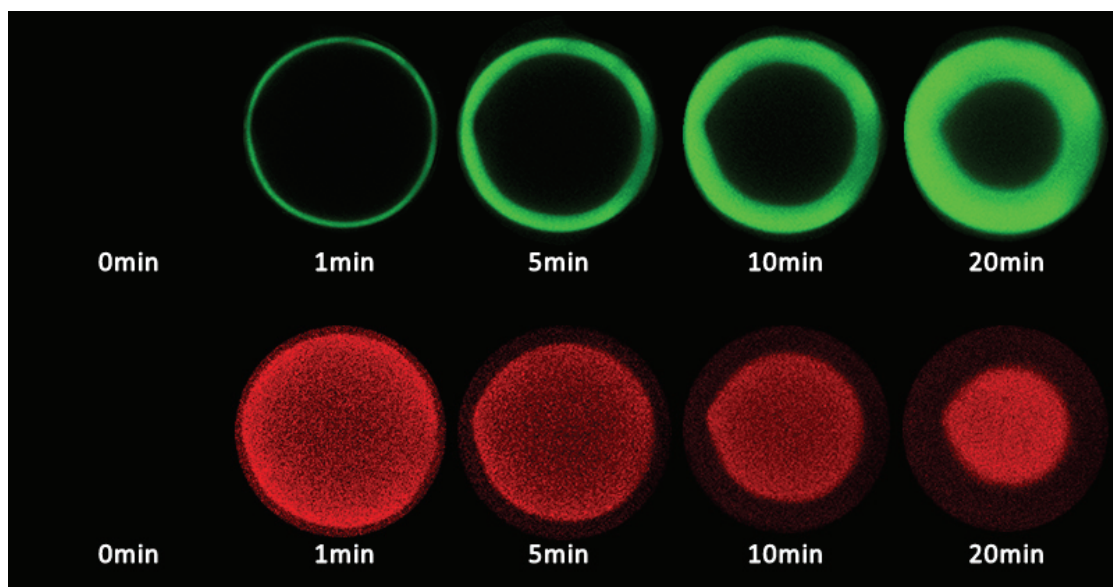


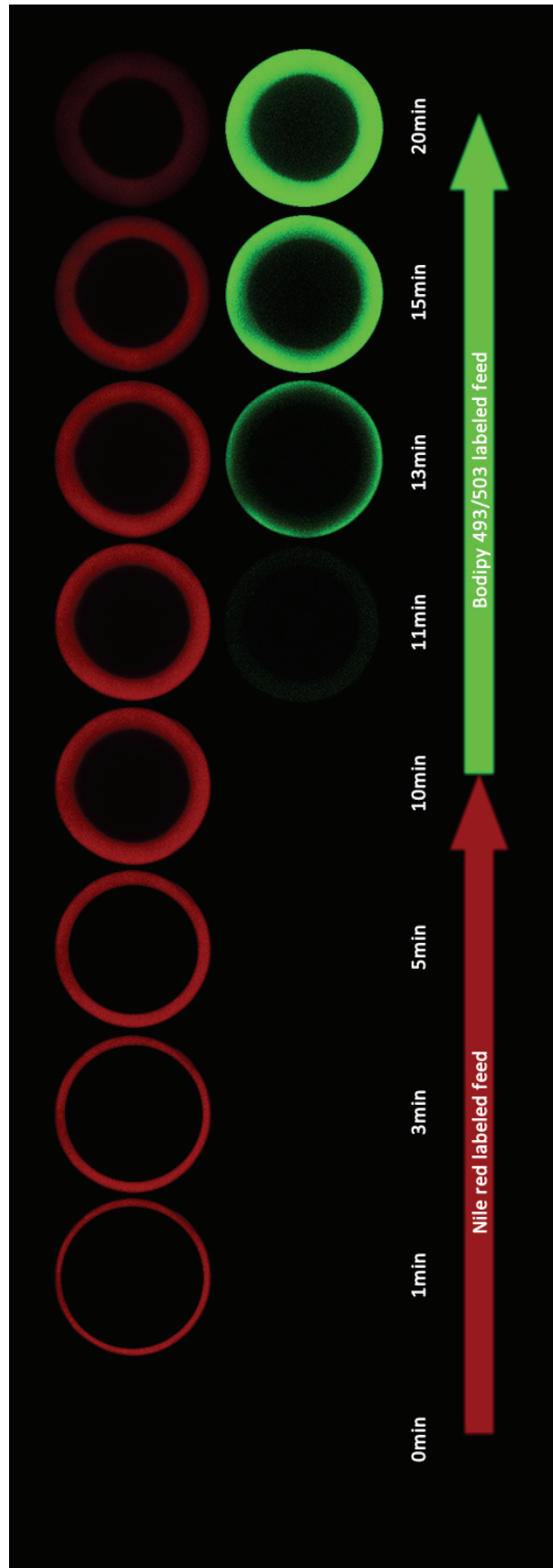
Figure 4-20: Time series of bead cross-sections (1, 5, 10, and 20 min) during the competitive uptake of Bodipy[®] 493/503 labelled lipids (green and solid lines) and BSA-Alexa[®] 555 (red and dash lines) from process feed to fresh Sepharose[®] Butyl-S 6 Fast Flow beads at 0.6 M $(\text{NH}_4)_2\text{SO}_4$, pH 7.0 and flow rate of 200 cm/h.

4.3.4.3 Irreversible adsorption of lipids

Pore blockage is thought to be caused by multilayer adsorption under favourable binding conditions (Dziennik et al., 2005). Thus, it would be interesting to visualise the origin and build-up of such multilayer at the intra-particle level. However, limited by the current CLSM system, it was not possible to obtain such information, thus alternative must be sought.

At adsorption equilibrium, there is a constant exchange of the adsorbed and free materials at the binding sites (Smith et al., 1953). One prerequisite of multilayer adsorption is the irreversible binding, as the vertical build up of materials requires an immobilised foundation. Once bound, the top layer will shield and prevent the lower layers from participating in the equilibrium. Therefore, by monitoring lipid exchange, the extent of irreversible binding within the beads can be revealed, which serves as an indication of multilayer adsorption.

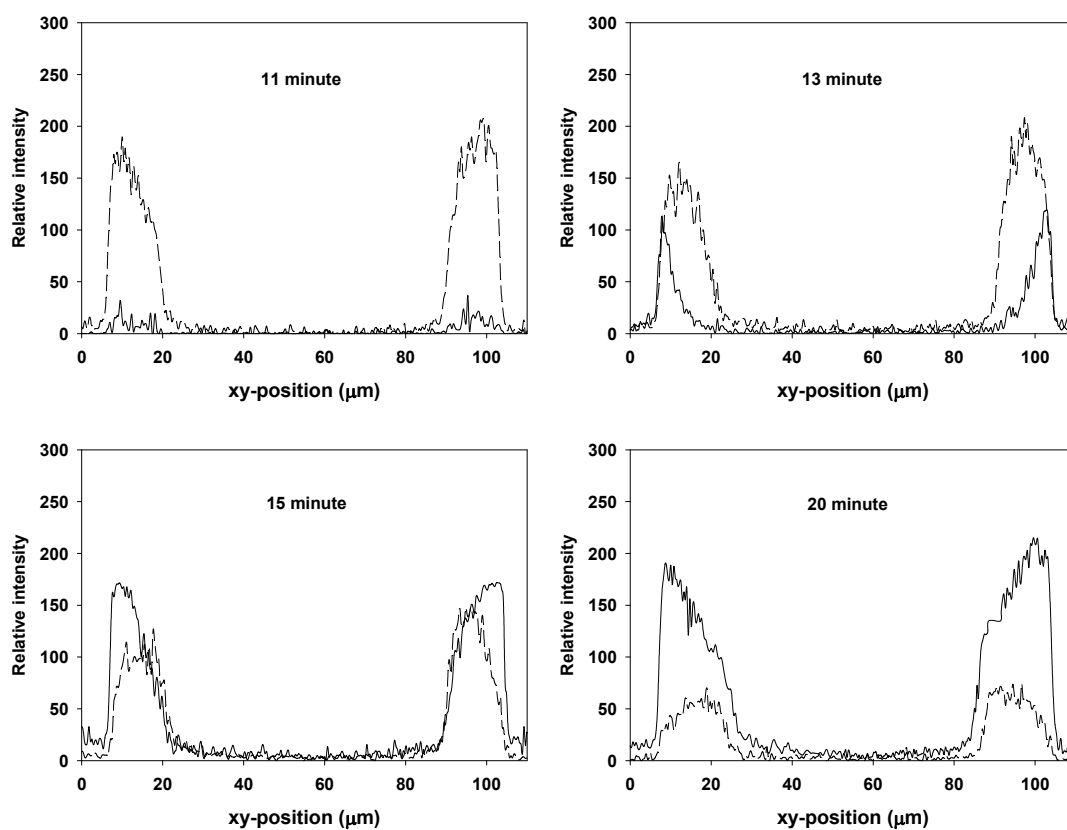
In the experiment (Section 2.4.5), the Nile red labelled feed was first loaded onto the flow cell for 10 minutes. It was then switched to the Bodipy[®] 493/503 labelled feed, and the loading continued for another 10 minutes. As shown in Figure 4-21, within three minutes of applying the Bodipy[®] 493/503 labelled feed, a thin concentration ring of the ‘new’ lipids was visible at the particle boundary, which rapidly displacing the adsorbed ‘old’ lipids. As the loading continued, there was still a significant amount of the ‘old’ lipids remained adsorbed. In order to quantify this, relative capacity was calculated from the fluorescence intensity profiles using the method described in Section 4.2.3.2. Figure 4-22 shows that displacement of the ‘old’ lipids started to level off at 40% towards the end of the 10 minute loading of the Bodipy[®] 493/503 labelled feed. Therefore, about 40% of the lipids adsorbed during



(a)

Figure 4-21: (a) Time series of bead cross-sections during the uptake of neutral lipids from process feed to fresh Sepharose® Butyl-S 6 Fast Flow beads. The column was first loaded with the Nile red labelled feed (red and dash lines) for 10 min, followed by another 10 minutes with the Bodipy® 493/503 labelled feed (green and solid lines). The operating conditions were 0.6 M $(\text{NH}_4)_2\text{SO}_4$, pH 7.0 and flow rate of 200 cm/h.

the first 10 minutes of loading were irreversible bound, a significant portion of which was likely to be in the multilayer state.



(b)

Figure 4-21: (b) Time series of bead cross-sections (11, 13, 15, and 20 min) during the uptake of neutral lipids from process feed to fresh Sepharose[®] Butyl-S 6 Fast Flow beads. The column was first loaded with the Nile red labelled feed (red and dash lines) for 10 min, followed by another 10 minutes with the Bodipy[®] 493/503 labelled feed (green and solid lines). The operating conditions were 0.6 M (NH₄)₂SO₄, pH 7.0 and flow rate of 200 cm/h.

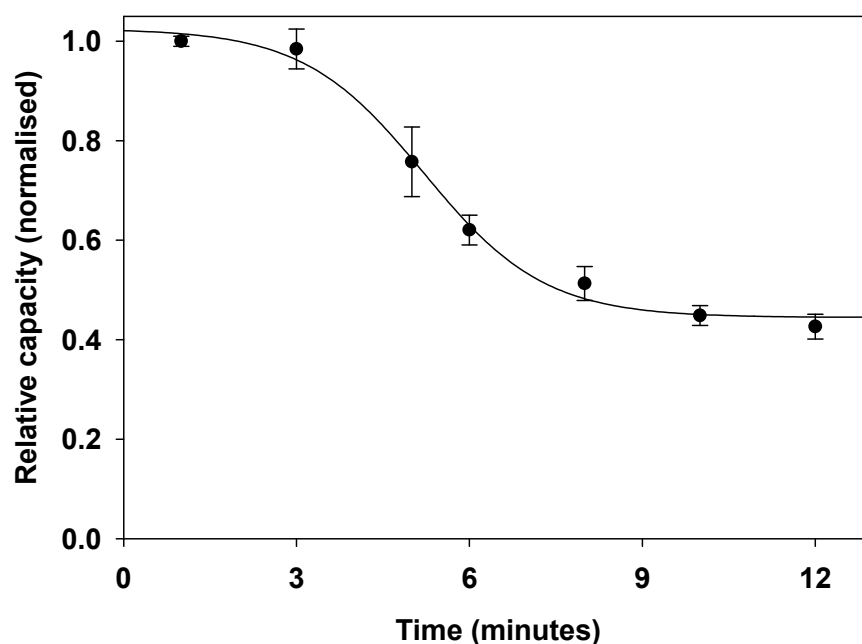


Figure 4-22: Fractions of the remaining adsorbed Nile red labelled lipids from the previous 10 minute during the continuous loading of Bodipy[®] 493/503 labelled lipids from the process feed. The operating conditions were 0.6 M (NH₄)₂SO₄, pH 7.0 and flow rate of 200 cm/h. Error bars correspond to standard deviation from triplicate samples.

So far, the investigation had been focused on material uptake during the loading stage, which addressed the immediate effect of lipid fouling on product binding capacity. In order to further account for the long-term deteriorative impact on column performance as seen in Chapter 3, bead samples collected at different stages during the column life-time were examined.

4.3.5 Visualisation of lipid fouling by SEM

Results from previous experiments confirmed that there were significant amount of lipids irreversibly bound to the resin during loading. However, whether these irreversible bindings were permanent, i.e. they were not subsequently removed at the elution or CIP stage, was still unknown. Therefore, in order to visualise the lipid accumulation that resulted from repeated cycles of operation under real process conditions, bead samples from the fouling experiment described in Section 3.2.5 were examined using SEM (Section 2.2.7).

High-resolution SEM images show a distinct difference in bead surface morphology between the resin samples (Figure 4-23). In a fresh bead, the texture of the bead surface was well-defined and the highly porous ultra-structure was clearly visible. Such state remained largely unaltered even after the first cycle of operation. In contrast, after 40 cycles an apparent bulky layer of materials was caking up on the surface covering all pores. Figure 4-24, which was imaged at lower magnification, gave a wider coverage of the bead, confirming the thickness of this foulant layer. Several large pieces of material were also seen attached to bead surface. Their unique texture suggests they were of biological origin, presumably lipid-containing aggregates, rather than artefacts from sample preparation.

The severity of this foulant build-up gives the strongest indication of pore blockage yet. Although such diffusion hindrance will not affect HBsAg VLP to the same extent as proteins and other small molecules, the gradual changes in resin surface properties due to this material build-up will inevitably affect the binding capacity and strength of HBsAg VLP over time. Such deviations in column performance were evidenced in Section 3.2.5, which showed that column became

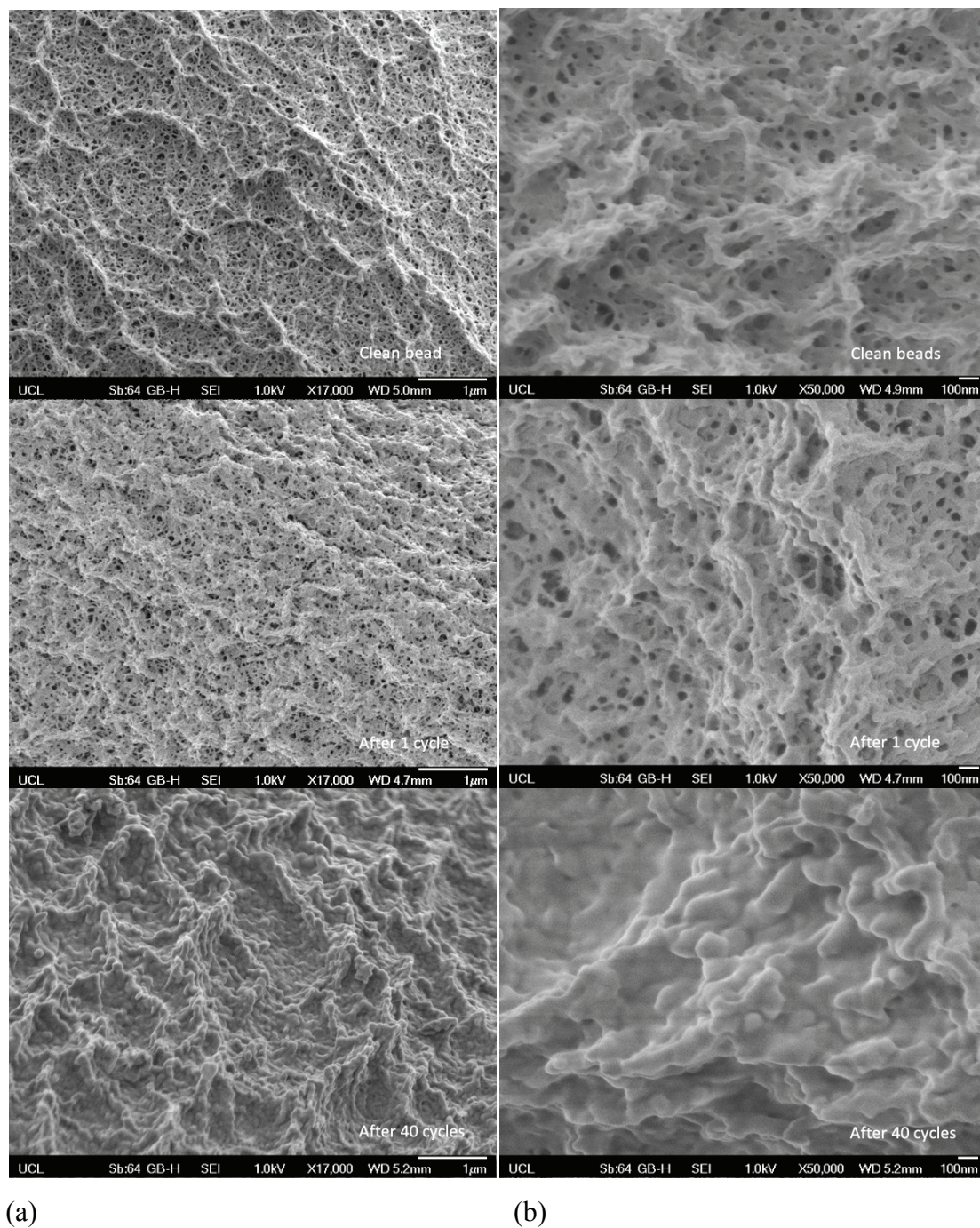


Figure 4-23: Scanning electron microscopy images of Sepharose® Butyl-S 6 Fast Flow bead from fresh resin and those at the end of 1 and 40 cycles of operation. (a) Magnification X17,000. (b) Magnification X50,000.

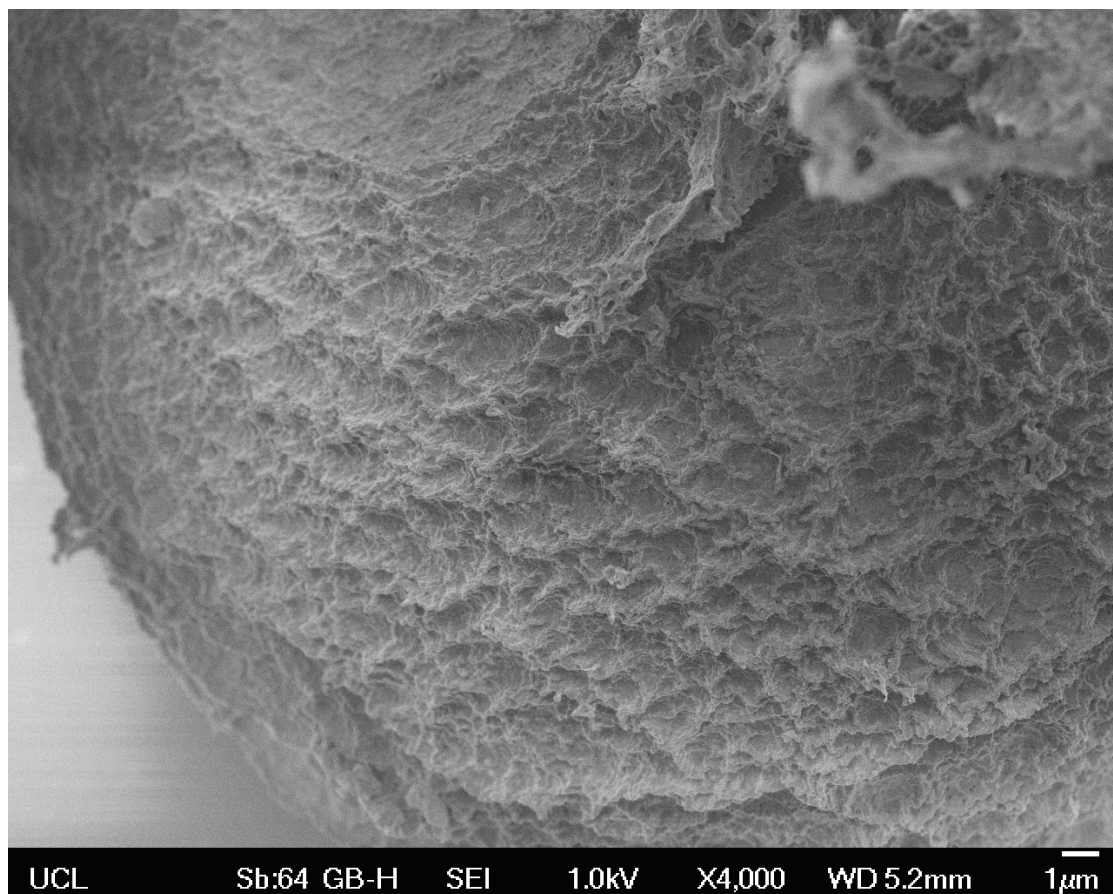


Figure 4-24: Scanning electron microscopy images of Sepharose® Butyl-S 6 Fast Flow bead at the end of 40 cycles of operation. Magnification X4,000.

more hydrophobic over its lifetime, leading to a higher capacity but lower recovery for the HBsAg VLP.

As previously mentioned, there was restricted mass transport at the contact point between two beads in a packed bed. The area inside and outside the contact point will therefore experience different amounts of feed material hence the levels of fouling. Such instance was captured in Figure 4-25, which shows a circular patch that is distinguishable from rest of the bead surface. As expected, within the boundary (area B) there was a clear area showing pores and surface texture similar to those in

the fresh beads. In comparison, the area outside the contact point (area A) resembled the foulant coating as seen previously after 40 cycles.

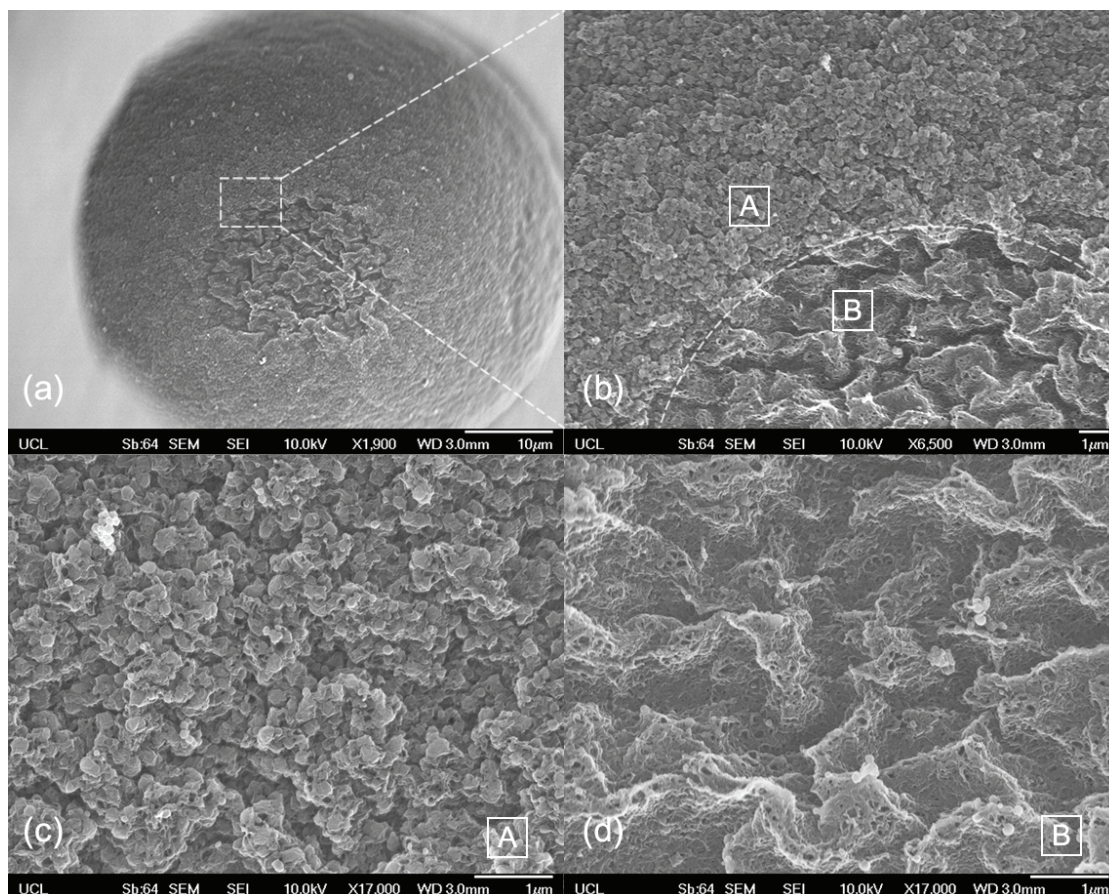


Figure 4-25: Scanning electron microscopy images of a fouled Sepharose[®] Butyl-S 6 Fast Flow bead showing an area of contact between beads, i.e. bead contact point. (a) Whole bead. Magnification X1,900. (b) Boundary of the bead contact point. Magnification X6,500. (c) Bead surface outside the contact point. Magnification X17,000. (d) Bead surface inside the contact point. Magnification X17,000.

In order to confirm that lipids were the major component in the surface material layer, samples were treated with osmium tetroxide (Section 1.4.4), which stains cellular lipids through the oxidative reaction with their unsaturated carbon-

carbon bonds. As a heavy metal, osmium atoms are extremely electron dense, thus detector can easily pick up the resulting secondary backscattered electrons revealing spatial distribution of the lipids. SEM images produced as such (Figure 4-26) confirm the abundance of lipids in the area outside (area A) but not within the contact point (area B).

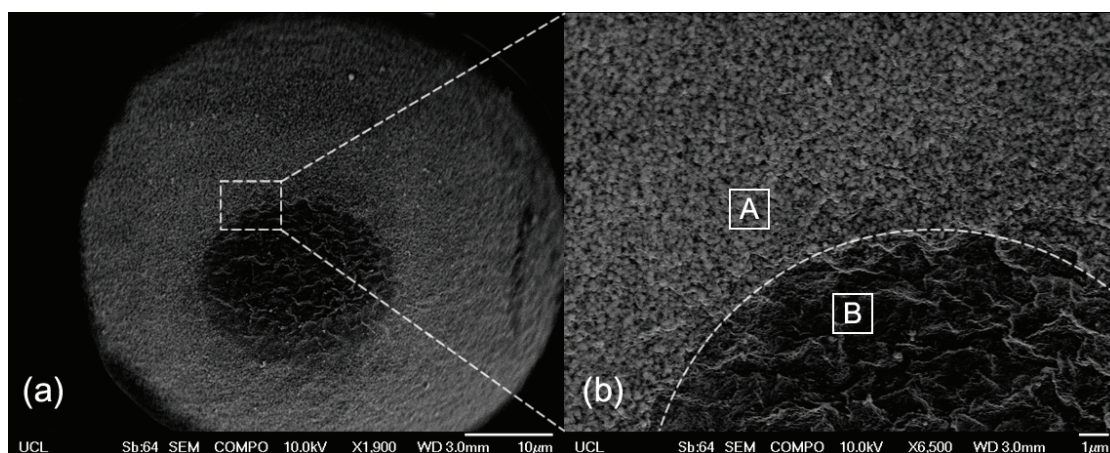


Figure 4-26: Scanning electron microscopy images from secondary emissions of a fouled Sepharose Butyl-S 6 Fast Flow bead labelled with Osmium showing an area of contact between beads, i.e. bead contact point. (a) Whole bead. Magnification X1,900. (b) Boundary of the bead contact point. Magnification X6,500.

4.3.6 Investigation of lipid fouling within a column

4.3.6.1 Quantitation of lipid fouling within a column

In order to quantify lipid fouling within a column, the process feed was labelled with Bodipy[®] 493/503. Following the method described in section 2.3.4, the

columns were operated for various numbers of cycles (1, 10 and 40 cycles). For in-column spatial information of the lipid build-up, at the end of each experiment resin was pushed out in three equal portions (top, middle and bottom) using a custom column sectioning tool (Section 2.4.6) and examined under CLSM immediately.

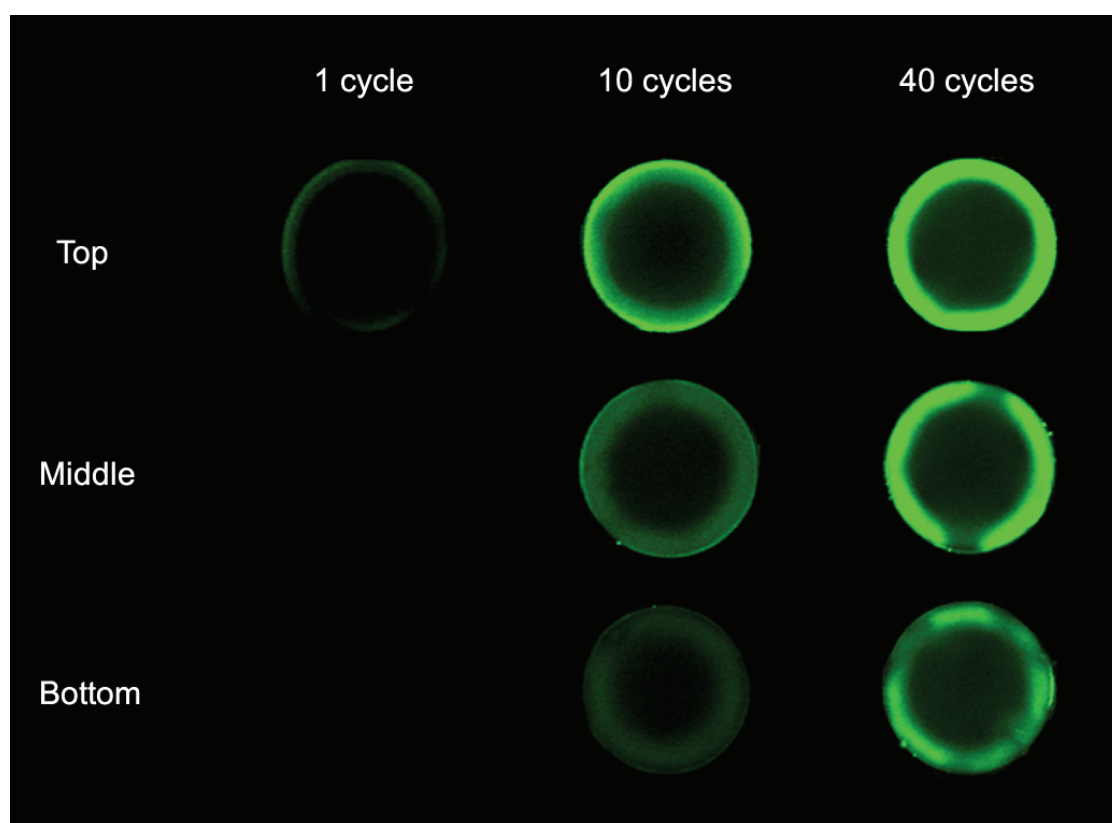


Figure 4-27: Typical beads chosen from the three column sections (top, middle and bottom) after 1 cycle, 10 cycles and 40 cycles of operation. Neutral lipids in the process feed were labelled with Bodipy[®] 493/503 (green). Bead contact point can be seen as breaks in otherwise bright rings.

The CLSM images (Figure 4-27) showed that the level of lipid foulant accumulation increased with the cycles of operation. Within a column, the top section was subjected to the heaviest fouling, followed by the middle and then the bottom

section. In addition, contact points were clearly visible as breaks in otherwise bright rings, supporting the previous finding that mass transport was severely restricted inside the area (Hubbuch et al., 2002; Siu et al., 2006b)(Dziennik et al., 2005; Hubbuch et al., 2002; Siu et al., 2006b).

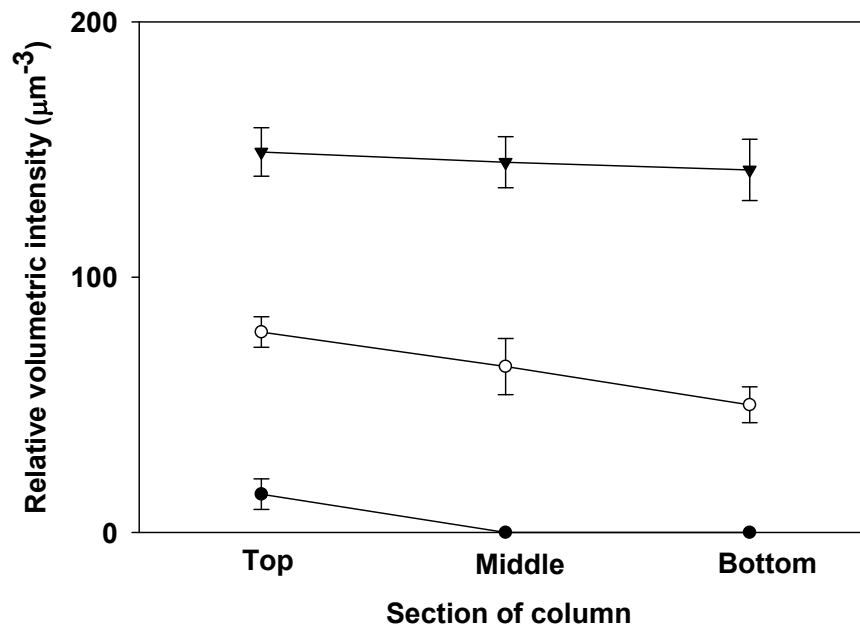


Figure 4-28: Intra-particle relative volumetric intensity of fluorescence from the Bodipy[®] 493/503 labelled process feed at top, middle and bottom section of the column, after 1 cycle (●), 10 cycles (○) and 40 cycles (▼) of operation. Error bars correspond to standard deviation from thirty samples.

Quantification was performed by calculating the relative volumetric intensity of fluorescence using the method described by (Hubbuch et al., 2002) (Section 4.2.3.2). Apart from the lower two sections of the 1 cycle column, all other samples showed various degrees of lipid accumulation (Figure 4-28). In the top section, where

fouling was thought to be the heaviest, the volumetric intensities were 15, 78.5 and 149 in the 1, 10 and 40 cycle column respectively. Meanwhile, the levels of lipid deposit were significantly lower towards the bottom half in both the 1 and 10 cycle columns. This suggests that lipid foulant bound to the top section of the column more readily, probably due to the fact that it was the first area that they came into contact with during loading. Thus, very limited lipid foulants were available for the lower sections, hence they were less affected. However, such variation was less noticeable in the 40 cycle column. This is possible due to the saturation of lipid foulant in the top section after prolong exposure to the process feed. So instead, lipid foulant started to accumulate in the lower sections of the column.

As the circular shape of the column cross-section was reasonably maintained when transferring the column section onto the glass slide, it was possible to examine the variation of lipid foulant deposits in the horizontal cross-section of the column. T-test result (standard error = 2.4, standard deviation = 10.9, two tailed P = 0.83) indicated no significant difference between the centre and outer edge (column wall adjacent) of the column. However, issues of accuracy were present when attempting to slice the column into thin pieces without disrupting the location of beads.

To investigate whether there was any correlation between origin of the long-term lipid foulant accumulation and the short-term lipid uptake during loading, comparisons were made with results from the flow cell uptake experiment (Section 4.3.4.1). Figure 4-29 shows that despite having processed approximately 80 column volumes (80 mL at 1 mL/min) of the process feed after 40 cycles of operation, vast internal area of the bead was still relative unaffected. Nevertheless, lipid foulant deposits at the rim of the bead was seen exceedingly fast. Such observation is

reasonable as can be seen from Figure 4-30 that during the 2 minute loading time of each cycle lipid foulant could only travel a very limited radial distance. Thus, a small portion of the bead, presumably only at the rim, was repeated challenged with an otherwise significant amount of process feed, leading to the severe lipid foulant build-up at the outer surface of the bead as evidenced from the SEM images.

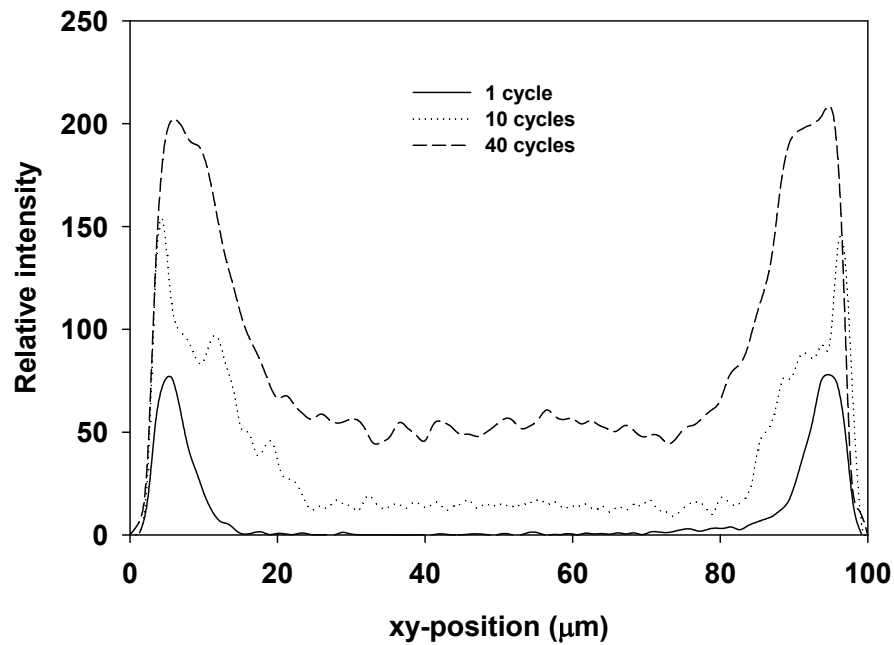


Figure 4-29: Bead cross-section intensity profiles of Bodipy[®] 493/503 labelled lipids from process feed after 1 cycle, 10 cycles and 40 cycles of operation. Bead samples were from top third section of the column.

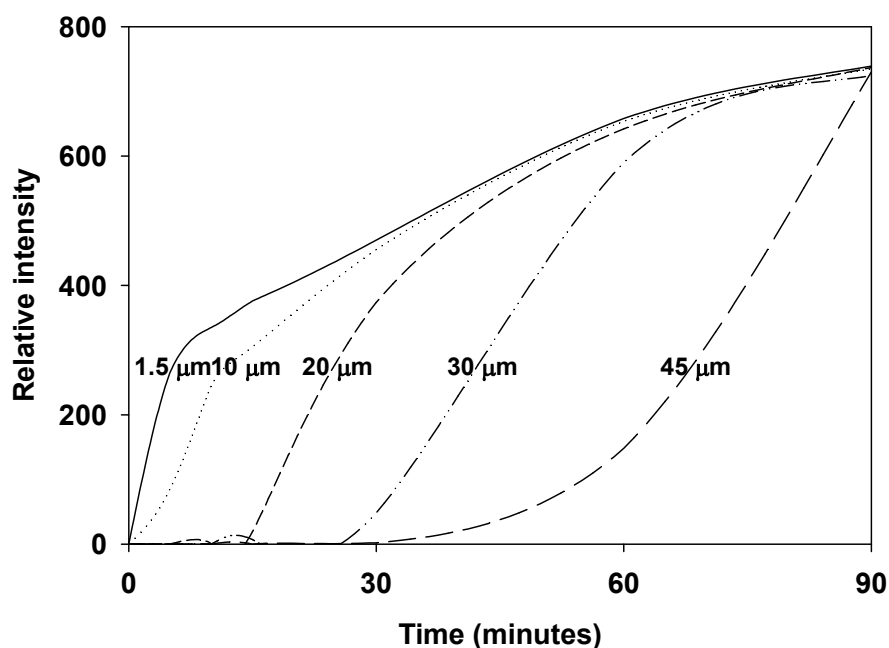


Figure 4-30: Fluorescence intensity of Bodipy[®] 493/503 labelled lipids from process feed at various intra-particle radial position during the uptake by Sepharose[®] Butyl-S 6 Fast Flow beads. Experimental conditions were 0.6 M (NH₄)₂SO₄ pH 7.0 at flow rate of 200 cm/h.

4.3.6.2 Progression of lipid fouling within a column

In order to further confirm the variation in foulant build-up seen at the different column heights, the progression of lipid fouling within a column was followed. Two sets of process feed were labelled with Bodipy[®] 493/503 and Nile red independently (Section 2.4.7). The Bodipy[®] 493/503 labelled feed was used for the first 10 cycles of operation, after which the operation commenced with the Nile red labelled feed for the next 10 cycles. At the end, resin in the column was pushed out, sectioned and imaged under CLSM as previously.

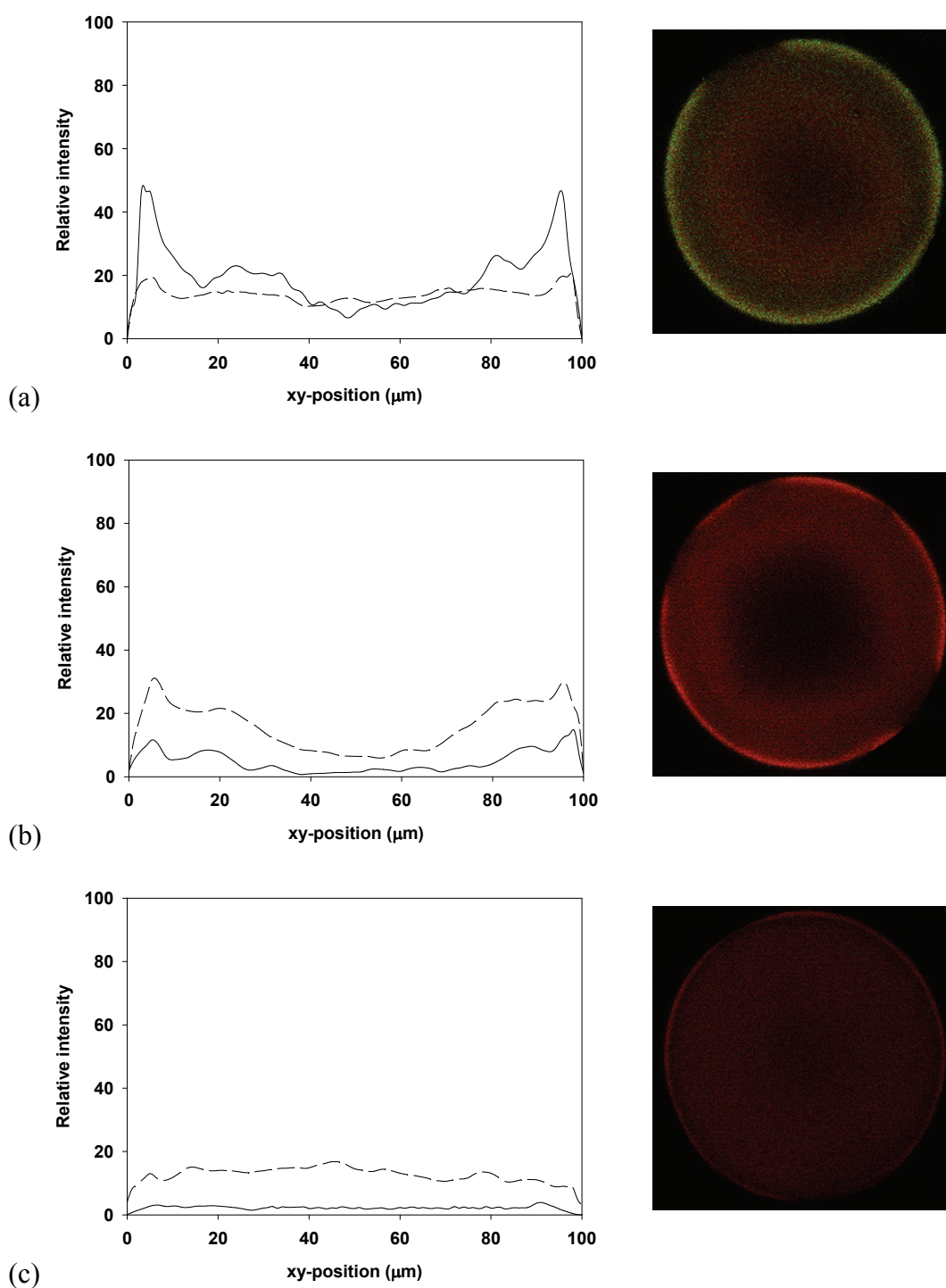


Figure 4-31: Intra-particle distribution of lipid foulant. Fresh Sepharose[®] Butyl-S 6 Fast Flow columns were challenged with Bodipy[®] 493/503 (green and solid) labelled process feed for first 10 cycles of operation and Nile red (red and dash) labelled process feed for the next 10 cycles of operation. (a) Top section. (b) Middle section. (c) Bottom section.

Figure 4-31 shows a different spatial distribution of lipid foulant from the two sets of feeds. The majority of lipid foulant from the first 10 cycles was retained by the top section of the column, while lipid foulant from the next 10 cycles was seen in all three sections, with the middle section contained the most followed by the top and the bottom sections. Thus, this gives a clear indication on the course of lipid fouling within a column. In the early cycles, as the level of lipid foulant was not significant, most of them were retained by the top section. However, as operation continued, more lipid foulant was able to travel downward to the next section, possibly due to either the saturation of the top section or the pore blockages caused by lipid build-up.

4.3.6.3 Dual-peak phenomenon

During data analysis in the previous experiments, it was observed that a large proportion of the beads display a visible outer ring. As seen in Figure 4-32, the outer ring was indicated by the additional peak on the outside edge of the main peak. After quantification (Table 4-7), it became apparent that the occurrence of such dual-peak phenomenon was much more frequent in the bottom half of the column. In fact, more than 50% of the bead samples in the bottom sections showed such phenomenon after 10 or 40 cycles of operation.

Similar phenomena have also been reported by others in studies on competitive uptake between proteins. Dziennik et al. (2005) observed the displacement of adsorbed Cy5-lysozyme by FITC-lysozyme in the outer shell of the bead. The trough of dual peaks in the FITC-lysozyme intensity profile corresponded with an area containing high a level of adsorbed Cy5-lysozyme. Siu et al. (2006)

reported a slight ‘hump’ in the intensity profiles of Cy3-labelled HCP as BSA moved inwards causing them to desorb. Although in the former case the dual-peak phenomenon was observed for the competing material, in the latter case it was the one being desorbed. Thus, competition effects in general may be the cause for such an anomaly. In the current situation, the dual-peak phenomenon could be a result of the competition between lipid foulants and other materials, such as HBsAg VLP or host proteins. However, it is worth pointing out that the subject examined in the current experiments was the permanently adsorbed lipid foulants at the end of a purification cycle, while in those studies it was the material adsorbed during loading.

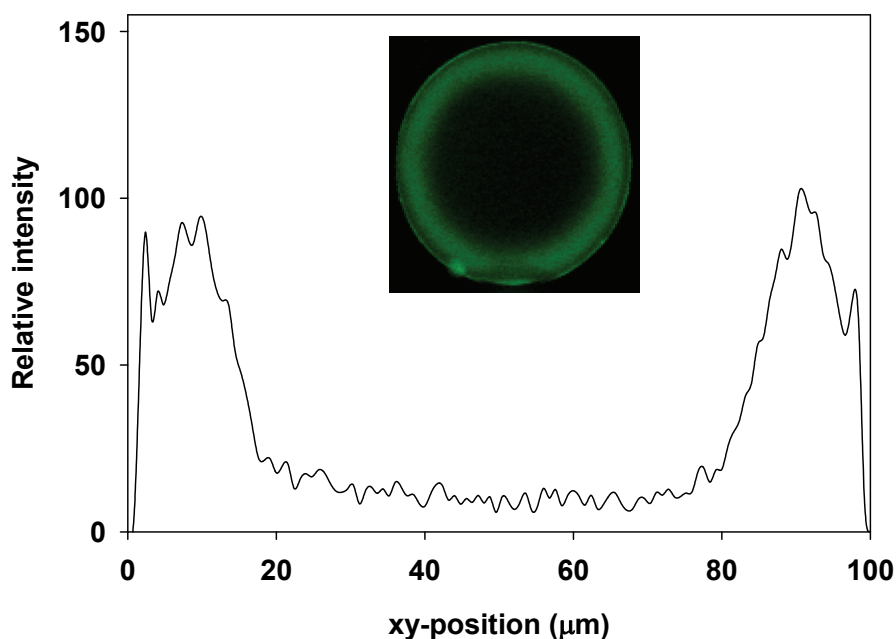


Figure 4-32: Dual-peak phenomenon. Intra-particle intensity profile of Bodipy[®] 493/503 labelled neutral lipids in the bottom section of the column after 10 cycles of operation.

Table 4-7: Percentage of beads displaying dual-peak phenomenon. Each value was determined from an average bead population of 100.

Column section	1 cycle	10 cycles	40 cycles
Top third	0%	0%	0%
Middle third	N.A.	8%	6%
Bottom third	N.A.	55%	50%

N.A: Not available

4.4 Conclusions and proposed lipid fouling mechanism

4.4.1 Summary of findings

Understanding the underlying mechanism of lipid fouling is the prerequisite for process improvement in order to limit its impact on column performance as evidenced in the previous chapter. This study has demonstrated the potential of using novel microscopy techniques in obtaining such knowledge.

In order to first investigate the competitive effect from lipid foulants on other feed components, material adsorption isotherms and batch uptake profiles were followed. In comparison, lipids displayed a disproportionally higher binding capacity. The resulting preferential binding posed strong competition for HBsAg VLP capacity, even causing the displacement of already adsorbed VLP. In addition, the influence on both material adsorption level and uptake rate differed significantly between the low and high salt concentrations, with more deviations from the standard Langmuir model

observed in the latter condition where the hydrophobic interaction was heightened. This salt effect was also evidenced in the CLSM examination, where intra-particle diffusion and adsorption profiles of the fluorescently labelled lipid foulants were monitored microscopically at various salt concentrations. The CLSM images showed a distinct change from pore to homogenous diffusion as the salt concentration decreased, a phenomenon also observed by Dziennik et al. (2005), Harinarayan et al. (2006) and Linden et al. (2002). Furthermore, the accumulation of lipids at the rim of the beads was seen to occur exceedingly fast. Consequently, external protein probes were excluded from the bead due to pore blockage or diffusion hindrance resulted from the adsorbed lipid layer. The elevated level of irreversible binding within the area was then confirmed in the subsequent dual-colour labelling experiment, where exchange of lipids was monitored.

The investigation then proceeded to the examination of the resin conditions caused by the long-term impact of lipid fouling. The intra-particle fluorescence intensity profiles of bead samples collected at different stages during the column life-time showed that lipid accumulation increased with number of operation cycles and majority of the lipid deposits concentrated at the rim of bead, corroborating with the fast lipid build-up in the region observed previously during loading. This was consistent with the small loading volume of each cycle, which led to the rim of the bead being repeatedly challenged with an otherwise significant amount of feed. High-resolution images of the fouled bead surfaces were also obtained using SEM, serving as confirmation of the build-up of a lipid layer on its surface. Additionally, in-column spatial distribution and progression of lipid fouling were visualised by examining bead samples from different positions within the column. Fouling in the top section was

shown to be the heaviest, while significant amount of the beads in the bottom sections displayed the dual-peak phenomenon as evidenced by Dziennik et al. (2005) and Siu et al. (2006b).

From the results, the potential lipid fouling mechanism at both intra-particle and column level are proposed as follows.

4.4.2 Characteristics of lipids and their roles in fouling

Lipids are highly hydrophobic material that have a strong tendency to form aggregates either themselves or other materials. Even though lipid molecules are usually small (~ 1 kDa), the size of its multimers in the form of structures such as micelles (which can self-assemble from lipids) can sometimes be very significant. As a result, high level of lipids in the process feed will present a unique challenge in chromatography purification, especially for hydrophobic interaction chromatography.

Two possible roles of neutral lipids, the most hydrophobic lipid class, in fouling are proposed. First, they compete with HBsAg VLP and proteins for binding sites. This is clearly evident from the previous results that lipid-depleted feed gave a high HBsAg VLP capacity (Section 3.2.5). Further, as seen during the batch uptake experiments, they were able to displace already adsorbed HBsAg VLP under the current process condition. Second, taking into account the hydrophobic nature of lipids, multilayer adsorption of neutral lipids or their multimers is a distinct possibility under favourable adsorption condition, as they could serve potentially as anchors or building blocks.

4.4.3 Effect of adsorption condition on diffusion

The rates of diffusion and adsorption determine the overall rate of material uptake in porous particles, thus it is important to understand the interactions between these two phenomena in the presence of fouling. In a simplistic view, any diffusing molecule is considered to be subject to both the diffusive and adsorptive force (Figure 4-33). At high salt concentration, the heightened hydrophobic interaction will increase the adsorption strength (binding strength), leading to greater conformational ‘spreading’ of the molecule upon adsorption in order to minimise surface exposure to

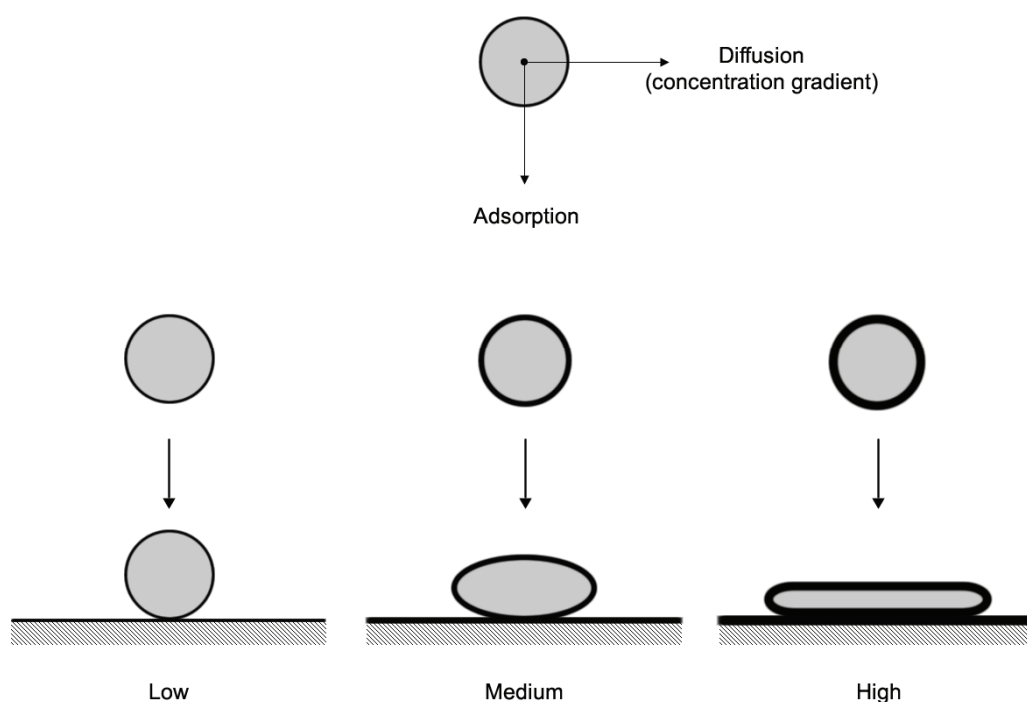


Figure 4-33: Interaction between adsorptive and diffusive forces on a molecule in HIC at low, medium and high adsorption conditions. The hydrophobic strength is indicated by the thickness of the molecule boundary. The extents of conformational change upon adsorption are also illustrated.

the polar mobile phase (Corradini et al., 1994; Oscarsson, 1995b; Tibbs Jones and Fernandez, 2003; Wu et al., 1986; Zoungrana et al., 1997). Such strong interaction makes the adsorbed molecule less mobile, raising the activation energy for lateral movement, i.e. surface diffusion. Thus, the overall diffusion rate is lowered. Furthermore, this localised adsorptive potential will significantly promote the build-up of materials, especially the highly hydrophobic neutral lipids. The resulting multilayer adsorption may lead to the eventual pore blockage causing further diffusion hindrance, the exact phenomenon reported by several other studies (Dziennik et al., 2005; Harinarayan et al., 2006; Linden et al., 2002, Susanto et al., 2007).

4.4.4 Multilayer adsorption

Although multilayer adsorption is a common occurrence, high level of lipids in the process feed will accelerate its formation considerably. As discussed in Section 4.3.3.3, a significant portion of the large increase in lipid capacity from the low to high salt concentration was most likely to be contributed by the multilayer adsorption through lipid-lipid interactions. Due to the highly hydrophobic nature of lipid molecules, once adsorbed they can not only act as anchors slowing down lateral movement and disassociation of the surrounding adsorbed materials, but also provide a stable foundation, which critically also possess the sufficient hydrophobic characteristics required for secondary adsorption. Figure 4-34 illustrates the build-up of a typical multilayer consisting of lipids and other materials.

Once formed, such a layer will be able to attract more materials due to the greater hydrophobicity of its surface, thus accelerating the build-up of the multilayer.

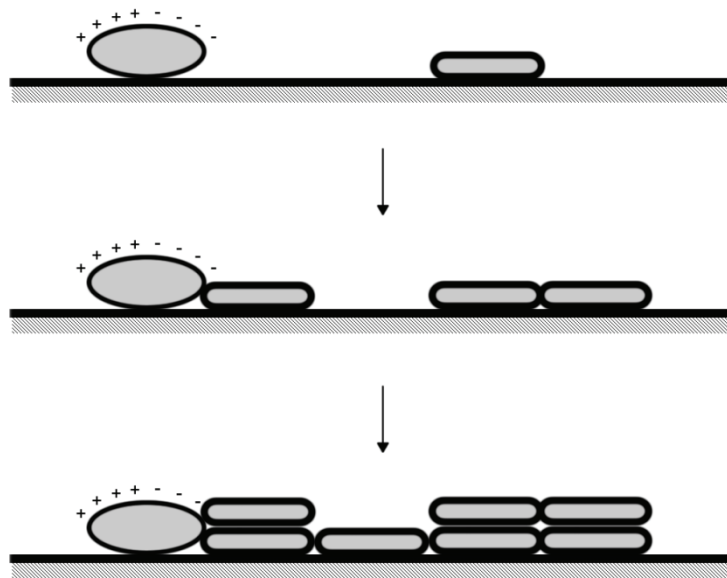
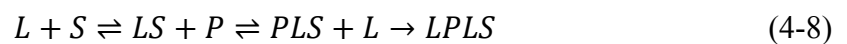


Figure 4-34: Proposed multilayer adsorption in the presence of lipid foulants.

Furthermore, the top layer will not only prevent the lower layers from participating in the material exchange at equilibrium, but also shield them from eluents or CIP cleaning agents. Thus, the level of permanent lipid deposit at the end of each cycle of operation is directly related to the degree of multilayer adsorption. The mechanism of multilayer adsorption in the presence of lipid foulants therefore can be expressed as either



where L is lipid molecule, P is a protein molecule and S is an adsorption site.

4.4.5 Pore blockage

The SEM images (Section 4.3.5) gives the strongest indication of pore blockage, which was caused by the permanent lipid foulant build-up on the bead surface. Even though neutral lipid monomer is small, its more thermodynamically stable micellised or membrane form can however be of significant sizes. Considering the average pore diameter of the Sepharose[®] is approximately 30 nm (Janson and Rydén, 1998; Lenhoff and To, 2007), pore blockages can frequently occur as a result of the extensive multilayer adsorption, leading to the hindered diffusion or even the complete exclusion of incoming materials. As evidenced in Section 4.3.4.2, the BSA probe, which has a hydrodynamic radius 4.3 nm (Bohidar, 1989), were unable to diffuse through the adsorbed lipid layer as illustrated in Figure 4-35.

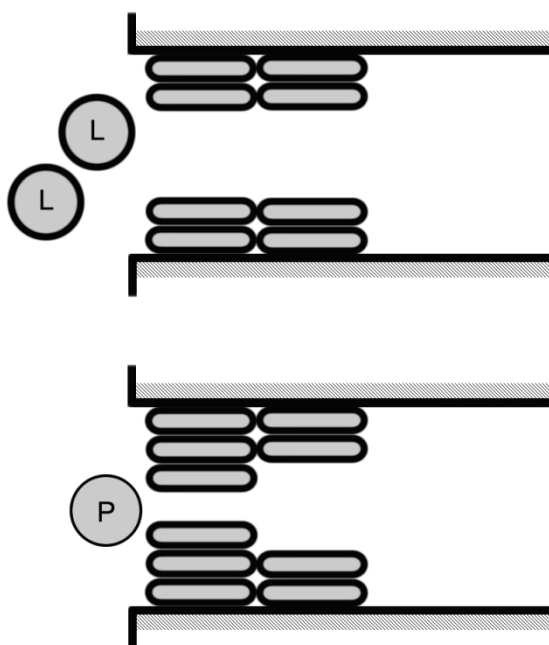


Figure 4-35: Pore blockage due to multilayer adsorption. L: lipids or lipid aggregates. P: proteins.

4.4.6 Lipid fouling mechanism

Based on the findings from the studies performed so far, the following lipid fouling mechanism is proposed (Figure 4-36). Both the immediate and long-term effects on column performance are indicated at the corresponding stages in the lipid fouling process.

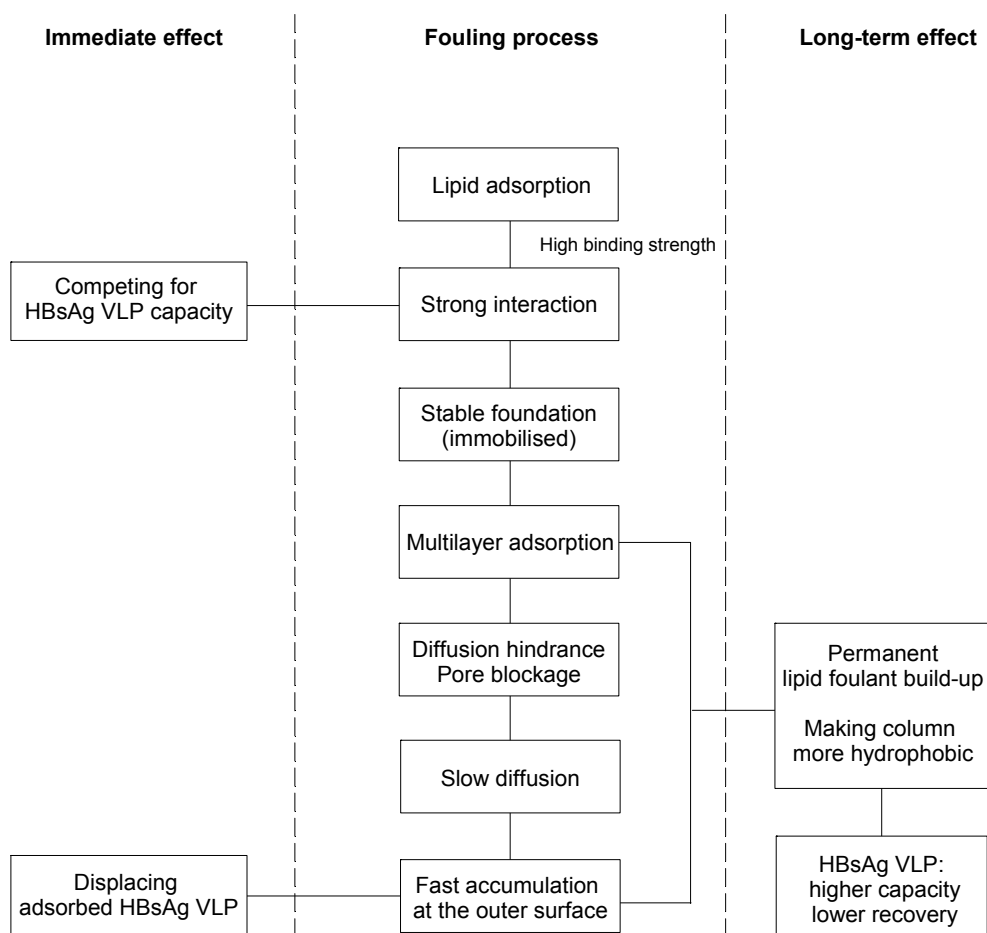


Figure 4-36: Proposed lipid fouling mechanism during the chromatographic purification of yeast-derived HBsAg VLP, including accounts for both the immediate and long-term effects on column performance.

Chapter 5

Investigating the efficacy of pretreatments in lipid removal

This chapter explores the pretreatment options for improving feed quality. Operating conditions in the current downstream process and dedicated lipid removal steps are examined. The efficacy of each strategy in limiting both the short and long-term impacts of lipid fouling is then verified by measuring the improvement on product capacity and robustness in HIC performance.

5.1 Introduction

In the multistage process of HBsAg VLP purification from *Saccharomyces cerevisiae*, the yeast cells need to be first retained and then ruptured as any other process that involves intracellularly expressed products. However, this is further complicated by the fact HBsAg VLP is associated with the ER membrane in manners that cell disruption alone cannot achieve complete isolation, hence an additional detergent liberation step is required. Consequently, such route inevitably introduces a higher level of intracellular contents into the process stream, and these process-related contaminants will adversely affect the performance of the downstream processing steps that follow, such as the HIC capture step as evidenced from the previous chapters. In the current process, relative harsh column regeneration (30% isopropanol) and CIP (0.5 M NaOH) regime were already in place but proved to be ineffective in resisting the lipid build-up. Furthermore, as seen from the previous results the exceedingly high lipid capacity for even the Sepharose[®] Butyl-S resin, the least hydrophobic in the series, suggesting the introduction of feed pre-treatment steps to reduce the lipid level prior to chromatographic purification would be more beneficial. Therefore, this study was setup with aims to improve the feed quality by exploring not only the potential optimised operating conditions in the current process but also the efficiency of dedicated lipid removal steps.

Possible areas of improvement include homogenisation pressure, an additional centrifugation step to remove cytosolic materials after cell disruption, selective precipitation with ammonium sulphate, the use of an adsorptive step such as a depth

filter, e.g. Zeta Plus[®] Delipid filters (3M, Bracknell, UK), or a particulate sorbent e.g. Lipid Removal Agent (Advanced Minerals Corporation, California, USA). Such options have the potential to increase capacity and prolong product recovery over a larger number of loading cycles, thus helping to maintain column performance and so improve the cost-effectiveness of VLP manufacture.

5.2 Theory

5.2.1 Homogenisation

Purification of intracellular products requires cell disruption in order to release the desired material, which is often the first unit of operation immediately after fermentation harvesting. Although a large number of options are available, such as grinding, ultrasonication and enzymatic digestion, high-pressure homogenisation remains the most widely used technique for cell disruption. One such device is the Manton-Gaulin homogeniser as shown in Figure 5-1. This high-pressure pump incorporates an adjustable valve with restricted orifice through which cells are forced at pressures up to 1300 bar (Balasundaram et al., 2009; Doran, 1995).

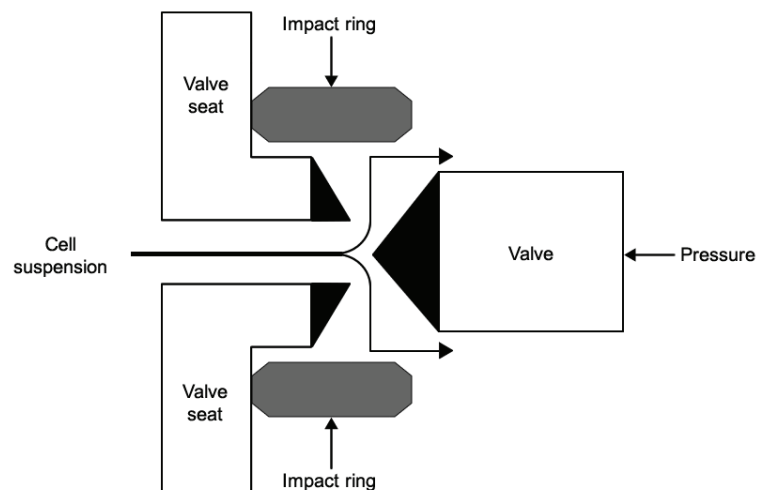


Figure 5-1: Schematic diagram of a typical valve unit inside the high-pressure Manton-Gaulin homogeniser.

The underlying mechanism of disruption in the Manton-Gaulin homogeniser was found to be due to impingement, and the rate of cell breakage related to the stagnation pressure or maximum wall stress of the fluid jet (Moore et al., 1990). Hetherington et al (1971) described the relationship between rate of protein release and operating conditions in such system as (for feed concentration under 600 g/L)

$$\ln\left(\frac{R_m}{R_m - R}\right) = kNp^\alpha \quad (5-1)$$

where R_m is the maximum amount of protein available for release, R is the amount of protein released, k is a rate constant that normally increases with temperature (up to 50 °C), N is the number of passes and p is the operating pressure. The exponent α is a measure of the resistance to disruption from the cells, which varies between cell types and growth conditions (Engler and Robinson, 1981). For *Saccharomyces cerevisiae*, it has an estimated value of 2.9 (Hetherington et al., 1971). Although Equation 5-1 shows that high-temperature, high-pressure and multiple passes are all beneficial to protein release, in practise generally only the high-pressure condition is adopted. This is because the fine cell debris resulted from the large number of passes will often create unnecessary burden for the subsequent clarification steps, and constant cooling (0-4 °C) is required to dissipating the excessive heat generated throughout the homogenisation operation in order to prevent protein denaturation.

5.2.2 Detergent: Triton X-100

Detergents have major applications in protein purifications. In particular, membrane proteins require detergent treatment before they can be solubilised into the process stream and subjected to subsequent operations, such as chromatography.

Being amphipathic, each detergent molecule contains both a polar head group and a neutral (non-polar) carbon tail. While the polar head group interacts with water molecules by forming hydrogen bonds, the carbon tail self-aggregates due to hydrophobic interactions. Unlike membrane lipids such as cholesterol or phospholipids, detergents can form micelles more readily, thus making them significantly more soluble in aqueous solutions (Neugebauer, 1990). Based on the hydrophilic head group, detergents are classified as ionic, zwitterionic or non-ionic. Non-ionic detergents are more efficient at breaking lipid-lipid and lipid-protein interactions than protein-protein interactions and generally considered as mild and non-denaturing in comparison to the other two classes (Linke, 2009). Thus, they dominate the detergent-mediated liberation processes of membrane proteins (Barbero et al., 1984). One of the most commonly used non-ionic detergents is Triton X-100, which contains uncharged polyoxyethylene head groups (Figure 5-2).

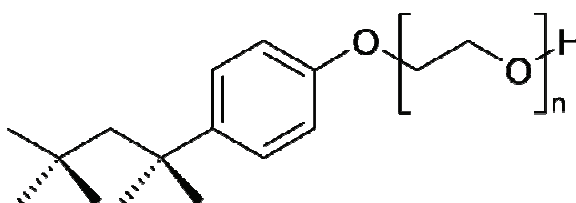


Figure 5-2: Molecular structure of Triton X-100 detergent. $n = 9 - 10$.

According to various studies, membrane protein solubilisation is a three-stage process (Jackson et al., 1982; Levy et al., 1990; Lichtenberg et al., 1983; Paternostre et al., 1988). In the first stage, detergent incorporates into the membrane without solubilisation. As thermodynamic activity approaches critical micellar concentration (CMC), the detergent-saturated membranes then coexist with the newly formed mixed-micelles in the second stage, where the hydrophobic regions of proteins anchor into micelles via hydrophobic interactions and the hydrophilic moieties are exposed to the aqueous environment. In the final stage, all membrane components are micellised and become soluble. Kragh-Hansen et al. (1998) further proposed the transbilayer mechanism for molecular interactions between detergents and membrane components, in which the mixed-micelle formation is greatly assisted by the cooperative attack of monomeric detergent that has a rapid flip-flop from both sides of the membrane.

5.2.3 Ammonium sulphate precipitation

At high salt concentrations, the solubility of proteins usually decreases, leading to precipitation, an effect known as salting-out (Green and Hughes, 1955). The mechanism of salting-out is based on the preferential solvation due to exclusion of salt from the hydration layer on protein surface (Wingfield, 1998). The addition of salt raises the surface tension of the water, promoting hydrophobic interaction in the system. In order to minimise the solvent contact area that creates energetically unfavourable ordered water molecules at the hydrophobic side chains, protein will re-fold and then self-associate, leading to precipitation. The release of bound water molecules upon precipitation makes it an energetically favourable process. These

complex effects have been examined in details elsewhere (Creighton, 1997; Kita et al., 1994).

Selective precipitation provides an efficient mean of proteins fractionation, for example, in antibody purifications (Schagger, 1994; Page and Thorpe, 1996). Due to its high solubility and salting-out strength, ammonium sulphate precipitation is one of the most widely adopted processes, in particular for feed with high levels of lipid impurities (Bracewell et al., 2008). As low density lipid precipitates often float to the top during the subsequent centrifugation, protein-only precipitates pellets can be collected at the bottom.

5.2.4 LRA (Lipid Removal Agent)

LRA (Lipid Removal Agent) is a synthetic calcium silicate hydrate developed by Advance Minerals Corp (California, USA) for the selective removal of lipids in the production of biopharmaceuticals (Zhang et al., 2005). Made from gyrolite, a naturally occurring mineral of calcium silicate hydrate, LRA is highly specific for lipids and lipoproteins in the presence of other biological materials, which is evidenced from the high recovery of most cellular proteins at LRA concentration up to 80 g/L (Smith, 2001). Combined with high removal capacity (Table 5-1), it has a number of reported applications in bioprocesses. Kent and Drohan (2001) developed a technique using LRA to separate cholesterol, triglyceride, phospholipids and lipoproteins from human blood plasma. Rolf (2003) and Zhang et al. (2005) used the media to remove endotoxins (lipopolysaccharide) from aqueous solutions.

Table 5-1: LRA lipid removal capacity (Sigma-Aldrich, 2010).

Lipid class	Removal capacity (mg/g of LRA)
Cholesterol	40
Triacylglyceride	82
Apolipoprotein A1	160
HDL	73
Phosphatidylcholine	265

5.2.5 Amberlite[®] XAD-4

Holloway (1973) first used polystyrene beads to remove Triton X-100 from samples in order to avoid its interference during protein assay. Since then, a series of polystyrene resins such as Amberlite[®] XAD 1, 2, 4, 7 and IRC 50 have been successfully applied in detergent removal applications, which remain a popular choice for bioprocess developers (Cheetham, 1979; Horigome and Sugano, 1983; le Maire et al., 1987; Scheule and Gaffney, 1981; Ueno et al., 1984).

Similar to chromatographic resins, XAD-4 is a non-ionic cross-linked polymer that features a large surface area ($\geq 725 \text{ m}^2/\text{g}$). Although it has been exclusively used for detergent removals, the aromatic surface does allow XAD-4 to adsorb other hydrophobic compounds such as lipids in the process stream. With an average pore size of 5 nm, it was suggested that XAD-4 should have a higher adsorptive potential for monomeric hydrophobic molecules than those in micellar forms (Rigaud et al., 1998b).

5.2.6 CUNO Zeta Plus® depth filtration

Zeta Plus® DEL Series (Cuno 3M, Bracknell, UK) (Chu and Babineau, 1986; Hou, 1986; Olsen et al., 1999) is a family of depth filter media which incorporates lipid-specific adsorbents such as calcium silicates for the selective removal of lipids, detergents and hydrophobic compounds from biological samples. Not only the cellulose-based depth filtration media can retain submicron contaminants such as cell debris and aggregates by size exclusion, also the embedded silica adsorbents have high capacities for a board range of lipids (mono-, di-, and triglycerides, fatty acids, cholesterol, phospholipids, and lipoproteins). At the same time, these filters are highly scalable and can be streamlined in production-scale cGMP manufacturing facilities, replacing the labour-intensive and difficult to prepare bulk silica batch operations.



Figure 5-3: CUNO Zeta Plus® DEL depth filtration cartridges (Cuno 3M, Bracknell, UK).

5.3 Results and Discussion

5.3.1 Effect of homogenisation pressure and centrifugation

In the current process, homogenisation is the first point of entry, through which intracellular content is introduced into the process stream. The two key parameters in homogenisation, pressure and number of passes, are therefore the main focus for process improvement. 1200 bar and 3 passes were employed and has been reported to be the optimum for VLP release from *Saccharomyces cerevisiae* (Sitrin and Kubek, 1992; Milburn and Dunnill, 1994; Pointek and Weniger, 2002). As discussed previously, it is generally undesirable to use high number of passes as the resulting fine particles will complicate feed stream for the subsequent operations, while the downward degree of freedom in passage number is also rather limited (one or two passes). Therefore, this investigation concentrated only on the pressure aspect in the overall homogenisation condition with the aim to realise lipid reduction while maintaining HBsAg VLP yields.

Homogenisations were carried out at four different pressures (100, 400, 800 and 1200 bar) at 3 passes with an undisrupted control sample (Section 2.5.1). An additional centrifugation step, reported to be beneficial in lipid removal (Kee et al., 2010), was also included as the selective method. Both homogenates and the re-suspended sediments from centrifugation were then subjected to the detergent and XAD-4 treatments, after which the levels of HBsAg VLP and lipids were determined.

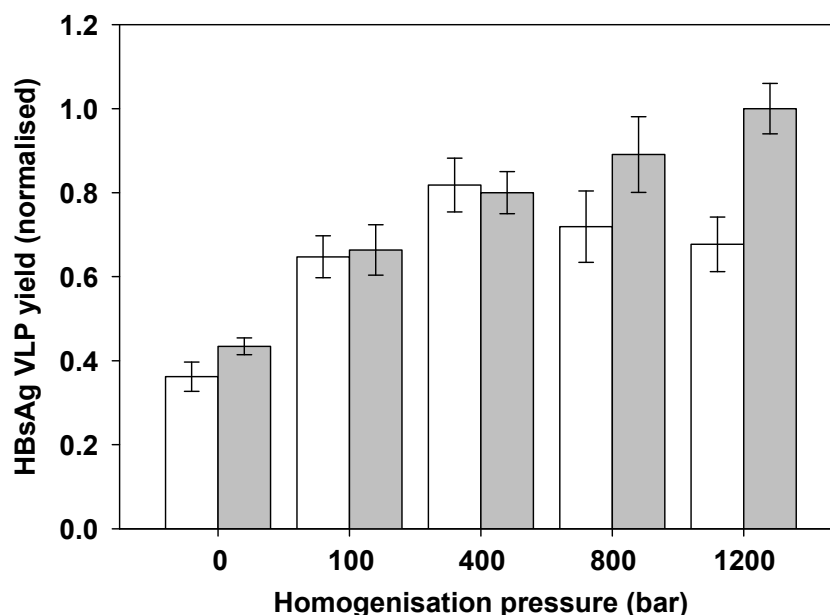


Figure 5-4: The yields of HBsAg VLP at various homogenisation pressures (0, 100, 400, 800 and 1200 bar) in both conventional (dark) and selective (light) method. Conventional method: homogenates were directly subjected to Triton X-100 detergent and subsequent XAD-4 treatments. Selective method: homogenisations were followed by an immediate centrifugation, sediments were re-suspended and then subjected to Triton X-100 detergent and subsequent XAD-4 treatments. Normalisation was carried out against the highest HBsAg VLP level (conventional method at 1200 bar). Error bars correspond to standard deviation from triplicate samples.

As shown in Figure 5-4, the level of HBsAg VLP released increased steadily with homogenisation pressure in the conventional method, which is consistent with previous studies that greater cell breakage at the higher pressure led to more effective release of the HBsAg VLP during the subsequent detergent step (Sitrin and Kubek, 1992). However, in the selective method where the homogenisation was followed by an immediate centrifugation step, the level of VLP released peaked at 400 bar, despite being 20% lower than the maximum achieved in the conventional method at 1200 bar,

and began to decrease afterwards. The difference between the two methods is a clear indication that the loss of HBsAg VLP observed was primarily due to the incomplete sedimentation of the HBsAg VLP containing cell fragments from supernatant during the centrifugation. It is possible that cell fragments are more micronised at homogenisation pressure above 400 bar, hence the inadequate settling velocity to achieve full sedimentation. It is, however, surprising to notice that a substantial amount of the HBsAg VLP is recoverable even without homogenisation, i.e. in the control sample. There could be a number of reasons for this. A substantial amount of yeast cells could have already been ruptured as a result of the cell death observed towards the end of the fermentation (after 50th hour). Also this might be an unintended effect from the freeze-thaw process, in which ice crystals formed during freezing caused the yeast cells to swell and ultimately break. Nevertheless, detergent is also capable of increasing membrane permeability leading to the release of solubilised HBsAg VLP.

In the conventional method, the level of lipid release was almost linear with homogenisation pressure (Figure 5-5), thus suggesting lipid reduction was not possible without sacrificing HBsAg VLP yield. Results from the selective method were, however, rather encouraging, showing significant lower amount of lipid release at all homogenisation pressures. In particular at 400 bar and above, the reduction in lipid level was as high as 70% from those in the conventional method. Considering the fact that lipid composition in the current process feed resembles that of lipid particles within the yeast cells i.e. high in triacylglyceride (Section 3.2.3), it is very likely that the additional centrifugation served as an important step to remove the supernatant containing a high level of lipid particles and triacylglyceride released from the lipid

particles. Because both lipids and lipid particles were low in density, thus it was possible to achieve high degree of separation from the HBsAg VLP sediments. High homogenisation pressures caused more lipid particles to rupture and release the internal triacylglyceride, thus the advantageous effect of the selective method became more apparent.

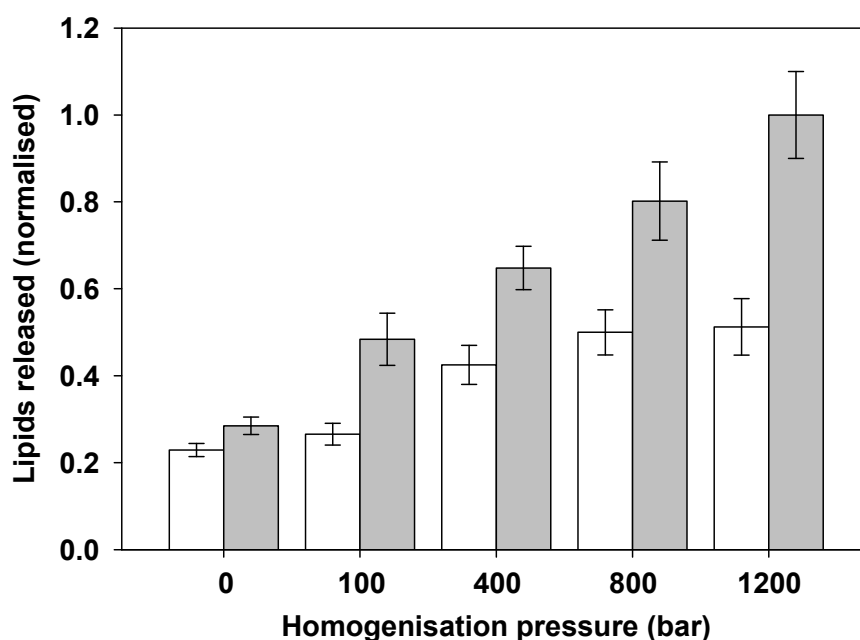


Figure 5-5: The levels of lipid released at various homogenisation pressures (0, 100, 400, 800 and 1200 bar) in both conventional (dark) and selective (light) method. Conventional method: homogenates were directly subjected to Triton X-100 detergent and subsequent XAD-4 treatments. Selective method: homogenisations were followed by an immediate centrifugation, sediments were re-suspended and then subjected to Triton X-100 detergent and subsequent XAD-4 treatments. Normalisation was carried out against the highest lipid level (conventional method at 1200 bar). Error bars correspond to standard deviation from triplicate samples.

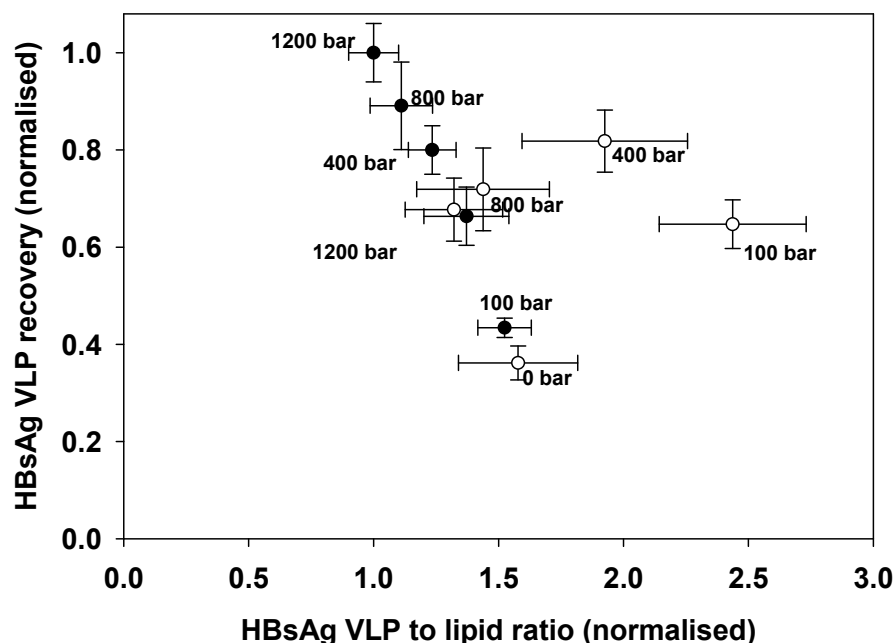


Figure 5-6: Screening of optimal homogenisation pressure condition. The effects of various homogenisation pressures (0, 100, 400, 800 and 1200 bar) in both conventional (●) and selective (○) were represented by HBsAg VLP to lipid ratio versus HBsAg VLP recovery plots. Error bars correspond to standard deviation from triplicate samples.

In order to pinpoint the optimal homogenisation pressure, HBsAg VLP to lipid ratios were plotted against HBsAg VLP recovery (Figure 5-6), which set the maximum level of HBsAg VLP achieved in the conventional method at 1200 bar as reference. The result shows that selective method at 400 bar was the optimum, as it gave a high HBsAg VLP to lipid ratio while maintaining more than 80% of the product yield. It is, however, important to emphasise that although pressure is a major component in the overall homogenisation condition, other factors such as number of passes and valve seat design (Moore et al., 1990) can still have a significant impact on feed characteristics (debris profile, total release of VLP, host proteins and lipid

content). Therefore, an in-depth trade-off study between total VLP release and host contaminant release is required in order to identify the optimum homogenisation condition, which will help to further improve the process economics.

5.3.2 Effect of Triton X-100 concentration

Following homogenisation, impacts of the detergent step on lipid release were investigated, as it was the second most likely point of entry for intracellular content. As discussed previously, yeast produces high level of host lipids that are essential for cellular activities during growth, most of which are stored in the form of lipid particles (lipid rafts) or organelle membranes. The non-selective nature of the detergent step for HBsAg VLP liberation from the ER membranes will inevitably cause other lipid components to co-release. Thus, it is important to determine the most suitable detergent condition in order to improve the quality of the feed stream in terms of host lipid contents.

Triton X-100 concentrations were screened in the range between 0.1% and 7% (v/v) (Section 2.5.2). Corresponding XAD-4 steps were then followed to remove the detergent prior to quantitation on the levels of HBsAg VLP and lipids. Figure 5-7 shows that the yield of HBsAg VLP increased with the initial Triton X-100 concentrations until 0.4% when it reached the maximum. From that point onwards, the yield of HBsAg VLP fell noticeable, and it was not until 3% the measured HBsAg VLP level rose again. For the rising trend, a few studies reported similar phenomena with a view that increasing detergent concentration accelerates the dispersion of membrane components and promotes VLP vesicle formation by inward budding of the

ER membrane leading to the more effective disassociation of the HBsAg VLP (Kreibich et al., 1982; Sitrin and Kubek, 1991; Chi et al., 1994; Smith et al., 2002; Kee et al., 2008).

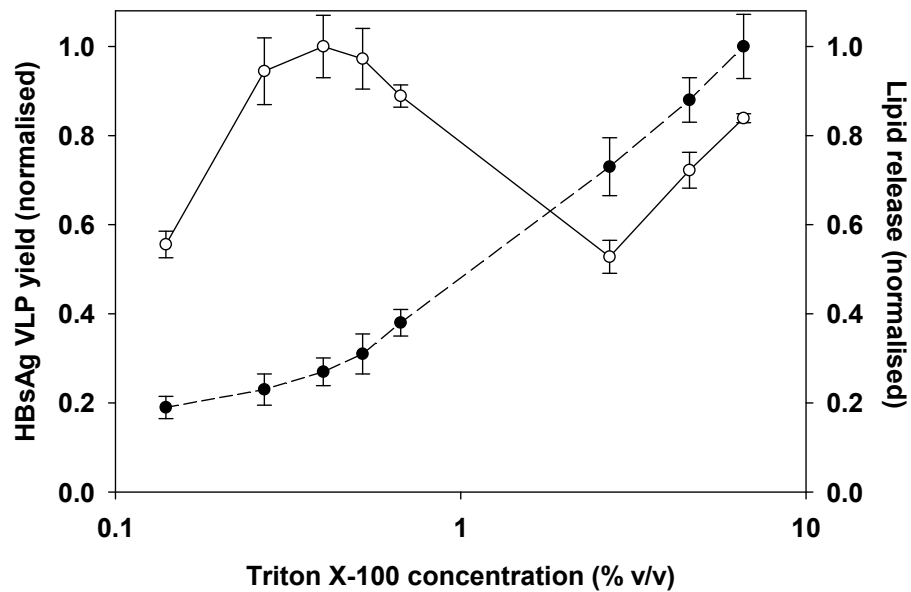


Figure 5-7: The yield of HBsAg VLP (\circ , solid line) versus the levels of lipid release (\bullet , dash line) at various Triton X-100 concentrations (0.1% - 7%). Normalisations were carried out against the highest HBsAg VLP (0.4% Triton X-100) and lipid level (7% Triton X-100) respectively. Error bars correspond to standard deviation from triplicate samples.

As for the subsequent V-shape profile of the HBsAg VLP activity, several possible explanations have been discussed (Kee et al., 2008). Structural lipids are essential for the antigenicity of the HBsAg VLP (Gavilanes et al., 1982b). At Triton X-100 concentrations above 0.5%, delipidation of the HBsAg VLP could occur due to the more effective extraction of the structural lipids by the readily available detergent

molecules. Thus, the resulting conformational rearrangement might engulf certain portion of the embedded HBsAg proteins (P24s), leading to the loss of antigenicity. As detergent concentration continued to rise past 3%, more monomeric P24s were extracted and solubilised. Additionally, the high level of lipids seen at the elevated Triton X-100 concentration (which will be discussed in the following paragraph) greatly hindered the detergent removal by XAD-4 (Rigaud et al., 1998a), leaving sufficient Triton X-100 molecules to form thermodynamically stable micelles at the end. Upon incorporation of the monomeric P24s, this gave rise to a more antigenic water-soluble protein micelle (Skelly et al., 1981; Sanchez et al., 1983), hence the higher ELISA measurements.

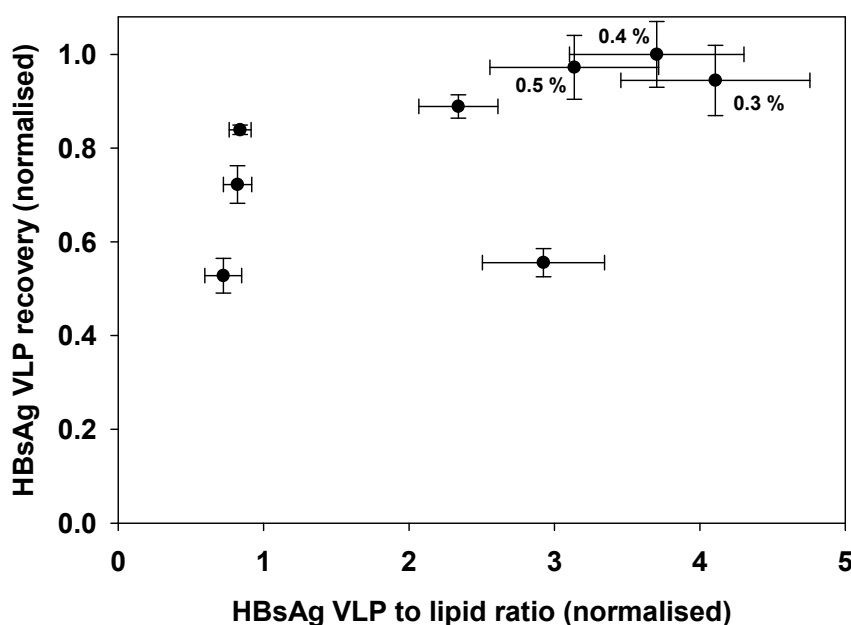


Figure 5-8: Screening of optimal Triton X-100 concentration. The effects of various Triton X-100 concentrations (0.1% - 7%) were represented by HBsAg VLP to lipid ratio versus HBsAg VLP recovery plots. Error bars correspond to standard deviation from triplicate samples.

Meanwhile, the level of lipid release increased steadily with Triton X-100 concentration (Figure 5-7), which was consistent with the expectation that the mechanism of detergent solubilisation was predominantly through the interactions with the lipid components (Kragh-Hansen et al., 1998). As the maximum of HBsAg VLP yield achieved early at the relative low detergent concentration (0.4%), where the rate of lipid release was still low, there should not have significant improvements on quality of the feed by using lower detergent concentrations. Figure 5-8 confirms this to be the case, in which both the HBsAg VLP to lipid ratios and VLP recoveries are in close range for the 0.3%, 0.4% and 0.5% Triton X-100 concentrations.

Although the beneficial effect of adjusting Triton X-100 concentration was rather limited, other parameters such as incubation temperature may offer potential improvement in the current process. Kragh-Hansen et al. (1998) showed that detergent-modified membrane fragments have a pronounced tendency toward secondary, temperature driven aggregation, a feature especially prominent in the case of Triton X-100. And as incubation temperature lowered to 4 °C, aggregation was completely absent. Thus, this offer means of controlling aggregate sizes in the process feed, which would be of great importance in preventing column fouling. Another possible area of improvement is to screen for a milder detergent that will maintain an acceptable product yield while releasing less hydrophobic components, for example polysorbate 20 (Tween[®] 20), whose use was reported in HBsAg VLP purification (Wijnendaele and Simonet, 1985), has been suggested. Both of these areas warrant further studies in hope to fully utilising the potential benefits.

5.3.3 Additional lipid removal step

Due to the significant impact lipid fouling has on column performance, it is justifiable to include a dedicated lipid removal step prior to chromatography in order to raise the robustness of the overall process. Therefore, in addition to exploring the optimised conditions in the homogenisation and detergent liberation steps, several scalable options were also examined, which included ammonium sulphate precipitation, LRA (Lipid Removal Agent) treatment, extended polystyrene bead (XAD-4) treatment and CUNO Zeta Plus[®] Delipid filtration.

Selective precipitation by ammonium sulphate provides an efficient means of proteins fractionation, and is widely used in protein purifications (Schagger, 1994; Page and Thorpe, 1996), particularly for feed with high levels of lipid impurities (Bracewell et al., 2008). LRA has a high removal capacity that is specific for lipids and lipoproteins in the presence of other biological materials. Kent and Drohan (2001) developed a technique using LRA to separate cholesterol, triglyceride, phospholipids and lipoproteins from human blood plasma. Similarly, aromatic surface of the polystyrene bead XAD-4 makes it an ideal adsorbent in removing not only detergent molecules but also other hydrophobic compounds such as lipids in the process stream (Rigaud et al., 1998a). CUNO Zeta Plus[®] Delipid filters combine high lipid specificity with cellulose-based depth filtration, achieving removal of both hydrophobic components and particulates such as cell debris and aggregates in a single operation.

For comparability of the results, all four options were subjected to the same starting feed material, which was at the end of the two step filtration (Section 2.5.3) before chromatography. In ammonium sulphate precipitation, saturations up to 35% were screened. Process feed was adjusted to required ammonium sulphate

concentration by mixing with small volume of the $(\text{NH}_4)_2\text{SO}_4$ stock while keeping the overall volume constant for all samples. It was then briefly mixed, incubated and centrifuged, after which the supernatant excluding the floating precipitate was analysed. For LRA, concentrations up to 80 mg/mL were added to the process feed, followed by the similar mixing, incubation and centrifugation condition. At the end, the supernatant was analysed. Meanwhile, the process feed was mixed with up to 500 mg/mL of XAD-4 beads. After incubation, the feed was passed through a 1.0 μm glass-fibre filter before quantitation. Three flow rates, hence the contact time, was chosen for the CUNO Zeta Plus[®] Delipid filters following the manufacture recommendation (Product Information sheet, Cuno 3M, Bracknell, UK). The filtrate at the end of the operation was assayed for its HBsAg VLP and lipid level.

Figure 5-9 and Figure 5-10 show that in both ammonium sulphate precipitation and LRA treatment, the decline in lipid level matched exactly that in the HBsAg VLP, which suggests that the removal capabilities in these two methods were not specific. This is not surprising considering the large size and hydrophobic nature of the HBsAg VLP, it may behave the same way as most lipids in terms of the tendency to aggregate and adsorb to other hydrophobic materials. In ammonium sulphate precipitation, a thick layer of material was found floating on top of the supernatant with little or no sediment observed, indicating that the majority of the precipitates formed during the operation were of low density, presumably lipids. Thus, the loss of HBsAg VLP in this case was most likely due to with co-precipitation with lipids. In contrast, all the LRA media was settle at the bottom after centrifugation, which suggested that HBsAg VLP was either adsorbed to silica surface or just depositing into the sediment without

interaction. However, in the latter case, there was not practical way of isolating the HBsAg VLP from the sediment.

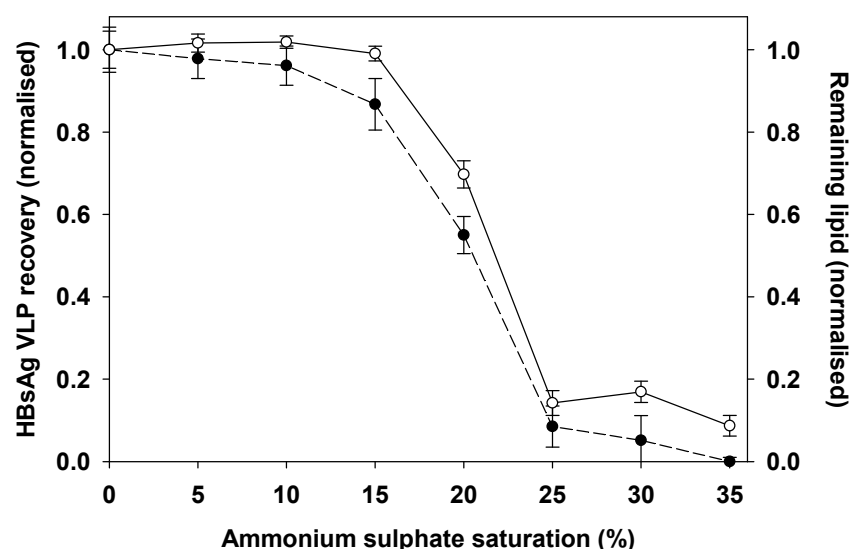


Figure 5-9: The effects of ammonium sulphate precipitation on HBsAg VLP recovery (○, solid line) and remaining lipid levels (●, dash line). Normalisation was carried out against material concentrations in the control sample. Error bars correspond to standard deviation from triplicate samples.

For the XAD-4 treatment, the rate of lipid removal was far higher than the loss of HBsAg VLP (Figure 5-11). After 200 mg/mL, the level of remaining HBsAg VLP stayed constantly above 80%, while the amount of lipid removed continued to rise, achieving a five-fold reduction at the end. The porous, chromatographic resin like, structure is most likely to be the reason for such high specificity. The polystyrene beads have a narrow distribution of pore sizes, which averages at 5 nm. Thus, similar to the situation with Sepharose[®] Butyl-S 6 Fast Flow resin, the 22 nm HBsAg VLP is

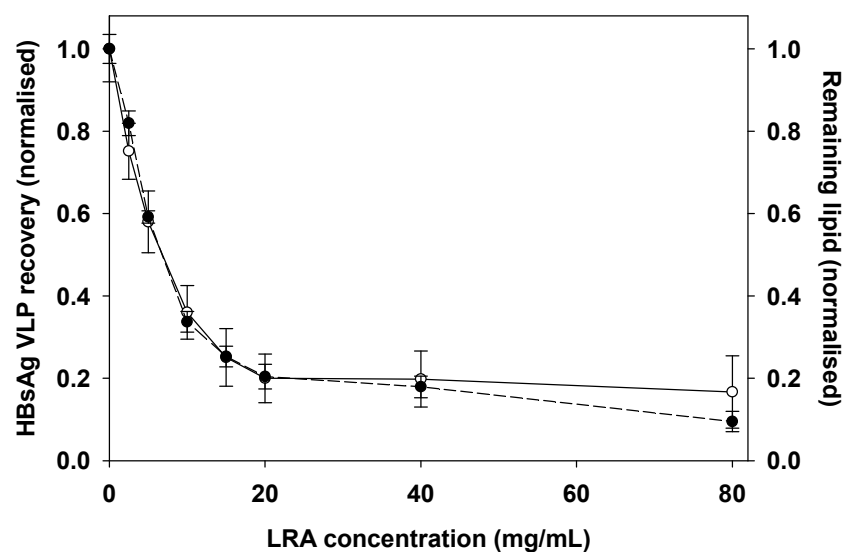


Figure 5-10: The effects of LRA treatment on HBsAg VLP recovery (\circ , solid line) and remaining lipid levels (\bullet , dash line). Normalisation was carried out against material concentrations in the control sample. Error bars correspond to standard deviation from triplicate samples.

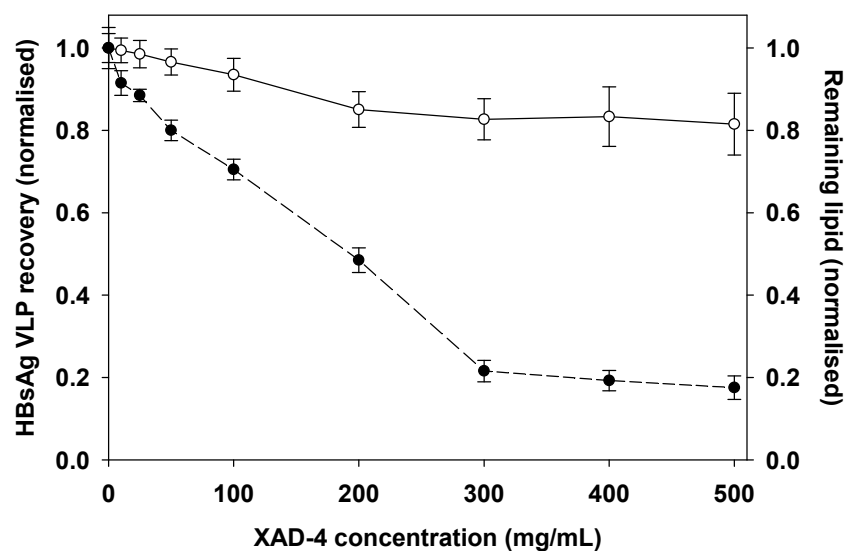


Figure 5-11: The effects of XAD-4 treatment on HBsAg VLP recovery (\circ , solid line) and remaining lipid levels (\bullet , dash line). Normalisation was carried out against material concentrations in the control sample. Error bars correspond to standard deviation from triplicate samples.

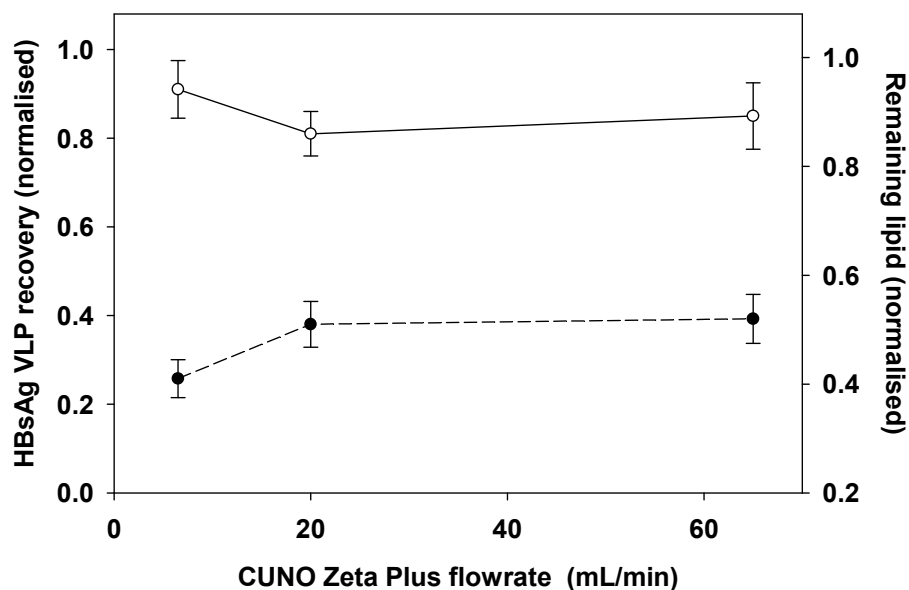


Figure 5-12: The effects of CUNO Zeta Plus[®] Delipid filtration on HBsAg VLP recovery (○, solid line) and remaining lipid levels (●, dash line). Normalisation was carried out against material concentrations in the control sample. Error bars correspond to standard deviation from triplicate samples.

excluded from the internal bead surface, while the much small lipid molecules can freely diffuse through, hence the large difference in capacity between the two.

Equally promising was the result from CUNO Zeta Plus[®] Delipid filtration. At 6.5 mL/min, the recovery of HBsAg VLP was more than 90%, while the rate of lipid removal almost reached 80%. As the flow rate increased to 20 mL/min, the level of HBsAg VLP fell marginally to 80% but remained stable thereafter. The high shear generated from the increasing flow rate could potential cause VLP to aggregate (Shi et al., 2005), leading to the loss of activity. Lipid removal, however, was slightly lowered at the higher flow rates, which was expected from the shorter residence time.

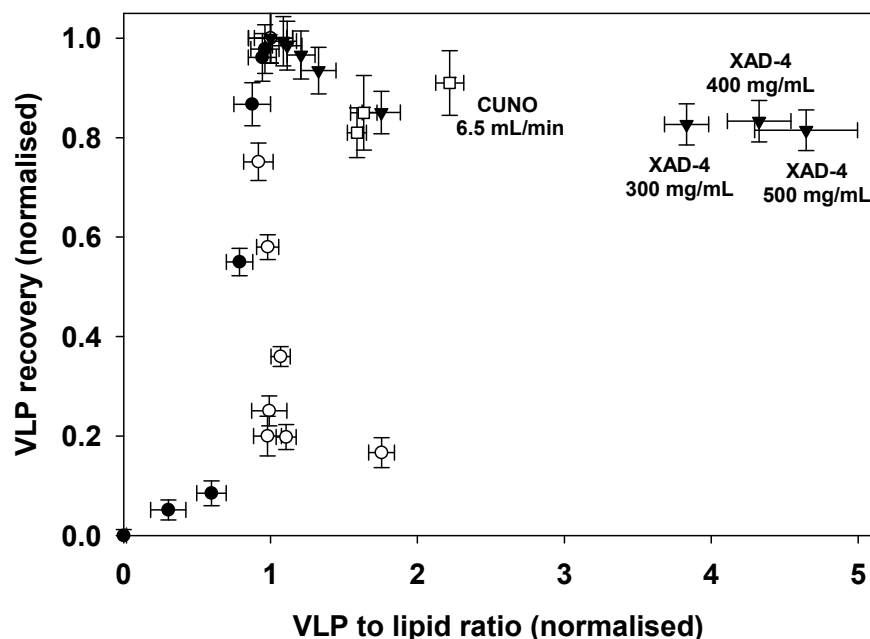


Figure 5-13: Screening of lipid removal performance in HBsAg VLP process feed. The effects of ammonium sulphate precipitation (●, 0-35% saturation), LRA treatment (○, 0-80 mg/mL), XAD-4 treatment (▼, 0-500 mg/mL) and CUNO Zeta Plus[®] Delipid filtration (□, 6.5-65 mL/min) were represented by HBsAg VLP to lipid ratio versus HBsAg VLP recovery plots. Error bars correspond to standard deviation from triplicate samples.

In order to quantitatively compare the performance of the four operations, HBsAg VLP to lipid ratios were plotted against HBsAg VLP recovery (Figure 5-13). The result shows that the optimal conditions for achieving improved feed quality were dominated by XAD-4 treatment (300-500 mg/mL), followed by CUNO Zeta Plus[®] Delipid filtration (6.5 mL/min). Furthermore, as the current process already includes a XAD-4 treatment step for removing Triton X-100, an extended operation condition with higher XAD-4 concentration can be adopted to accomplish the additional goal of lipid removal. This will cost significantly less than the introduction of an extra unit of

operation in the process. Similarly, CUNO Zeta Plus[®] Delipid filtration can, if not partially, replace the current two-step filtration for XAD-4 removal, thus at the same time improving feed quality with little overheads.

5.3.4 HIC performance improvement

To demonstrate the effectiveness in limiting lipid fouling, HIC performances were compared for the optimal operating conditions in current process and the additional lipid removal options investigated. Percentage loadings and elutions of the HBsAg VLP were monitored between the first and 40th cycle of operation, in this way, effects of both competitive binding and permanent accumulation can be properly accounted for.

In addition to the Conventional (I) feed as described in Section 2.3.2, the three feed candidates chosen (Section 2.5.3) included the Selective (II) feed, prepared from homogenisation at 400 bar with an immediate centrifugation; the XAD-4 (III) feed, prepared from treatment with 500 mg/mL XAD-4; and the CUNO (IV) feed, prepared from CUNO Zeta Plus[®] Delipid filtration at 6.5 mL/min. Fresh columns were used for each feed stream, following the HIC method described in Section 2.3.4. Loading volumes were adjusted to contain the same amount of HBsAg VLP per cycle as that in conventional feed, from which equivalent lipid amounts were calculated and normalised.

Table 5-2 summarises the result. The improvements on HBsAg VLP capacity, concluded from the percentage loading in the first cycle of operation, were substantial in the optimised feed streams (II, III and IV) with reduced amount of lipids. In the

XAD-4 feed (III), where the level of lipids was the lowest, nearly all of the available HBsAg VLP was captured. This is in stark contrast to the poor capacity observed in the Conventional (I) feed. Thus, this result indirectly re-confirms the significant impact lipids have on HBsAg VLP capacity due to competitive binding.

*Table 5-2: HIC performance from the four feed streams as described in Section 2.5.3: (I) Conventional feed, (II) Selective feed, (III) XAD-4 feed and (IV) CUNO feed. *Loading volumes were adjusted to contain the same amount of HBsAg VLP per cycle, and the equivalent percentage lipid amounts were calculated. Percentage loadings and elutions of the HBsAg VLP were compared between the first and 40th cycle of operation. Standard deviations of all data (triplicate samples) were within 10%.*

		Conventional (I)	Selective (II)	XAD-4 (III)	CUNO (IV)
Lipid loaded per cycle *		100	50	22	43
First cycle	Loading	33	78	99	80
	Elution	93	98	65	90
	Yield	31	76	64	72
40th cycle	Loading	62	90	96	87
	Elution	29	46	58	43
	Yield	18	41	56	37
% Change	Loading	88	15	-3	9
	Elution	-69	-53	-11	-52
	Yield	-41	-46	-13	-48

When examining the HBsAg VLP recovery, values from the XAD-4 (III) and CUNO (IV) feed streams were however lower than the rest. In particular, more than one-third of the captured HBsAg VLP was unrecoverable in the XAD-4 case, which causes serious concerns about the HBsAg VLP structure integrity. Shi et al. (2005) demonstrated that the presence of low level of detergents and lipids was beneficial to the structural stability of VLPs. Thus, it is possible that the aggressive lipid removal strategies used in the XAD-4 (III) and CUNO (IV) feed preparations may extract structural lipids from the HBsAg VLP at the same time as the host lipids, making them less stable. Consequently, adsorption to the resin surface causes irreversible conformational change in the HBsAg VLP, leading to poor recoveries. This reiterates the need for a secondary assay such as SEC that can provide structural information of the HBsAg VLP.

Comparing the HBsAg VLP capacities and recoveries between the first and the 40th cycle, the general trend was the rise in capacity but lowered recovery as the number of cycle increased, and the degrees of change appear to correlate well with the levels of lipid in the starting feeds. Thus, the results corroborate with the previous findings that lipid fouling alters resin property, making it more hydrophobic. The XAD-4 (III) feed once again shows the smallest change, whose yield stayed constantly above 50%, while the Selective (II) and CUNO (IV) feeds display noticeable improvements on the resistance to the deleterious effects from lipid fouling.

5.4 Conclusions

The high level of lipid foulants present in the HBsAg VLP feed stream and their severe impact on column performance evidenced from the preceding chapters warrant this study, which aims to improve the feed quality by exploring not only the optimisation of the existing unit operations but also the efficiency of dedicated lipid removal steps.

Substantial improvement on feed quality in terms of high HBsAg VLP yield and low lipid release was seen at a reduced homogenisation pressure (400 bar, 3 passes) followed by centrifugation step, whereas no noticeable gain was observed in the Triton X-100 concentrations screened. From the four dedicated operations investigated, polystyrene XAD-4 treatment and CUNO Zeta Plus[®] Delipid filtration demonstrated promising lipid removal capabilities with satisfactory HBsAg VLP recoveries. Finally, the efficacy of each strategy in reducing lipid fouling was studied by evaluating HIC performance in terms of capacity and recovery over multiple cycles. The results showed a three-fold increase in capacity in the best case, suggesting reduced competition on the column between VLP and lipid. Additionally, this performance remained constant over 40 cycles, indicating lipid fouling was now well managed on the HIC column. As a result, process modifications such as those shown in Figure 5-14 can be incorporated to minimise the impact of lipid fouling, leading to improved process economics.

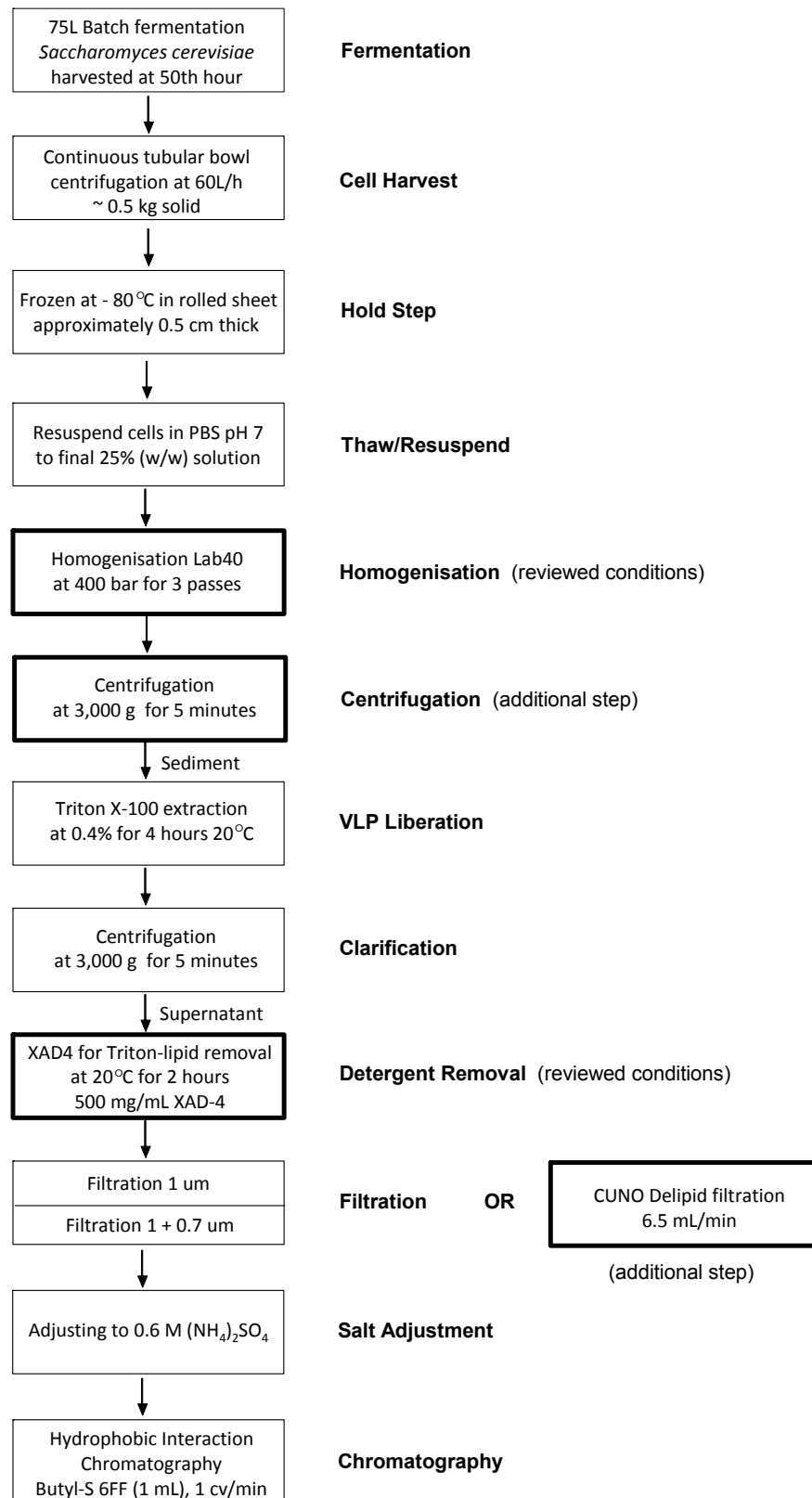


Figure 5-14: Revised process flow chart for HBsAg VLP purification. Bold boxes indicate modifications from the current process as shown in Figure 2-4.

Chapter 6

Conclusions

Recommendations for future work

6.1 Overview

The ever increasing challenge on productivity and robustness in process chromatography emphasise the urgent need for a better understanding of the fouling process and the consequent optimisation on adsorbent designs and operating conditions. The absence of systematic study in the literature on chromatography fouling from industrially relevant process feed streams means little is established in the area. The objective of this thesis was to develop a mechanistic understanding of lipid fouling through the investigation of a capture step hydrophobic interaction chromatography (HIC). Although the focus of this study is on lipid fouling in HIC, the systematic approach and novel analytical techniques employed can potentially provide a unique platform to study fouling of other chromatographic adsorbents and process feed materials.

HIC is employed as a primary capture step in the purification of yeast derived HBsAg VLP vaccine, where the required cell disruption and detergent liberation steps release high levels of lipid content into the feed stream. Bracewell et al. (2008) reported that lipid fouling from yeast homogenate can have a major impact on HIC performance. Due to the hydrophobic nature of lipid-column interaction, this HIC step will thus be particularly susceptible to lipid fouling. If it is not possible to control this fouling, it will render such a process sequence economically unfeasible. Therefore, this scenario presents an excellent example of lipid fouling in process chromatography.

Using a three-step approach, the investigation started by ascertaining the foulant species and their effect on column performance. This was then followed by

efforts to determine the underlying mechanism of fouling. Finally, from the knowledge acquired strategies to limit fouling were suggested and evaluated.

6.2 Quantification of the deterioration in column performance from lipid fouling (Chapter 3)

6.2.1 Study objectives (Chapter 3)

Quantification of the impact lipid fouling has on HIC performance is essential in establishing the difficulty in dealing with feeds containing high levels of host lipids, such as those obtained from yeast fermentations. For a realistic representation of the industrial process, the fouling challenges were performed as successive cycles of operation, which also incorporated CIP at the recommended strength and frequency as would be deployed for life-time studies of process chromatography. Comparative analysis was then performed on key performance parameters including binding capacities, purities and recoveries in each cycle between lipid-rich and lipid-depleted feedstocks, which was produced from extensive centrifugation. Thus, both the immediate competitive effect on product binding capacity and the long-term deteriorative impact on column performance were examined. In addition, full mass balance on host lipids was performed to identify the lipid class that has the highest fouling potential.

6.2.2 Summary of findings (Chapter 3)

The results from this study demonstrate clearly the difficulties in chromatographic purification when dealing with high lipid content feeds, such as those obtained from yeast fermentations. Both lipid mass balance and confocal data confirmed lipid accumulation within the column over time, which caused the properties of the matrix to change and made the purification process less consistent after repeated rounds of feed application. In terms of compliance with stringent regulatory requirements, this could result in a much shorter column lifetime due to the reduced recovery in elution. Hence, this study has laid down the foundations for carrying out further microscopic investigations in order to gain a better understanding of detailed lipid fouling mechanisms. Based on the results of such studies, improvements to adsorbent design and operating protocols could then be explored, such as by optimising the ligand density and spacer arm length, or by using stronger CIP conditions. In this study, however, the relatively harsh CIP was shown to be ineffective and improvements to the regenerating buffer alone would be unlikely to tackle the problem of reduced column capacity caused by the presence of competing lipids and would present challenges during column operation. Alternatively and of potentially greater utility could be the introduction of feed pre-treatment steps to reduce the lipid level prior to chromatographic purification. Such options have the potential to increase capacity and prolong product recovery over a larger number of loading cycles, thus helping to maintain column performance and so improve the cost-effectiveness of VLP manufacture.

6.3 Investigation on lipid fouling mechanism (Chapter 4)

6.3.1 Study objectives (Chapter 4)

Experimental verification of the material intra-particle diffusion and adsorption profiles is crucial for understanding the mechanism of fouling, and it was made possible by the use of CLSM. In order to first corroborate the competitive effect from lipid foulants on other feed components, material adsorption isotherms and batch uptake profiles were followed. The uptake of fluorescently labelled lipid foulants was then monitored microscopically at various salt concentrations, which also aimed to relate the extent of fouling with HIC operating conditions. Additionally, by measuring the intra-particle foulant accumulation, inspections on resin condition were performed for samples collected at different stages during the column life-time. High-resolution images of the fouled bead surfaces were also obtained using SEM, serving as a visual confirmation for quantitative analysis from CLSM. Furthermore, in-column spatial distribution and progression of lipid fouling were measured by examining bead samples from different positions in the packed bed. From the results, potential lipid fouling mechanism was proposed.

6.3.2 Summary of findings (Chapter 4)

The investigation started by characterising the interactions between lipid foulant and other feed components through the analysis of material adsorption isotherms and batch uptake profiles. In comparison to HBsAg VLP and proteins,

lipids displayed a disproportionally higher binding capacity. The resulting preferential binding posed strong competition for HBsAg VLP capacity, even causing the displacement of already adsorbed VLP. In addition, the influence on both material adsorption level and uptake rate differed significantly at the low and high salt concentrations, with more deviation from the standard Langmuir model observed in the latter condition where the hydrophobic interaction was heightened. This salt effect was evidenced in the CLSM examination, where intra-particle diffusion and adsorption profiles of the fluorescently labelled lipid foulants were monitored microscopically at various salt concentrations. The CLSM images showed a distinct change from pore to homogenous diffusion as the salt concentration decreased, a phenomenon also observed by Dziennik et al. (2005), Harinarayan et al. (2006) and Linden et al. (2002). Furthermore, the accumulation of lipids at the rim of the beads was seen to occur exceedingly fast. Consequently, external protein probes were not excluded from bead due to pore blockage or diffusion hindrance resulted from the adsorbed lipid layer. The elevated level of irreversible binding within the area was then confirmed in subsequent dual-colour labelling experiment, where exchange of lipids was monitored.

The investigation then proceeded to the examination of the resin conditions caused by the long-term impact of lipid fouling. The intra-particle fluorescence intensity profiles of bead samples collected at different stages during the column life-time showed that lipid accumulation increased with number of operation cycles and majority of the lipid deposits concentrated at the rim of bead, corroborating with the fast lipid build-up in the region observed previously during loading. This was consistent with the small loading volume of each cycle, which led to the rim of the

bead being repeatedly challenged with an otherwise significant amount of feed. High-resolution images of the fouled bead surfaces were also obtained using SEM, serving as confirmation of the build-up of a lipid layer on its surface. Additionally, in-column spatial distribution and progression of lipid fouling were visualised by examining bead samples from different positions of the column. Fouling in the top section was shown to be the heaviest, while significant amount of the beads in the bottom sections displayed the dual-peak phenomenon as evidenced by Dziennik et al. (2005) and Siu et al. (2006b).

6.4 Investigating on the efficacy of pretreatments in lipid removal (Chapter 5)

6.4.1 Study objectives (Chapter 5)

Results from the preceding investigations provided valuable information for the design of an effective strategy in reducing lipid fouling. On account of the already harsh, yet ineffective column regeneration and CIP regime that were currently employed, emphasis has since been placed on pretreatments. With the aim to improve feed quality, further study was performed to explore not only the VLP liberation operating conditions in the current downstream process but also the efficiency of dedicated lipid removal steps. The efficacy of each strategy in limiting both the short and long-term impacts of lipid fouling was then verified by measuring the improvement on product capacity and robustness in HIC performance.

6.4.2 Summary of findings (Chapter 5)

Substantial improvement on feed quality in terms of high HBsAg VLP yield and low lipid release was seen at a reduced homogenisation pressure (400 bar, 3 passes) followed by centrifugation step, whereas no noticeable gain was observed in the Triton X-100 concentrations screened. From the four dedicated operations investigated, polystyrene XAD-4 treatment and CUNO Zeta Plus[®] Delipid filtration demonstrated promising lipid removal capabilities with satisfactory HBsAg VLP recoveries. Finally, the efficacy of each strategy in reducing lipid fouling was studied by evaluating HIC performance in terms of capacity and recovery over multiple cycles. The results show a three-fold increase in capacity in the best case, suggesting reduced competition on the column between VLP and lipid. Additionally, this performance remained constant over 40 cycles, indicating lipid fouling was now well managed on the HIC column.

6.5 Recommendation for future work

The objective of this study was to understand the mechanism of lipid fouling in chromatography through the investigation of a hydrophobic interaction chromatography (HIC) operation. The systematic approach and novel analytical techniques employed can create a unique platform to study fouling of other chromatographic adsorbents and process feed materials, with the ultimate goal to improve overall process economics. Suggestion of future works will thus not only seek to further develop the investigative platform by addressing the difficulties so far encountered, but also identify the potential research areas of interest in reducing fouling in process chromatography.

6.5.1 HBsAg VLP quantification

In this study, the quantification of HBsAg VLP relied solely on the ELISA assay, which predominately measures activity of the p24 surface antigen. In addition to the large errors in measurement arisen from the relative manual procedures, it does not provide information on the actual HBsAg VLP conformation. Although one can argue that antigenicity is the key measure of vaccine quality, structural changes may destabilise the VLP and lead to the eventual loss in antigenicity that is not apparent at the beginning. The unexpectedly low recovery detected from the feed sample treated with XAD-4 (Section 5.3.4) could potentially be the case. Therefore, this reiterates the need for a size-based secondary assay for HBsAg VLP. Two SEC columns have been examined, including Superose[®] 6 10/300 GL (GE Healthcare, Amersham, UK) and

TSK[®] gel G5000_{PWXL} (Tosoh Bioscience GmbH, Stuttgart, Germany). The resolution, however, proved to be inadequate due to nonspecific hydrophobic interactions between the resins and HBsAg VLP, even in presence of organic additive as suggested. Thus, at the same time of optimising the SEC column operating conditions, other options need to be evaluated, such as dynamic light scattering and circular dichroism based methods.

6.5.2 Further characterisation of HBsAg stability

In spite of the importance of HBsAg VLP, its structural stability is less well understood, especially during the manufacturing process in comparison to other VLP vaccines, such as HPV. As illustrated by Buckland (2005), ‘the process of producing the VLP defines the final product’. This will thus add another layer of complexity in the process development in terms of the trade-off between process yield and product quality. As demonstrated previous, even though the aggressive lipid removal regime (the use of XAD-4) was effective in providing a more clarified feed stream and higher capacity, the resulted VLP was significantly less stable, leading to the eventual loss in recovery. There are a number of factors that may influence the stability of HBsAg VLP, including but not limited to shear, temperature, pH, ionic strength, protein concentration, the presence of stabiliser, such as detergents. Therefore, a high-throughput screening, possibly micro-well based, may be required to provide a better understanding of the interactions between the HBsAg VLP and its manufacturing process.

6.5.3 Improved labelling techniques and conditions

During the CLSM and SEM studies, attempts to label HBsAg VLP were proven unsuccessful. The immunolabelling technique used a primary antibody that identifies the surface antigen p24s and a secondary fluorescent or gold labelled antibody that specifically binds to the primary antibody. The result showed no difference to the control experiment, where wild-type yeast homogenate was labelled. Labelling specificity due to material interactions is thus an issue in complex process feed stream, such as the one currently investigated. Additionally as mentioned previously, there is no effective means of removing the unbound dye molecules without significantly altering the feed property. For example, the most commonly used SEC method will at the same time unavoidably eliminate feed components that are of similar size to the dye molecule. Therefore, in order further improve the applicability of the current fouling study approach on other process feed materials, it is essential to screen for more effective labelling techniques and conditions. One alternative suggested is the ‘add-back’ approach, where the targets are first isolated by conventional means such as chromatography prior to labelling and small volume of the labelled species are then added back to starting material. However, the efficacy of the initial isolation remains to be determined.

6.5.4 Alternative lipid removal strategies

In addition to the current chemical based lipid removal strategies (Section 5.3.3), the investigation may be extended to exploring other physical and biological based methods, such as ultracentrifugation and enzymatic digestion. The successfully

applications of density gradient ultracentrifugation in isolating lipids, lipid particles or even HBsAg VLP have been reported on both laboratory and production scales (Even-Chen, 1993; Phogat et al., 2008). Tahoun (1986) has also shown that agarose beads containing immobilised lipase can be used for the hydrolysis of triglycerides on a reasonable scale. Thus, methods as such may provide alternative or supplementary lipid removal capability to the current process, thorough examinations of their efficacy and economics are required though.

The *in-vitro* use of lipase does raise the question on whether it would be more efficient and cost-effective to achieve lipid removal on a molecular level. Lipase and other molecular machineries can be easily incorporated into an expression system through genetic manipulation (Xu et al., 2008). Thus, the levels of the foulants present later in the process stream, such as intracellular lipid particles containing significant amount of neutral lipids, can be reduced even before primary recovery. Therefore, if the toxicity on cell growth and impact on product formation can be properly managed, this would be an attractive option to improve overall process economics.

6.5.5 Alternative capture step chromatography

Previous studies (Belew et al., 1991; Dekleva, 2002; Zhou et al., 2007) identified HIC as a potential step for VLP purification. Thus, we have established that due to the hydrophobic nature of lipids, HIC step is particularly susceptible to lipid fouling as evident from the current study. Thus, the use of an alternative capture step, such as IEX, may have the potential to mitigate these deleterious effects. However, there are several possible limiting factors that may require further examinations. First,

IEX columns may not have adequate binding capacities for VLP due to its insufficient ionic characteristics. This is further challenged by the fact that the large size of for VLP will limit its binding sites to only the outer bead surface for most commercial resins, although new column format such as monolith may provide a remedy. Second, thanks to the refolding process upon desorption from HIC resin, product aggregation, a widely-acknowledged problem for VLP purification (Kim et al., 2007), is generally suppressed (Li et al., 2004). Thus, in IEX, extent of the possible VLP aggregation remains to be determined. Finally, even though less critical, fouling due to lipids or other host materials may still occur in IEX through non-specific binding. A detailed investigation using the systematic approach developed in this study may provide a good performance appraisal between the alternative and current process.

6.5.6 Column design

The pretreatment XAD-4 step examined in Section 5.3.3 can be considered to effectively function as a guard column for the capture HIC. Thus, this demonstrates the potential benefits of changing column configuration on process performance. However, the properties and operating conditions of the guard column need to be carefully determined in order to achieve the optimal balance between lipid removal and product recovery.

As evidenced previously, the permanent lipid build-up progressed along the flow direction (Section 4.3.6.2), and fouling effect of lipid escalated only after it had reached certain degree of saturation (Section 4.3.3.3). Therefore, by periodically alternating the flow direction between the cycles of operation, lipid accumulation can

be mitigated to both sides of the column, limiting the fouling effect for a longer period. Combining with the guard column concept, new column design, such as the one suggested in Figure 6-1, will have the potential to not only reduce the fouling effect, but also provide a mean of managing in-process fouling.

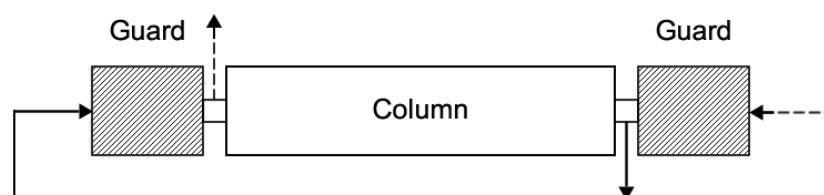


Figure 6-1: Chromatograph column equipped with guard columns at the both ends. Flow direction is alternated between cycles of operation. Two outlets are incorporated in to order to bypass the guard column used by the opposite flow direction. Both guard columns can be periodically replaced according to usage.

6.5.7 Resin design

Although improvement on feed stream quality targets the source of the fouling problem, resin development is of equal importance. As evident from the current findings, lipid fouling affects the material adsorption and diffusion process in HIC. Fexby et al. (2007) showed that HIC resin hydrophobicity can be precisely controlled through a new manufacturing process, leading to a reduced effect of protein denaturation. Similarly, Chen et al. (2008) reported a significant improvement on binding capacity of monoclonal antibody (mAB) on a new generation of HIC resin with optimised pore size. Thus, both these affecting areas can be potentially addressed via advances in resin design and its production process.

Chapter 7

References

Aggerbeck, L.P. & Peterson, D.L., 1985. Electron microscopic and solution X-ray scattering observations on the structure of hepatitis B surface antigen. *Virology*, 141(1), 155-161.

Arakawa, T., 1986. Thermodynamic analysis of the effect of concentrated salts on protein interaction with hydrophobic and polysaccharide columns. *Archives of Biochemistry and Biophysics*, 248(1), 101-105.

Arakawa, T. & Timasheff, S.N., 1982. Preferential interactions of proteins with salts in concentrated solutions. *Biochemistry*, 21(25), 6545-6552.

Arve, B.H. & Liapis, A.I., 1987. Modeling and analysis of biospecific adsorption in a finite bath. *AIChE Journal*, 33(2), 179-193.

Balasundaram, B., Harrison, S. & Bracewell, D.G., 2009. Advances in product release strategies and impact on bioprocess design. *Trends in Biotechnology*, 27(8), 477-485.

Barbero, M.C. et al., 1984. Effect of the nonionic detergent Triton X-100 on mitochondrial succinate-oxidizing enzymes. *Archives of Biochemistry and Biophysics*, 228(2), 560-568.

Bayer, M.E., Blumberg, B.S. & Werner, B., 1968. Particles associated with Australia antigen in the sera of patients with leukaemia, Down's Syndrome and hepatitis. *Nature*, 218(5146), 1057-1059.

Belew, M. et al., 1991. Purification of recombinant hepatitis B surface antigen produced by transformed Chinese hamster ovary (CHO) cell line grown in culture. *Bioseparation*, 1, 397-408.

Belfort, G. & Nagata, N., 1985. Fluid mechanics and cross-flow filtration: some thoughts. *Desalination*, 53(1-3), 57-79.

Benedek, K., 1988. Thermodynamics of [alpha]-lactalbumin denaturation in hydrophobic-interaction chromatography and stationary phases comparison. *Journal of Chromatography A*, 458, 93-104.

Berggrund, A. et al., 1994. Chemical and chromatographic characterization of a new bioprocess(TM) medium for hydrophobic interaction chromatography: Butyl Sepharose® 4 FastFlow. *Process Biochemistry*, 29(6), 455-463.

Berna, P.P. et al., 1998. Comparison of the protein adsorption selectivity of salt-promoted agarose-based adsorbents. Hydrophobic, thiophilic and electron donor-acceptor adsorbents. *Journal of Chromatography. A*, 800(2), 151-159.

Biemans, R. et al., 1992. Immunoelectron microscopic detection of the hepatitis B virus major surface protein in dilated perinuclear membranes of yeast cells. *DNA and Cell Biology*, 11(8), 621-626.

Bird, J. & Ross, C., 2002. *Mechanical engineering principles*, Newnes.

Bitter, G.A. et al., 1988. Hepatitis B vaccine produced in yeast. *Journal of Medical Virology*, 25(2), 123-140.

Blagović, B. et al., 2005a. Characterization of lipid components in the whole cells and plasma membranes of baker's yeast. *Croatica Chemica ACTA*, (78), 479-484.

Blagović, B. et al., 2005b. Lipid analysis of the plasma membrane and mitochondria of brewer's yeast. *Folia Microbiologica*, 50(1), 24-30.

Blumberg, B.S., Millman, I. & London, W.T., 1985. Ted Slavin's blood and the development of HBV vaccine. *The New England Journal of Medicine*, 312(3), 189.

Bohidar, H.B., 1989. Light scattering study of solution properties of bovine serum albumin, insulin, and polystyrene under moderate pressure. *Colloid & Polymer Science*, 267(4), 292-300.

Bracewell, D. et al., 2008. Impact of clarification strategy on chromatographic separations: Pre-processing of cell homogenates. *Biotechnology and Bioengineering*, 100(5), 941-949.

Bromley, E.H.C. & Hopkinson, I., 2002. Confocal Microscopy of a Dense Particle System. *Journal of Colloid and Interface Science*, 245(1), 75-80.

Buckholz, R.G. & Gleeson, M.A., 1991. Yeast systems for the commercial production of heterologous proteins. *Bio/Technology (Nature Publishing Company)*, 9(11), 1067-1072.

Buckland, B.C., 2005. The process development challenge for a new vaccine. *Nature Medicine*, 11(4 Suppl), S16-19.

Chang, C. & Lenhoff, A.M., 1998. Comparison of protein adsorption isotherms and uptake rates in preparative cation-exchange materials. *Journal of Chromatography A*, 827(2), 281-293.

Cheetham, P.S., 1979. Removal of triton X-100 from aqueous solution using amberlite XAD-2. *Analytical Biochemistry*, 92(2), 447-452.

Chen, J., Tetrault, J. & Ley, A., 2008. Comparison of standard and new generation hydrophobic interaction chromatography resins in the monoclonal antibody purification process. *Journal of Chromatography. A*, 1177(2), 272-281.

Chen, W. et al., 2003. Effect of Temperature on Hydrophobic Interaction between Proteins and Hydrophobic Adsorbents: Studies by Isothermal Titration Calorimetry and the van't Hoff Equation. *Langmuir*, 19(22), 9395-9403.

Chi, W.K. et al., 1994. Two-step cell disruption for the extraction of membrane-associated recombinant protein from *Saccharomyces cerevisiae*. *Annals of the New York Academy of Sciences*, 721, 365-373.

Chu, C. & Babineau, R.A., 1986. Modified cellulose separation matrix. US Patent: 4,606,824.

Clausen, M.K. et al., 1974. Isolation of lipid particles from baker's yeast. *FEBS Letters*, 43(2), 176-179.

Coates, T. et al., 2001. Hepatitis B vaccines: assessment of the seroprotective efficacy of two recombinant DNA vaccines. *Clinical Therapeutics*, 23(3), 392-403.

Corradini, D., Capitani, D. & Cellai, L., 1994. Salt Concentration Effects in High-Performance Hydrophobic-Interaction Chromatography in Comparison with NMR of Proteins in Solution. *Journal of Liquid Chromatography*, 17(20), 4335-4347.

Creighton, T.E., 1997. *Protein structure: a practical approach*, Oxford University Press.

Dahim, M. et al., 1998. Solubilization of phospholipid/triacylglycerol aggregates by non-ionic surfactants. *Chemistry and Physics of Lipids*, 97(1), 1-14.

Dekleva, M.L., 2002. Vaccine Technology. In M. C. Flickinger & S. W. Drew, eds. *Encyclopedia of Bioprocess Technology*. Hoboken, NJ, USA: John Wiley & Sons, Inc.

Dismer, F. & Hubbuch, J., 2007. A novel approach to characterize the binding orientation of lysozyme on ion-exchange resins. *Journal of Chromatography. A*, 1149(2), 312-320.

Doran, P.M., 1995. *Bioprocess Engineering Principles*, Academic Press.

Dreesman, G.R. et al., 1972. Biophysical and biochemical heterogeneity of purified hepatitis B antigen. *Journal of Virology*, 10(3), 469-476.

Dziennik, S.R. et al., 2003. Nondiffusive mechanisms enhance protein uptake rates in ion exchange particles. *Proceedings of the National Academy of Sciences of the United States of America*, 100(2), 420-425.

Dziennik, S.R. et al., 2005. Effects of ionic strength on lysozyme uptake rates in cation exchangers. I: Uptake in SP Sepharose FF. *Biotechnology and Bioengineering*, 91(2), 139-153.

Edwards, K. et al., 1989. Effects of Triton X-100 on sonicated lecithin vesicles. *Langmuir*, 5(2), 473-478.

Engler, C.R. & Robinson, C.W., 1981. Effects of organism type and growth conditions on cell disruption by impingement. *Biotechnology Letters*, 3(2), 83-88.

Even-Chen, Z., 1993. Method for production and purification of hepatitis B vaccine. US Patent: 5242812.

Fausnaugh, J., Kennedy, L. & Regnier, F., 1984. Comparison of hydrophobic-interaction and reversed-phase chromatography of proteins. *Journal of Chromatography A*, 317, 141-155.

Fausnaugh, J. & Regnier, F., 1986. Solute and mobile phase contributions to retention in hydrophobic interaction chromatography of proteins. *Journal of Chromatography A*, 359, 131-146.

Fernandez-Lahore et al., 1999. The influence of complex biological feedstock on the fluidization and bed stability in expanded bed adsorption. *Biotechnology and Bioengineering*, 64(4), 484-496.

Feuser, J. et al., 1999. Cell/adsorbent interactions in expanded bed adsorption of proteins. *Bioseparation*, 8(1-5), 99-109.

Fexby, S. et al., 2007. Novel in situ polymerized coatings for hydrophobic interaction chromatography media. *Journal of Chromatography. A*, 1161(1-2), 234-241.

Follows, M. et al., 1971. Release of enzymes from bakers' yeast by disruption in an industrial homogenizer. *Biotechnology and Bioengineering*, 13(4), 549-560.

Ganem, D. & Prince, A.M., 2004. Hepatitis B virus infection--natural history and clinical consequences. *The New England Journal of Medicine*, 350(11), 1118-1129.

Gao, J. & Dubin, P., 1999. Binding of proteins to copolymers of varying hydrophobicity. *Biopolymers*, 49(2), 185-193.

Garland, S.M. et al., 2007. Noninferiority of antibody response to human papillomavirus type 16 in subjects vaccinated with monovalent and quadrivalent L1 virus-like particle vaccines. *Clinical and Vaccine Immunology: CVI*, 14(6), 792-795.

Gavilanes, F. et al., 1990. Hepatitis B surface antigen. Role of lipids in maintaining the structural and antigenic properties of protein components. *The Biochemical Journal*, 265(3), 857-864.

Gavilanes, F., Gonzalez-Ros, J.M. & Peterson, D.L., 1982b. Structure of hepatitis B surface antigen. Characterization of the lipid components and their association with the viral proteins. *The Journal of Biological Chemistry*, 257(13), 7770-7777.

GE Healthcare, 2010. *Hydrophobic Interaction and Reversed Phase Chromatography, Principles and Methods*.

GE Healthcare, Phenyl Sepharose High Performance/Butyl Sepharose High Performance. Available at: <http://www.gelifesciences.com/> [Accessed September 13, 2009].

GE Healthcare, Sepharose 4 Fast Flow/Sepharose 6 Fast Flow. Available at: <http://www.gelifesciences.com/> [Accessed September 13, 2009].

Geng, X., Guo, L. & Chang, J., 1990. Study of the retention mechanism of proteins in hydrophobic interaction chromatography. *Journal of Chromatography A*, 507, 1-23.

Goheen, S.C. & Engelhorn, S.C., 1984. Hydrophobic interaction high-performance liquid chromatography of proteins. *Journal of Chromatography A*, 317, 55-65.

Green, A.A. & Hughes, W.L., 1955. Protein fractionation on the basis of solubility in aqueous solutions of salts and organic solvents. *Methods in Enzymology*, 1, 67-90.

Green, D.W. & Perry, R.H., 2007. *Perry's Chemical Engineers' Handbook, Eighth Edition* 8th ed., McGraw-Hill Professional.

Grgacic, E.V.L. & Anderson, D.A., 2006. Virus-like particles: passport to immune recognition. *Methods (San Diego, Calif.)*, 40(1), 60-65.

Guiochon, G. et al., 2006. *Fundamentals of preparative and nonlinear chromatography*, Academic Press.

Hagel, L., Jagschies, G. & Sofer, G.K., 2007. *Handbook of Process Chromatography: Development, Manufacturing, Validation and Economics* 2nd ed., Academic Press.

Hahn, R. et al., 2003. Hydrophobic interaction chromatography of proteins. II. Binding capacity, recovery and mass transfer properties. *Journal of Chromatography. B, Analytical Technologies in the Biomedical and Life Sciences*, 790(1-2), 99-114.

Hajibagheri, M.A.N., 1999. *Electron microscopy methods and protocols*, Humana Press.

Hale, G. et al., 1994. Repeated cleaning of protein A affinity column with sodium hydroxide. *Journal of Immunological Methods*, 171(1), 15-21.

Harinarayan, C. et al., 2006. An exclusion mechanism in ion exchange chromatography. *Biotechnology and Bioengineering*, 95(5), 775-787.

de Harven, E., Leung, R. & Christensen, H., 1984. A novel approach for scanning electron microscopy of colloidal gold- labeled cell surfaces. *The Journal of Cell Biology*, 99(1), 53-57.

Haugland, R.P., Spence, M.T.Z. & Johnson, I.D., 2005. *The handbook: a guide to fluorescent probes and labeling technologies*, Molecular Probes.

Heinemann, M., Limper, U. & Büchs, J., 2004. New insights in the spatially resolved dynamic pH measurement in macroscopic large absorbent particles by confocal laser scanning microscopy. *Journal of Chromatography. A*, 1024(1-2), 45-53.

Heinemann, M. et al., 2002. A new approach for the spatially resolved qualitative analysis of the protein distribution in hydrogel beads based on confocal laser scanning microscopy. *Biotechnology Letters*, 24(10), 845-850.

Heinitz, M.L. et al., 1988. Chromatography of proteins on hydrophobic interaction and ion-exchange chromatographic matrices: mobile phase contributions to selectivity. *Journal of Chromatography A*, 443, 173-182.

Hermanson, G.T., 2008. *Bioconjugate techniques*, Academic Press.

Hetherington, P.J. et al., 1971. Release of protein from baker's yeast (*Saccharomyces cerevisiae*) by disruption in an industrial homogenizer. *Transactions of the American Institute of Chemical Engineers*, 49, 142-148.

Hilleman, M.R., 2001. Overview of the pathogenesis, prophylaxis and therapeutics of viral hepatitis B, with focus on reduction to practical applications. *Vaccine*, 19(15-16), 1837-1848.

Hilleman, M.R., 2003. Critical overview and outlook: pathogenesis, prevention, and treatment of hepatitis and hepatocarcinoma caused by hepatitis B virus. *Vaccine*, 21(32), 4626-4649.

Hinkeldey, B., Schmitt, A. & Jung, G., 2008. Comparative Photostability Studies of BODIPY and Fluorescein Dyes by Using Fluorescence Correlation Spectroscopy. *ChemPhysChem*, 9(14), 2019-2027.

Hitzeman, R.A. et al., 1983. Expression of hepatitis B virus surface antigen in yeast. *Nucleic Acids Research*, 11(9), 2745-2763.

Holloway, P.W., 1973. A simple procedure for removal of Triton X-100 from protein samples. *Analytical Biochemistry*, 53(1), 304-308.

Horigome, T. & Sugano, H., 1983. A rapid method for removal of detergents from protein solution. *Analytical Biochemistry*, 130(2), 393-396.

Hou, K.C., 1986. Fibrous media containing millimicron-sized particulates. US Patent: 4,578,150.

Hubbuck, J. & Kula, M.R., 2008. Confocal laser scanning microscopy as an analytical tool in chromatographic research. *Bioprocess and Biosystems Engineering*, 31(3), 241-259.

Hubbuck, J. et al., 2002. Dynamics of protein uptake within the adsorbent particle during packed bed chromatography. *Biotechnology and Bioengineering*, 80(4), 359-368.

Hubbuck, J. et al., 2003. Mechanism and kinetics of protein transport in chromatographic media studied by confocal laser scanning microscopy. Part II. Impact on chromatographic separations. *Journal of Chromatography. A*, 1021(1-2), 105-115.

Huovila, A.P., Eder, A.M. & Fuller, S.D., 1992. Hepatitis B surface antigen assembles in a post-ER, pre-Golgi compartment. *The Journal of Cell Biology*, 118(6), 1305-1320.

Invitrogen, 2010. *Molecular Probes: The Handbook*, Invitrogen.

Jackson, M.L. et al., 1982. Solubilization of phosphatidylcholine bilayers by octyl glucoside. *Biochemistry*, 21(19), 4576-4582.

Janson, J. & Rydén, L., 1998. *Protein purification: principles, high-resolution methods, and applications*, Wiley-VCH.

Jennings, G.T. & Bachmann, M.F., 2008. The coming of age of virus-like particle vaccines. *Biological Chemistry*.

Jin, J. et al., 2009. Evaluation of the impact of lipid fouling during the chromatographic purification of virus-like particles from *Saccharomyces cerevisiae*. *Journal of Chemical Technology & Biotechnology*, 85(2), 209-215.

Johnston, A. & Hearn, M., 1991. High-performance liquid chromatography of amino acids, peptides and proteins : CXIV. Protein interactions with porous coulombic sorbents: comparison of experimental findings with predictions of several adsorption models. *Journal of Chromatography A*, 557, 335-358.

Joseph, J. et al., 2007. A Framework for the Prediction of Scale-Up When Using Compressible Chromatographic Packings. *Biotechnology Progress*, 23(2), 413-422.

Kasche, V. et al., 2003. Direct observation of intraparticle equilibration and the rate-limiting step in adsorption of proteins in chromatographic adsorbents with confocal laser scanning microscopy. *Journal of Chromatography. B, Analytical Technologies in the Biomedical and Life Sciences*, 790(1-2), 115-129.

Kato, Y. et al., 2002. Separation of proteins by hydrophobic interaction chromatography at low salt concentration. *Journal of Chromatography. A*, 971(1-2), 143-149.

Katti, A., Maa, Y.-. & Horváth, C., 1987. Protein surface area and retention in hydrophobic interaction chromatography. *Chromatographia*, 24(1), 646-650.

Kee, G.S. et al., 2010. Exploiting the intracellular compartmentalization characteristics of the *S. cerevisiae* host cell for enhancing primary purification of lipid-envelope virus-like particles. *Biotechnology Progress*, 26(1), 26-33.

Kee, G.S., Pujar, N.S. & Titchener-Hooker, N.J., 2008. Study of detergent-mediated liberation of hepatitis B virus-like particles from *S. cerevisiae* homogenate: identifying a framework for the design of future-generation lipoprotein vaccine processes. *Biotechnology Progress*, 24(3), 623-631.

Kelly, S.T. & Zydney, A.L., 1997. Protein fouling during microfiltration: comparative behavior of different model proteins. *Biotechnology and Bioengineering*, 55(1), 91-100.

Kent, R.S. & Drohan, W.N., 2001. Methods for the selective separation of organic components from biological fluids. US Patent: 6,193,891.

Kim, S.N. et al., 2007. Purification and immunogenicity study of human papillomavirus type 16 L1 protein in *Saccharomyces cerevisiae*. *Journal of Virological Methods*, 139(1), pp.24-30.

Kita, Y. et al., 1994. Contribution of the surface free energy perturbation to protein-solvent interactions. *Biochemistry*, 33(50), 15178-15189.

Kragh-Hansen, U., le Maire, M. & Møller, J.V., 1998. The mechanism of detergent solubilization of liposomes and protein-containing membranes. *Biophysical Journal*, 75(6), 2932-2946.

Kreibich, G. et al., 1982. Recovery of ribophorins and ribosomes in "inverted rough" vesicles derived from rat liver rough microsomes. *The Journal of Cell Biology*, 93(1), 111-121.

Kuo, J., 2007. *Electron Microscopy: Methods and Protocols*: 369 2nd ed., Humana Press.

Langmuir, I., 1916. The constitution and fundamental properties of solids and liquids. Part i. solids. *Journal of the American Chemical Society*, 38(11), 2221-2295.

Lenhoff, A.M. & To, B.C.S., 2007. Hydrophobic interaction chromatography of proteins. I. The effects of protein and adsorbent properties on retention and recovery. *Journal of Chromatography. A*, 1141(2), 191-205.

Levison, P.R. et al., 1995. Validation studies in the regeneration of ion-exchange celluloses. *Journal of Chromatography A*, 702(1-2), 59-68.

Levy, D. et al., 1990. Phospholipid vesicle solubilization and reconstitution by detergents. Symmetrical analysis of the two processes using octaethylene glycol mono-n-dodecyl ether. *Biochemistry*, 29(40), 9480-9488.

Lewus, R.K., Altan, F.H. & Carta, G., 1998. Protein Adsorption and Desorption on Gel-Filled Rigid Particles for Ion Exchange. *Industrial & Engineering Chemistry Research*, 37(3), 1079-1087.

Li, J. et al., 2004. Hydrophobic interaction chromatography correctly refolding proteins assisted by glycerol and urea gradients. *Journal of Chromatography A*, 1061(2), pp.193-199.

Lichtenberg, D., Robson, R.J. & Dennis, E.A., 1983. Solubilization of phospholipids by detergents. Structural and kinetic aspects. *Biochimica Et Biophysica Acta*, 737(2), 285-304.

Lin, F.Y., Chen, W.Y. & Hearn, M.T., 2001. Microcalorimetric studies on the interaction mechanism between proteins and hydrophobic solid surfaces in hydrophobic interaction chromatography: effects of salts, hydrophobicity of the sorbent, and structure of the protein. *Analytical Chemistry*, 73(16), 3875-3883.

Lina, F.Y. et al., 2000. Microcalorimetric studies of interactions between proteins and hydrophobic ligands in hydrophobic interaction chromatography: effects of ligand chain length, density and the amount of bound protein. *Journal of Chromatography. A*, 872(1-2), 37-47.

Linden, T. et al., 1999. Visualizing two-component protein diffusion in porous adsorbents by confocal scanning laser microscopy. *Biotechnology and Bioengineering*, 65(6), 622-630.

Linden, T. et al., 2002. Visualizing patterns of protein uptake to porous media using confocal scanning laser microscopy. *Separation Science and Technology*, 37(1), 1-32.

Linke, D., 2009. Chapter 34 Detergents: An Overview. In *Methods in Enzymology*. Academic Press, pp. 603-617.

Ljunglöf, A. & Thömmes, J., 1998. Visualising intraparticle protein transport in porous adsorbents by confocal microscopy. *Journal of Chromatography. A*, 813(2), 387-395.

Ljunglöf, A. & Hjorth, R., 1996. Confocal microscopy as a tool for studying protein adsorption to chromatographic matrices. *Journal of Chromatography A*, 743(1), 75-83.

Ludwig, C. & Wagner, R., 2007. Virus-like particles-universal molecular toolboxes. *Current Opinion in Biotechnology*, 18(6), 537-545.

Maartens, A., Swart, P. & Jacobs, E.P., 1998. Humic membrane foulants in natural brown water: characterization and removal. *Desalination*, 115(3), 215-227.

le Maire, M., Møller, J.V. & Champeil, P., 1987. Binding of a nonionic detergent to membranes: flip-flop rate and location on the bilayer. *Biochemistry*, 26(15), 4803-4810.

Malmsten, M., Xing, K. & Ljunglöf, A., 1999. Confocal Microscopy Studies of Trypsin Immobilization on Porous Glycidyl Methacrylate Beads. *Journal of Colloid and Interface Science*, 220(2), 436-442.

Margadant, F., leemann, T. & Niederer, P., 1996. A precise light attenuation correction for confocal scanning microscopy with $O(n^4/3)$ computing time and $O(n)$ memory requirements for n voxels. *Journal of Microscopy*, 182(2), 121-132.

Marshall, A.D., Munro, P.A. & Trägårdh, G., 1993. The effect of protein fouling in microfiltration and ultrafiltration on permeate flux, protein retention and selectivity: A literature review. *Desalination*, 91(1), 65-108.

Mattiasson, B. & Nandakumar, M., 2000. Physicochemical basis of expanded-bed adsorption for protein purification. In *Handbook of Bioseparations*. Academic Press, pp. 417-430.

McAleer, W.J. et al., 1984. Human hepatitis B vaccine from recombinant yeast. *Nature*, 307(5947), 178-180.

Melander, W. & Horváth, C., 1977. Salt effect on hydrophobic interactions in precipitation and chromatography of proteins: an interpretation of the lyotropic series. *Archives of Biochemistry and Biophysics*, 183(1), 200-215.

Melander, W., Corradini, D. & Horváth, C., 1984. Salt-mediated retention of proteins in hydrophobic-interaction chromatography : Application of solvophobic theory. *Journal of Chromatography A*, 317, 67-85.

Melander, W.R., El Rassi, Z. & Horváth, C., 1989. Interplay of hydrophobic and electrostatic interactions in biopolymer chromatography : Effect of salts on the retention of proteins. *Journal of Chromatography A*, 469, 3-27.

Milburn, P.T. & Dunnill, P., 1994. The release of virus-like particles from recombinant *Saccharomyces cerevisiae*: effect of freezing and thawing on homogenization and bead milling. *Biotechnology and Bioengineering*, 44(6), 736-744.

Minsky, M., 1988. Memoir on Inventing the Confocal Scanning Microscope. *Scanning*, 10, 128-138.

Minsky, M., 1961. Microscopy Apparatus. US Patent: 3,013,467

Miyabe, K. & Guiochon, G., 2001. Correlation between Surface Diffusion and Molecular Diffusion in Reversed-Phase Liquid Chromatography. *The Journal of Physical Chemistry B*, 105(38), 9202-9209.

Mohammad, A.W., Stevenson, D.G. & Wankat, P.C., 1992. Pressure drop correlations and scale-up of size exclusion chromatography with compressible packings. *Industrial & Engineering Chemistry Research*, 31(2), 549-561.

Moore, E.K., Hoare, M. & Dunnill, P., 1990. Disruption of baker's yeast in a high-pressure homogenizer: New evidence on mechanism. *Enzyme and Microbial Technology*, 12(10), 764-770.

Morrow, K., 2006. Large-Scale Production of Antibodies. *GEN*, 26(4), 34-37.

Natter, K. et al., 2005. The spatial organization of lipid synthesis in the yeast *Saccharomyces cerevisiae* derived from large scale green fluorescent protein tagging and high resolution microscopy. *Molecular & Cellular Proteomics: MCP*, 4(5), 662-672.

Neugebauer, J.M., 1990. Detergents: an overview. *Methods in Enzymology*, 182, 239-253.

Noad, R. & Roy, P., 2003. Virus-like particles as immunogens. *Trends in Microbiology*, 11(9), 438-444.

Olsen, D.K. et al., 1999. Encapsulated lenticular filter cartridge. US Patent: 5,965,019.

Oscarsson, S., 1995. Influence of salts on protein interactions at interfaces of amphiphilic polymers and adsorbents. *Journal of Chromatography. B, Biomedical Applications*, 666(1), 21-31.

Oscarsson, S., 1995. Influence of salts on protein interactions at interfaces of amphiphilic polymers and adsorbents. *Journal of Chromatography B: Biomedical Sciences and Applications*, 666(1), 21-31.

Paavonen, J. et al., 2007. Efficacy of a prophylactic adjuvanted bivalent L1 virus-like-particle vaccine against infection with human papillomavirus types 16 and 18 in young women: an interim analysis of a phase III double-blind, randomised controlled trial. *Lancet*, 369(9580), 2161-2170.

Paddock, S.W., 1999. *Confocal microscopy methods and protocols*, Humana Press.

Page, M. & Thorpe, R., 1996. Purification of IgG by Precipitation with Polyethylene Glycol (PEG). In *The Protein Protocols Handbook*. pp. 731-731.

Paternostre, M.T., Roux, M. & Rigaud, J.L., 1988. Mechanisms of membrane protein insertion into liposomes during reconstitution procedures involving the use of detergents. 1. Solubilization of large unilamellar liposomes (prepared by reverse-phase evaporation) by triton X-100, octyl glucoside, and sodium cholate. *Biochemistry*, 27(8), 2668-2677.

Pattenden, L.K. et al., 2005. Towards the preparative and large-scale precision manufacture of virus-like particles. *Trends in Biotechnology*, 23(10), 523-529.

Perkins, T.W. et al., 1997. Protein retention in hydrophobic interaction chromatography: modeling variation with buffer ionic strength and column hydrophobicity. *Journal of Chromatography A*, 766(1-2), 1-14.

Peskin, A.P. & Rudge, S.R., 1992. Optimization of large-scale chromatography for biotechnological applications. *Applied Biochemistry and Biotechnology*, 34-35(1), 49-59.

Peterson, D.L., 1987. The structure of hepatitis B surface antigen and its antigenic sites. *BioEssays: News and Reviews in Molecular, Cellular and Developmental Biology*, 6(6), 258-262.

Phogat, S. et al., 2008. Analysis of the Human Immunodeficiency Virus Type 1 gp41 Membrane Proximal External Region Arrayed on Hepatitis B Surface Antigen Particles. *Virology*, 373(1), 72-84.

Pointek, M. & Weniger, M., 2001. Method for obtaining recombinant hbsag. US Patent: 6,428,984.

Ramsay, A.M. & Douglas, L.J., 1979. Effects of phosphate limitation of growth on the cell-wall and lipid composition of *Saccharomyces cerevisiae*. *Journal of General Microbiology*, 110(1), 185-191.

Ratray, J., 1988. *Microbial Lipids*, Academic Press.

Rigaud, J. et al., 1998. Detergent removal by non-polar polystyrene beads. *European Biophysics Journal*, 27(4), 305-319.

Rippel, G. & Szepeszy, L., 1994. Hydrophobic interaction chromatography of proteins on an Alkyl-Superose column. *Journal of Chromatography A*, 664(1), 27-32.

Roingeard, P. et al., 2008. Hepatitis C virus budding at lipid droplet-associated ER membrane visualized by 3D electron microscopy. *Histochemistry and Cell Biology*, 130(3), 561-566.

Rolf, J.M., 2003. Methods for the removal of organic substances from aqueous solutions.

Ruthven, D.M., 1984. *Principles of adsorption and adsorption processes*, Wiley-Interscience.

Sajbidor, J., Certík, M. & Grego, J., 1994. Lipid analysis of baker's yeast. *Journal of Chromatography A*, 665(1), 191-195.

Sanchez, Y. et al., 1983. Comparative studies of the immunogenic activity of hepatitis B surface antigen (HBsAg) and HBsAg polypeptides. *Journal of Medical Virology*, 11(2), 115-124.

Schagger, H., 1994. Chromatographic techniques and basic operations in membrane protein purification. In *In A Practical Guide to Membrane Protein Purification*. Academic Press, pp. 23-57.

Scheule, R.K. & Gaffney, B.J., 1981. Reconstitution of membranes with fractions of triton X-100 which are easily removed. *Analytical Biochemistry*, 117(1), 61-66.

Schmuck, M.N., Nowlan, M.P. & Gooding, K.M., 1986. Effect of mobile phase and ligand arm on protein retention in hydrophobic interaction chromatography. *Journal of Chromatography A*, 371, 55-62.

Shaeiwitz, J.A., Blair, J.B. & Ruaan, R., 1989. Evidence that yeast cell wall debris can separate proteins by ion-exchange during cell lysis. *Biotechnology and Bioengineering*, 34(1), 137-140.

Shepard, S.R. et al., 2000. Discoloration of ceramic hydroxyapatite used for protein chromatography. *Journal of Chromatography. A*, 891(1), 93-98.

Shi, L. et al., 2005. Stabilization of human papillomavirus virus-like particles by non-ionic surfactants. *Journal of Pharmaceutical Sciences*, 94(7), 1538-1551.

Shikary, T. et al., 2009. Epidemiology and risk factors for human papillomavirus infection in a diverse sample of low-income young women. *Journal of Clinical Virology: The Official Publication of the Pan American Society for Clinical Virology*, 46(2), 107-111.

Sigma-Aldrich, 2010. LRA product information technical note.

Sitrin, R.D. & Kubek, D.J., 1991. Method of stabilizing recombinant hepatitis B virus surface proteins from recombinant host cells.

Siu, S.C., Baldascini, H. et al., 2006. Effect of fouling on the capacity and breakthrough characteristics of a packed bed ion exchange chromatography column. *Bioprocess and Biosystems Engineering*, 28(6), 405-414.

Siu, S.C., Boushaba, R. et al., 2006. Visualising fouling of a chromatographic matrix using confocal scanning laser microscopy. *Biotechnology and Bioengineering*, 95(4), 714-723.

Skelly, J., Howard, C.R. & Zuckerman, A.J., 1981. Hepatitis B polypeptide vaccine preparation in micelle form. *Nature*, 290(5801), 51-54.

Smith, M.L. et al., 2002. Factors important in the extraction, stability and in vitro assembly of the hepatitis B surface antigen derived from recombinant plant systems. *Biotechnology Progress*, 18(3), 538-550.

Smith, R.N., Geiger, C.F. & Pierce, C., 1953. The Equilibrium Exchange Rates of Adsorbed Species with Un-adsorbed Species in Solution. *The Journal of Physical Chemistry*, 57(3), 382-384.

Smith, T.R., 2001. LRA product information technical note.

Soriano, G.A., Titchener-Hooker, N.J. & Shamlou, P.A., 1997. The effects of processing scale on the pressure drop of compressible gel supports in liquid chromatographic columns. *Bioprocess Engineering*, 17(2), 115.

Staby, A. et al., 1998. Comparison of loading capacities of various proteins and peptides in culture medium and in pure state. *Journal of Chromatography. A*, 827(2), 311-318.

Susanto, A., Herrmann, T. & Hubbuch, J., 2006. Short-cut method for the correction of light attenuation influences in the experimental data obtained from confocal laser scanning microscopy. *Journal of Chromatography. A*, 1136(1), 29-38.

Susanto, A. et al., 2007. Investigation of pore diffusion hindrance of monoclonal antibody in hydrophobic interaction chromatography using confocal laser scanning microscopy. *Journal of Chromatography A*, 1149(2), 178-188.

Susanto, A. et al., 2006. Developing a chromatographic column model for bovine serum albumin on strong anion-exchanger Source30Q using data from confocal laser scanning microscopy. *Journal of Chromatography. A*, 1137(1), 63-75.

Suzuki, M., 1990. *Adsorption Engineering*, Elsevier Science.

Szepesy, L. & Horváth, C., 1988. Specific salt effects in hydrophobic interaction chromatography of proteins. *Chromatographia*, 26(1), 13-18.

Tahoun, M.K., 1986. Large agarose-lipase beads for the hydrolysis of triglycerides. *Food Chemistry*, 22(4), 297-303.

Tallarek, U. et al., 2003. Quantitative Study of Electrokinetic Transport in Porous Media by Confocal Laser Scanning Microscopy. *Langmuir*, 19(11), 4527-4531.

Teske, C.A. et al., 2006. Competitive adsorption of labeled and native protein in confocal laser scanning microscopy. *Biotechnology and Bioengineering*, 95(1), 58-66.

Teske, C.A. et al., 2005. Protein-labeling effects in confocal laser scanning microscopy. *The Journal of Physical Chemistry. B*, 109(28), 13811-13817.

Teske, C.A. et al., 2007. Changes in retention behavior of fluorescently labeled proteins during ion-exchange chromatography caused by different protein surface labeling positions. *Biotechnology and Bioengineering*, 98(1), 193-200.

Tibbs Jones, T. & Fernandez, E.J., 2003. [alpha]-Lactalbumin tertiary structure changes on hydrophobic interaction chromatography surfaces. *Journal of Colloid and Interface Science*, 259(1), 27-35.

Timasheff, S.N., 1993. The control of protein stability and association by weak interactions with water: how do solvents affect these processes? *Annual Review of Biophysics and Biomolecular Structure*, 22, 67-97.

Timasheff, S.N. & Arakawa, T., 1988. Mechanism of protein precipitation and stabilization by co-solvents. *Journal of Crystal Growth*, 90(1-3), 39-46.

Ueberbacher, R. et al., 2010. Hydrophobic interaction chromatography of proteins: Thermodynamic analysis of conformational changes. *Journal of Chromatography A*, 1217(2), 184-190.

Ueno, M., Tanford, C. & Reynolds, J.A., 1984. Phospholipid vesicle formation using nonionic detergents with low monomer solubility. Kinetic factors determine vesicle size and permeability. *Biochemistry*, 23(13), 3070-3076.

Valenzuela, P. et al., 1982. Synthesis and assembly of hepatitis B virus surface antigen particles in yeast. *Nature*, 298(5872), 347-350.

Verhoff, F.H. & Furjanic, J.J., 1983. Compressible packed bed fluid dynamics with application to a glucose isomerase reactor. *Industrial & Engineering Chemistry Process Design and Development*, 22(2), 192-198.

Wachtler, V. & Balasubramanian, M.K., 2006. Yeast lipid rafts? - An emerging view. *Trends in Cell Biology*, 16(1), 1-4.

Walboomers, J.M. et al., 1999. Human papillomavirus is a necessary cause of invasive cervical cancer worldwide. *The Journal of Pathology*, 189(1), 12-19.

Wampler, D.E. et al., 1985. Multiple chemical forms of hepatitis B surface antigen produced in yeast. *Proceedings of the National Academy of Sciences of the United States of America*, 82(20), 6830-6834.

Wijnendaele, F. & Simonet, G., 1985. Method for the isolation and purification of hepatitis B surface antigen using polysorbate.

Wingfield, P., 1998. Protein Precipitation Using Ammonium Sulfate. In J. E. Coligan et al., eds. *Current Protocols in Protein Science*. Hoboken, NJ, USA: John Wiley & Sons, Inc.

Winters, M.A. et al., 2003a. Plasmid DNA purification by selective calcium silicate adsorption of closely related impurities. *Biotechnology Progress*, 19(2), 440-447.

Winters, M.A. et al., 2003b. Plasmid DNA purification by selective calcium silicate adsorption of closely related impurities. *Biotechnology Progress*, 19(2), 440-447.

Wu, S., Benedek, K. & Karger, B.L., 1986. Thermal behavior of proteins in high-performance hydrophobic-interaction chromatography On-line spectroscopic and chromatographic characterization. *Journal of Chromatography A*, 359, 3-17.

Xu, Y. et al., 2008. Enhancing functional expression of heterologous lipase in the periplasm of *Escherichia coli*. *World Journal of Microbiology and Biotechnology*, 24(12), 2827-2835.

Yamamoto, S., Nakanishi, K. & Matsuno, R., 1988. *Ion Exchange Chromatography of Proteins*, CRC Press.

Yang, K., Shi, Q. & Sun, Y., 2006. Modeling and simulation of protein uptake in cation exchanger visualized by confocal laser scanning microscopy. *Journal of Chromatography. A*, 1136(1), 19-28.

Yoshida, H., Yoshikawa, M. & Kataoka, T., 1994. Parallel transport of BSA by surface and pore diffusion in strongly basic chitosan. *AIChE Journal*, 40(12), 2034-2044.

Zhang, J.P. et al., 2005. Endotoxin removal using a synthetic adsorbent of crystalline calcium silicate hydrate. *Biotechnology Progress*, 21(4), 1220-1225.

Zhang, Y.P. et al., 1999. Stabilized plasmid-lipid particles for regional gene therapy: formulation and transfection properties. *Gene Therapy*, 6(8), 1438-1447.

Zhao, Q. et al., 2006. Maturation of recombinant hepatitis B virus surface antigen particles. *Human Vaccines*, 2(4), 174-180.

Zhou, W. et al., 2007. A highly efficient hydrophobic interaction chromatographic adsorbent improved the purification of hepatitis B surface antigen (HBsAg) derived from *Hansenula polymorpha* cell. *Process Biochemistry*, 42(5), 751-756.

Zoungrana, T., Findenegg, G.H. & Norde, W., 1997. Structure, Stability, and Activity of Adsorbed Enzymes. *Journal of Colloid and Interface Science*, 190(2), 437-448.

Appendix

Publication

Jin, J. et al., 2009. Evaluation of the impact of lipid fouling during the chromatographic purification of virus-like particles from *Saccharomyces cerevisiae*. *Journal of Chemical Technology & Biotechnology*, 85(2), 209-215. (DOI: 10.1002/jctb.2290)